Green synthesis of zinc oxide nanoparticles using *Ilex paraguariensis* leaves for application in antimicrobial polyelectrolyte biomaterials

being a thesis submitted for the degree of

Doctor of Philosophy

by

Marina Bandeira

based on a research carried out under the supervision of

Dr. Declan M. Devine

Dr. Janaina da Silva Crespo

Dr. Mariana Roesch-Ely

2021

Green synthesis of zinc oxide nanoparticles using Ilex paraguariensis leaves for applications in antimicrobial polyelectrolyte biomaterials

Marina Bandeira

A thesis submitted for the degree of Doctor of Philosophy in a collaboration between the Department of Polymer Engineering of Athlone Institute of Technology (AIT), Ireland and the Materials Science Engineering Postgraduate Program of Universidade de Caxias do Sul (UCS), Brazil.

27th July, 2021

Examiners:

_____
Dr. Cláudio Antônio Perottoni
Universidade de Caxias do Sul, Brazil

_____
Dr. Jacqueline Ferreira Leite Santos
Universidade Federal do Rio Grande do Sul, Brazil

_____
Dr. Michael Nugent
Athlone Institute of Technology, Ireland

_____
Dr. Patrick Murray
Limerick Institute of Technology, Ireland

Declaration

I hereby declare that this thesis submitted to the Athlone Institute of Technology and the Universidade de Caxias do Sul for the degree of Doctor of Philosophy, is a result of my own work and has not in the same or altered form, been presented to these institutes or any other institute in support for any degree other than for which I am now a candidate.

_____   27th July, 2021

Marina Bandeira   Date

Acknowledgments

I would like to thank my supervisors for all your support, guidance and for sharing your knowledge with me. To Dr. Janaina Crespo, also thank you for all the years we have worked together and for always believing in me. To Dr. Mariana Roesch-Ely, for your patience and essential contribution to the biological part of this project. And to Dr. Declan Devine, for the opportunity of turning this project into a joint Ph.D., to include me in your research group, and for the kind support in these last two years. I am very lucky to have worked with you all.

To Dr. Marcelo Giovanela, thank you for the important contributions, encouragement, and especially for sharing your knowledge.

To Caroline Menti, Sandra Pavin, and Rafaele Frassini, who kindly helped me with the biological tests. To Rodrigo Barbieri (LCMIC – UCS) and Alan Murphy (CISD – AIT), who kindly performed the microscopy analysis.

To Dr. Angela Gujel, thank you for firstly teaching me how to do research when I was an undergrad, and for kindly sharing your knowledge. But more importantly, thank you for your valuable friendship.

To my colleagues at PPGMAT – UCS, for the scientific discussions and fun moments, whether in classes or coffee breaks. A special thanks to Camila, Francisco, and Mario who I shared a good part of my days at the beginning of my Ph.D. journey.

To my colleagues at the Research Hub – AIT, thank you to all who helped me in any way, whether it was in scientific or English matter. Thank to my friends who shared uncountable 'cafezinhos' and for the joy moments along these years in AIT. A special thanks to Ana and Viviane for your support in the hardest time of this project.

And finally, I would like to thank my lovely mom, for all the unconditional love and support despite continuously complaining about the distance between Brazil and Ireland. The world would be better if we had more people like you. Also, thank to my awesome siblings, Tiago and Aline, André, and my little nephew Miguel, who is the joy of our days. I have no words to express how grateful I am for having you all in my life.

Table of contents

Abstract

This research aims to develop and characterize antimicrobial polymer biomaterials containing zinc oxide nanoparticles (ZnONPs) obtained using *Ilex paraguariensis* (IP) leaf extract by green synthesis. The biomaterials were investigated for biomedical device coating and tissue regeneration applications, considering that infections are one of the major complications in this field. The biomaterials were synthesized using the polyelectrolytes polyallylamine hydrochloride (PAH) and polyacrylic acid (PAA) and characterized according to their morphology, composition, and antimicrobial activity. The green synthesis of ZnONPs was optimized by evaluating the influence of ethanolic and aqueous plant extract and the zinc source on the morphological properties of the nanomaterial. Overall, ZnONPs exhibited hexagonal crystalline structure while the size and shape varied depending on the extract and zinc salt used. The most uniform and smallest ZnONPs were obtained using ethanolic extract and zinc nitrate, being spherical in shape and with a diameter of ~18nm. An investigation of the mechanism route for the green synthesis indicated that the formation of ZnONPs occurred due to the complexation of Zn(II) ions by antioxidants compounds present in the IP extract and further thermal degradation of the complexes. Cytotoxic analysis showed that L929 cell viability decreased in a dose-dependent manner for all ZnONPs samples. However, the nanomaterial with reduced size and uniform shape exhibited no cytotoxic effects up to a concentration of 10 µg mL^{-1} and was chosen to be incorporated in the polymeric biomaterials. Gram-positive bacteria were more vulnerable to the ZnONPs than Gram-negative, presenting a minimum inhibitory concentration of 45 µg mL^{-1}, while the Gram-negative bacteria showed only 10% inhibition at the same concentration. The thin films were characterized according to their morphology, ZnONPs content, and antimicrobial activity. The film composition was found to be dependent on the PAH pH and the IP concentration, where a more basic pH and lower IP extract concentration resulted in higher adsorption of ZnONPs, following a linear mathematical model. The thin films displayed no significant antimicrobial inhibition; however, many possibilities were addressed for this outcome. Conversely, the electrospun fibres containing ZnONPs presented a high antimicrobial activity against both *S. aureus* and *E. coli* bacteria strains, which is related to a higher content of ZnONPs. Also, morphological analysis of the fibre scaffold showed a three-dimensional structure formed by uniform fibres with a 230 nm diameter that mimics the extracellular matrix of natural tissue. Thus, ZnONPs were successfully synthesized using a green synthesis route and incorporated in two different biomaterials. While further studies need to be performed for the development of the thin film, the electrospun fibres showed promising properties for wound dressing applications.

Abbreviations

AA	Antioxidant activity
ANOVA	Analysis of variance
AuNPs	Gold nanoparticles
CFU	Colony-forming units
DLS	Dynamic light scattering
DMEM	Dulbecco's Modified Eagle Medium
DMSO	Dimethyl sulfoxide
DOE	Design of experiment
DRX	X Ray diffraction
EAG	Equivalent acid gallic
E. coli	*Escherichia coli*
EDS	Energy dispersive spectroscopy
FESEM	Field emission scanning electronic microscopy
IP	*Ilex paraguariensis*
LbL	Layer-by-layer
LC	Lethal concentration
MH	Muller Hinton
MI	Intensity mean
MIC	Minimum inhibitory concentration
MN	Number mean
MTT	Thiazolyl blue tetrazolium bromide

PAA	Polyacrylic acid
PAH	Polyallylamine hydrochloride
PBS	Phosphate buffer solution
PDDA	Polydiallydimethylammonium chloride
PEM	Polyelectrolyte multilayer
PLGA	Poly(lactic-co-glycolic acid)
PVA	Polyvinyl alcohol
ROS	Reactive oxygen species
S. aureus	*Staphylococcus aureus*
SDD	Silicon drift detector
SEM	Scanning electronic microscopy
TEM	Transmission electronic microscopy
UV-vis	Ultraviolet and visible
ZnO	Zinc oxide
ZnONPs	Zinc oxide nanoparticles

List of Figures

List of Tables

Introduction

CHAPTER 1: Introduction

1.1 Introduction

Nanotechnology has achieved great importance in scientific research and its applications are predicted to rise in the most varied fields of research and industries [1–4]. Zinc oxide nanoparticles (ZnONPs) are a type of ceramic nanomaterial with intrinsic properties with a wide range of applications, such as in photocatalysis, for semiconductor composites, and antimicrobial purposes [5–8]. This nanomaterial can be obtained through chemical, physical, or biological synthesis routes [9–10].

Nonetheless, the biological synthesis approach has come into focus as a solution to obtain a more sustainable product since it substitutes hazardous solvents with biological extracts from plants, bacteria, algae, and fungi. This process is called green synthesis as it agrees with green chemistry principles [11]. A variety of plant extracts have been used to synthesize metal and metal oxides nanoparticles with enhanced properties [12–20]. The mechanism of the formation of nanoparticles through green synthesis is yet to be understood. However, studies have concluded that antioxidant compounds present in the plant, such as flavonoids and polyphenols, reduce or form coordinated complexes with the targeted metal [21–23].

The green synthesis of ZnONPs has been reported using different biological extracts [16–22–24–27]. For example, Gunalan *et al.* [28] used *Aloe vera* extract and obtained ZnONPs with enhanced antibacterial effect in comparison to ZnONPs synthesized by chemical method, while Shahriyari Rad *et al.* [29] confirmed the antimicrobial activity of ZnONPs obtained using *Menta pulegium L.* leaves.

In this project, *Ilex paraguariensis* (IP) leaves, commonly found in the south of Brazil, Uruguay, and Argentina, was used in the green synthesis of the ZnONPs [30]. This plant has anxiolytic, antimicrobial, and anti-inflammatory properties, which have been associated with the presence of a high concentration of antioxidant compounds, which include chlorogenic acid, caffeic acid, and caffeine [31–33].

ZnONPs play an important role in the biomedical field, such as in the development of novel cancer therapies and wound healing and tissue regeneration scaffolds. For instance, this nanomaterial has been successfully employed in polymeric matrices aiming for bone regeneration and faster wound healing by inducing early mineralization and preventing infections [34–35].

Polymeric materials are widely used as biomaterials, as they have a variety of mechanical and chemical properties, enabling their application in the most diverse areas of medicine, such as tissue engineering, ophthalmology, dentistry, implants, among others [36]. The incorporation of nanoparticles in such materials has enhanced the performance of these biomaterials, like improving the antimicrobial activity, for example.

In this work, we are using polyelectrolyte complexes of polyallylamine hydrochloride (PAH) and polyacrylic acid (PAA) to produce thin films and electrospun fibres loaded with zinc oxide nanoparticles obtained by a green synthesis approach using plant extract to act as an antimicrobial biomaterial.

1.2 Research question

Considering the efforts towards a more sustainable world, this project was based on the possibility of obtaining zinc oxide nanoparticles *via* a green synthesis route by a

simple process with plant extract leaves, following the green chemistry principles. This approach was chosen not only aiming at an environmentally friendly process but also a product with lower cytotoxicity.

In addition, the ZnONPs are found to be important in the biomedical field, considering their low cytotoxicity and their antimicrobial activity, including against drug-resistant bacteria, showing promising properties for tissue regeneration and infection prevention. Nonetheless, such applications require this nanomaterial to be supported in a matrix as it is commonly employed in low concentrations, and also to achieve a material with greater mechanical properties. Therefore, considering the interesting characteristic of polymers, such as biocompatibility, flexibility, and mechanical properties, the ZnONPs were loaded in polymer thin films and electrospun fibers and evaluated in terms of their application as medical devices coating and tissue regeneration scaffolds. In this sense, the development of this research project was explored by addressing the following research questions:

I. Can zinc oxide nanoparticles be produced by green synthesis using plant extract leaves and be employed in polymeric matrices for the development of antimicrobial biomaterials?

> **(a)** Can ZnONPs be obtained by green synthesis using *Ilex paraguariensis* leaves extract?
>
> **(b)** How the mechanism route of the green synthesis occurs?
>
> **(c)** What are the cytotoxicity and antimicrobial activity of the green synthesised zinc oxide nanoparticles?
>
> **(d)** Is it possible to support the green synthesised ZnONPs in polyelectrolyte matrices?

(e) Can an antimicrobial thin film be obtained using a polyelectrolyte complex with incorporated ZnONPs and *Ilex paraguariensis* extract for medical devices coating?

(f) Can an antimicrobial polyelectrolyte electrospun fiber scaffold with incorporated green synthesised ZnONPs be obtained for wound healing purposes?

1.3   Proposed solution

The main objective of this project is to green synthesise and characterize zinc oxide nanoparticles from *Ilex paraguariensis* leaves extract for potential application as an antimicrobial biomaterial in polymeric matrices of polyallylamine hydrochloride and polyacrylic acid.

1.3.1   Project aims

- Synthesize zinc oxide nanoparticles *via* green route using *Ilex paraguariensis* extract.

- Characterize the zinc oxide nanoparticles obtained by the green synthesis according to its physical-chemical properties and biocompatibility.

- Evaluate and propose the reaction mechanism of the green synthesis.

- Develop and characterize PAH and PAA thin films with incorporated zinc oxide nanoparticles.

- Develop and characterize electrospun PAA and PAH fibres scaffold loaded with zinc oxide nanoparticles.

- Evaluate the antimicrobial activity and assess the application of the developed biomaterials.

1.4 Significance

Sustainability has become a critical topic among researchers from a necessity for environmental preservation and the production of less toxic materials. In this project, a sustainable approach to obtain ZnONPs was addressed in an attempt to obtain an important nanomaterial for different industries by a facile and greener synthesis, using a plant that is easily found in Brazil and already cultivated on a large scale. In addition, a careful analysis of the mechanism of formation of the nanoparticles by the green route was assessed, which is essential to guide the development of the production of such nanomaterials on an industrial scale.

Among different applications, ZnONPs have interesting properties as a biomaterial. Synthetic biomaterials have been vastly investigated for different biomedical applications such as wound healing adhesives, implant devices and drug delivery systems. The effort on this field of study promoted the development of novel medical treatments and therapies leading to a significantly enhancement on people's health and life expectancy.

Amid a variety of materials, nanoparticles play an important role on the development of biomaterials due to their unique properties and small size. However, they are usually supported by a polymeric structure to give stability and good mechanical properties for handling low amounts of material.

In this work, green synthesised ZnONPs were incorporated into polyelectrolyte thin films and electrospun fiber to obtain an antimicrobial biomaterial with structure

and mechanical properties for medical device coatings and tissue regeneration scaffolds. The ZnONPs polymeric composites developed in this project indicate promising characteristics that could enhance a variety of medical procedures while preventing infections and increasing cell proliferation, leading to an improvement in medical procedures and human health.

Literature review

CHAPTER 2:   Literature review

2.1   Nanotechnology

The development of nanomaterials is still of great interest in the scientific and technological area, given the possibility of manipulating its properties and the emergence of new applications [37]. In general, materials with particles that have at least one side between 1 and 100 nm are called nanomaterials [38]. Although interest and growth in the area of nanotechnology began only at the end of the 20th century, through the evolution of electronic microscopes, nanoparticles, both organic and inorganic, have been present in human life since ancient times [39]. For example, the Lycurgus Cup on display at the British Museum uses gold nanoparticles, providing a color change to the glass, depending on the light it receives [37].

The properties of nanoparticles depend, mainly, on their size and morphology, which are determined by the method used for their synthesis [10]. Researchers observed that changing the shape and size of colloidal gold nanoparticles resulted in different absorption bands in the visible spectrum, which can be observed with the naked eye, by changing the color of the solution [40]. Also, due to their high surface area and differentiated optical properties, resulting from the increase in free-electron energy in semiconductor nanomaterials and the higher absorption in the UV-vis region, nanoparticles have been showing greater efficiency in energy production in relation to larger particles [41–42]

Evidencing the advances of nanotechnology, currently studies on the development of nanomaterials approach a variety of areas. For example, nanoparticles

are used to treat effluents [43], drug-release [44], solar cells [45], bactericidal materials [64], among others.

2.2   Zinc oxide nanoparticles

Advances in the development of metal oxide nanoparticles have been the subject of studies in recent years due to the versatility of these nanomaterials and their interesting characteristics [46]. Among these oxides, zinc oxide nanoparticles (ZnONPs) have gained attention as they have diversified properties, which amplifies their field of applications in diverse areas of science [10]. Studies report that zinc oxide has semiconducting properties, high refractive index, thermal stability, low cytotoxicity, and bactericidal activity, among others. These properties can be manipulated and improved with the introduction of nanotechnology, increasing the surface area of the ZnO particles and modifying their morphology through the application of different synthesis methodologies [10–47].

The most commonly found and stable ZnO crystal at room temperature is formed by a hexagonal structure, called wurtzite (Figure 2.1), with three growth directions. This structure is formed through the tetrahedral coordination of O_2^- and Zn^{2+} ions [10–48–49]. Wang presents in his study that, by manipulating the combination of the surface polarity of ZnO with the growth direction, it is possible to obtain different morphologies, such as spirals, rings, and wires on a nanometre scale [49].
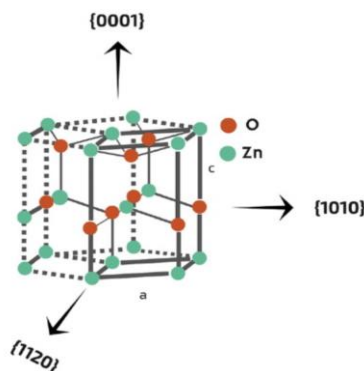
Figure 2.1: Wurtzite structure and its growth direction [10].

The synthesis of ZnO nanoparticles can be performed by chemical, physical or biological methods. Regarding the chemical method, techniques such as precipitation, microemulsion, chemical reduction, sol-gel, and hydrothermal synthesis are used, which may require high energy expenditure in some processes that operate at high pressures and/or temperatures [10–50]. However, one of the most common techniques for obtaining ZnONPs is the sol-gel synthesis, and was used primarily by Spanhel and Anderson [51].

The sol-gel synthesis uses a zinc precursor (sulfates, chlorides, nitrates, among others) and a chemical reagent to change the pH, precipitating the substance of interest, which will be subjected to a thermal treatment in temperatures that can reach up to 1000 °C [52–54]. Chemical stabilizers, such as citrates and polymers, can be added to the process to control the size of the nanoparticles avoiding their agglomeration [50–55]. In chemical synthesis, the concentration of each reagent can considerably influence the size and shape of the particles obtained, which can vary from just a few nanometers (5-10 nm) to particles of micrometric size [10–50].

Although less used than the chemical method, the synthesis of ZnONPs by physical method uses vapor deposition [56], plasma [57], and ultrasonic irradiation

[10] techniques and results in a high energy cost. Another methodology that has been widely investigated in recent years uses a biological approach. Commonly known as green synthesis, this method uses plants, fungi, bacteria, algae, among others, to obtain nanoparticles [13–58].

The main reason for the development of biological methods is the reduction of the environmental impact, since it does not use toxic chemical solvents. Also, this method has the potential to decrease the cost and complexity of the synthesis, increasing industrial interest [12]. The green synthesis is described in more detail in section 2.3.

With the evolution of scientific research, numerous applications have been developed for zinc oxide nanoparticles, in their pure form or composites. Due to their photocatalytic activity, ZnONPs have been widely applied for the degradation of dyes and drugs and has shown potential for clean energy produvcion through watter splitting [8–59–61]. Also, these nanoparticles can be used as dopants or in alloys for the development of sensors [62–63].

ZnO is also widely used in the rubber industry as a vulcanizing agent, a process that alters the mechanical properties of rubbers. With the introduction of ZnO nanoparticles, it is possible to increase the effectiveness of vulcanization and to reduce its consumption in elastomeric formulations [64]. Another segment that ZnO has a wide application is to produce sunscreens, due to its ability to absorb ultraviolet rays while presenting low cytotoxicity [7].

Another important feature is the antimicrobial activity of ZnONPs. Several studies report growth-inhibiting of bacteria, such as *Escherichia coli* and *Staphylococcus aureus*, and fungi, such as *Penicillium expansus* [65]. In general, the

mechanism of the bactericidal activity of ZnONPs can occur through the release of reactive oxygen species (ROS), the release of Zn^{2+} ions, or just by the contact of nanoparticles with the microorganism, altering bacterial metabolism, which can result in rupture of the cell membrane and damage to DNA and cellular proteins, for example [66]. Figure 2.2 presents an illustration of the possible mechanisms of antibacterial activity of ZnONPs.
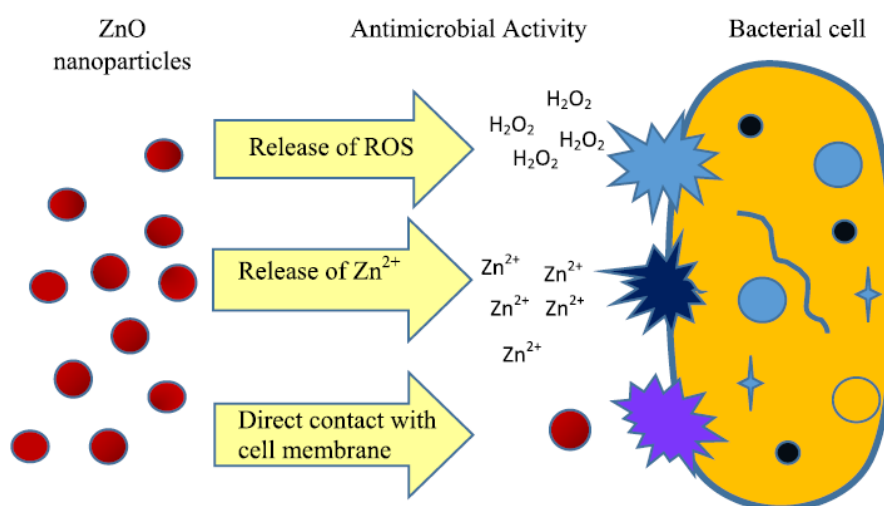
Figure 2.2: Antimicrobial mechanism of action of ZnONPs [66].

The formation of ROS from ZnONPs occurs due to their semiconduction property. When these nanoparticles are irradiated, the valence electrons go to the conduction band, creating a "hole" in the valence band (positive region) and presenting electrons in the conduction band (negative region). Thus, when in contact with water molecules, nanoparticles can separate the H_2O molecule, through the valence band, into H^+ ions and the free radical $\cdot OH^-$. On the other hand, when in contact with oxygen molecules, ZnONPs, with the presence of free electrons in the valence band, form the superoxide

radical ($\cdot O_2^-$). Species derived from these ions then form ROS, such as hydrogen peroxide (H_2O_2), which damages the cell membrane of microorganisms [10–66].

The toxicity of ZnONPs may also come from the release of Zn^{2+} ions into the growth medium of the bacteria, which are formed through the dissociation of the ZnO molecules. These metal ions directly affect the metabolism of the bacteria and the permeability of the cell wall, causing damage to the bacteria. Another mechanism of formation is the direct contact of the nanoparticles with the microorganism, which can penetrate the cell and/or break the cell membrane [10].

Due to their antimicrobial property, ZnONPs have been studied for application in water treatment [66], food packaging [67], and fabrics [68], for example. Another promising area for the application of ZnONPs is biomedicine, since these nanoparticles have low cytotoxicity and high bactericidal power, with great potential to become a lower cost option in some biomedical applications that use silver or gold nanoparticles as antimicrobial agents [69–70]. The high antimicrobial activity and low cytotoxicity of this nanomaterial can be explained due to the different structure and metabolism of bacteria and human cells. For instance, the mechanism of action of antimicrobial substances interferes directly in the bacteria cell membrane and affects their growth and absorption of nutrients. Both bacteria and human cells react differently to these substances as the cell membrane structure and composition and cell metabolism are not related [66–71].

The production of composite materials containing ZnONPs for biomedical application has also gained much attention. Studies report the production of biocompatible thin films containing ZnONPs to make these composites bactericidal. For example, Khalid *et al.* [72] produced cellulose films containing ZnONPs to treat

burn injuries, preventing them from becoming infected. Also, Bakhsheshi-Rad *et al.* [73] used ZnONPs to develop a film for coating orthopaedic implants, increasing resistance to corrosion and infections.

The role of ZnONPs in the development of wound healing materials has also been addressed. This fact is related not only to infection prevention due to their antimicrobial activity but also because it can improve the tissue regeneration process [74]. For example, several works report the improvement of angiogenesis and fibroblast migration after using composites doped with ZnONPs, which are intrinsic properties to enhance wound closure [74–77].

Studies also report the selective ability of ZnONPs to destroy cancer cells, while not damaging healthy cells [69]. Akhtar *et al.* [78] stated, through their experiments, that ZnONPs degraded three types of cancer cells while normal cells were not damaged. This selectivity was correlated to the action of ROS in the metabolism of cancer cells and to its high proliferation rate, which increases the production of ROS that causes oxidative stress in high concentrations. Also, preliminary studies developed in our research group have shown the cytotoxicity of ZnONPs in a colorectal cancer cell line, indicating induced autophagy as a contributing mechanism to cytotoxic activity [79]. Thus, it is evident that ZnONPs have the potential to treat cancers and tumors, but further studies are needed to understand the mechanism of action of this nanomaterial [80].

Therefore, the potential of using ZnO nanoparticles for the development of novel composites in the biomedical area has been addressed, aiming to benefit a range of medical treatments.

2.2.1   Cytotoxicity mechanism of ZnONPs

Even though ZnONPs are considered to present low cytotoxicity, their effect on human beings needs to be addressed when considering biomedical applications. According to Taccola *et al.* [93], the mechanism of cytotoxicity of zinc nanoparticles occurs through the release of reactive oxygen species (ROS), dissociation of these nanoparticles forming Zn^{2+} ions, or by internalization through endocytosis.

The endocytosis of nanoparticles is the main mechanism of entry of these substances in cells and has been studied both for the prevention of diseases and cellular dysfunctions and for the development of new therapies. Nanoparticles in general can penetrate cells through different mechanisms of endocytosis (Figure 2.3), depending on their physical-chemical properties such as size, shape, and chemical composition [81–83].

Endocytosis is a natural and vital process by which cells internalize substances or particles, providing and regulating the entry of nutrients, the transduction of signals, the composition of the plasma membrane, cell defence, among others [84]. This process can occur through pinocytosis or phagocytosis. In general, pinocytosis is the main route for entry of molecules suspended or dissolved in a fluid, creating an endosome inside the cell. Phagocytosis, on the other hand, involves the cell's immune system (macrophages, neutrophils, monocytes, among others), internalizing solid particles and creating a phagosome [85].
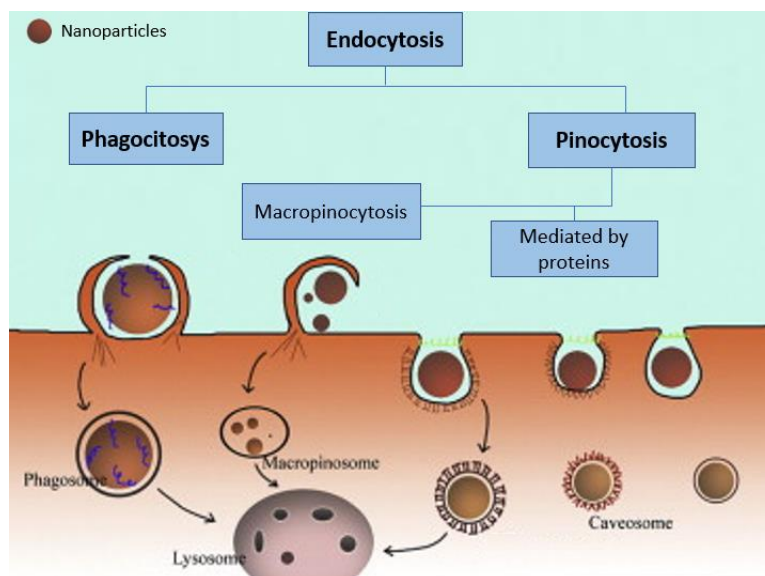
Figure 2.3: Nanoparticle internalization mechanism through endocytosis mechanism (adapted from [81])

For the nanoparticles to be internalized in the cell through phagocytosis they need to be recognized by opsonin - molecules that facilitate the phagocytosis process, such as antibodies and proteins - and then activate the cell surface and internal substances using a part of the plasma membrane, forming a phagosome with size between 0.5-10 µm that will be absorbed by the lysosome. On the other hand, the process of endocytosis of nanoparticles from micropinocytosis occurs through the internalization of extracellular fluid in large vacuoles, through undulations of the plasma membrane and without associated receptors, forming a macropinosome that is absorbed by the lysosome [81–82–85].

Regarding the mechanism of endocytosis of ZnONPs, proteins present in the cellular environment are adsorbed on the surface of the nanomaterial and bind to the cell membrane receptor proteins, triggering the receptor-mediated phagocytosis or pinocytosis process. Within the endosome or phagosome (pH~5.0), ZnONPs dissociate

to form Zn^{2+} ions that end up being released and accumulated inside the cell, which can trigger processes that lead to cell death [93,101].

The cytotoxicity of nanoparticles may also be related to the process of induced cell autophagy. Autophagy is a process in which the cell degrades damaged or aged cytoplasmic components, being essential for cell functioning and survival. Basically, this process is performed by the autophagosome, which absorbs a portion of the cytoplasm and merges with the lysosome, forming the autophagosome, responsible for the degradation and recycling of the absorbed components [86]. However, induced autophagy can cause cell death, due to the accumulation of autophagolysosomes inside the cell and the accelerated degradation of proteins and cytoplasmic organelles [87]. Studies report an increase in the autophagic process when cells are exposed to ZnONPs in concentrations greater than around 10 µg mL^{-1}, with this increase being directly dependent on the concentration of nanoparticles in the cellular medium [79–88].

The process of autophagy induced by nanoparticles begins with the internalization of these nanomaterials, subsequently forming an autophagosome [89]. This internalization depends directly on the physicochemical properties of the nanoparticles. Size is one of the most important factors, and the smaller the particle, the more easily it will be absorbed by the cell since there is a greater area of contact with the cell membrane due to the increase of surface area [82–90].

The morphology of nanoparticles can also affect cell internalization and, according to Salatin *et al.*, elongated particles are more likely to interact with the cell membrane [82]. However, the mechanism of internalization of nanoparticles depends on a set of factors and cannot be elucidated through physical-chemical properties only.

2.3   Green synthesis of nanoparticles

The interest in synthesizing ZnONPs *via* biological methods has increased considerably in the last decade. The development of this new approach and the significant interest in it is mainly related to the absence of toxic chemicals or a high amount of energy applied to the biological synthesis, which makes the process more cost-effective and eco-friendly [10–12–50–72–91].

Many reports in the literature indicate that the biological synthesis of metallic and metal oxides nanoparticles is more environmentally friendly than the conventional chemical or physical methods used nowadays [12–91]. Therefore, these biological methods have become more known as green synthesis. It was also given this term because it goes in agreement with the twelve principles of the green chemistry, which are shown in Figure 2.4 [11]. Nowadays, these principles are considered the fundaments to guide the   sustainable development and comprise instructions to implement new chemical products, new synthesis, and new processes.
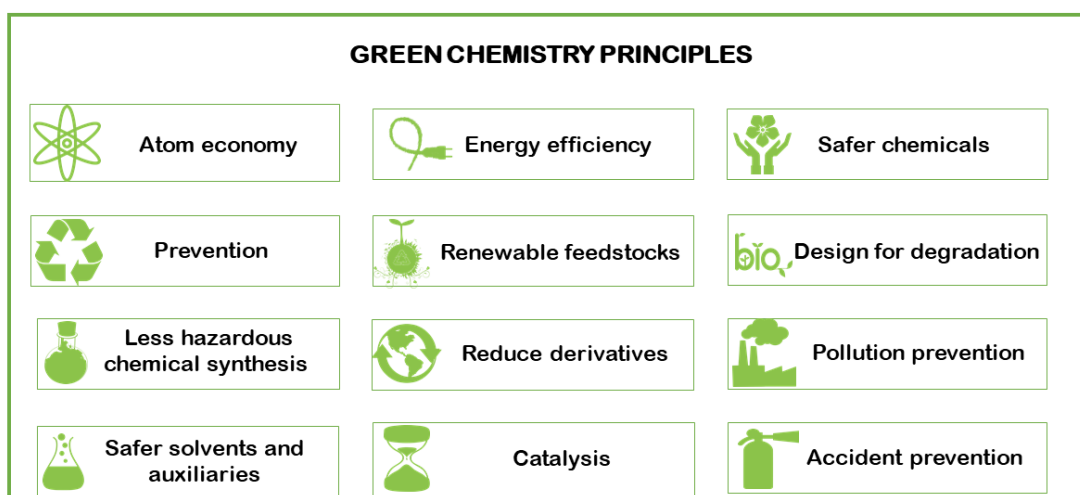
Figure 2.4: Green chemistry principles

Briefly, the green chemistry principles are based on 1) atom economy, to improve reaction efficiency, 2) energy efficiency, avoiding high energy consumption process, 3) safer chemicals, to minimize the toxicity of processes and products, 4) prevention, to minimize waste in every stage of the process, 5) renewable feedstocks, using chemicals made of renewable sources, 6) design for degradation, design biodegradable and non-toxic products, 7) less hazardous chemical synthesis, to design safer synthesis routes, 8) reduce derivatives, avoid the use of derivatives such as protectors or stabilizers, 9) pollution prevention, prevent the release of hazardous substances, 10) safer solvents and auxiliaries, to use the least possible solvent or chemical, 11) catalysis, use catalysis to improve processes like energy consumption or efficiency and 12) accident prevention, to minimize the risks of accident. For instance, the main advantages of biological synthesis are the employment of renewable sources, safer solvents, and auxiliaries while producing safer chemicals.

The large-scale production of nanoparticles by green synthesis remains a challenge, and these syntheses have been performed only at a laboratory scale. However, it is likely that its industrial application will take place in the near future as no robust equipment is necessary and significant advancements have been achieved on understanding the biological extracts composition and their interaction with the metal ions [12–69–91].

Essentially, green synthesis uses biological substrates such as plants, bacteria, fungi, and algae to replace chemical solvents and stabilizers to decrease the toxicity of both product and process [10–12]. In the case of ZnONPs synthesis, many different biological substrates have been successfully applied to obtain this metal oxide. In general, the biosynthesis of ZnONPs is a very straightforward process in which a zinc

salt, such as zinc nitrate or zinc acetate, is added to a biological extract previously prepared. After the reaction, this solution is submitted to a thermal treatment, and the ZnO powder is obtained [10–69–92]. The mentioned process is illustrated in Figure 2.5.
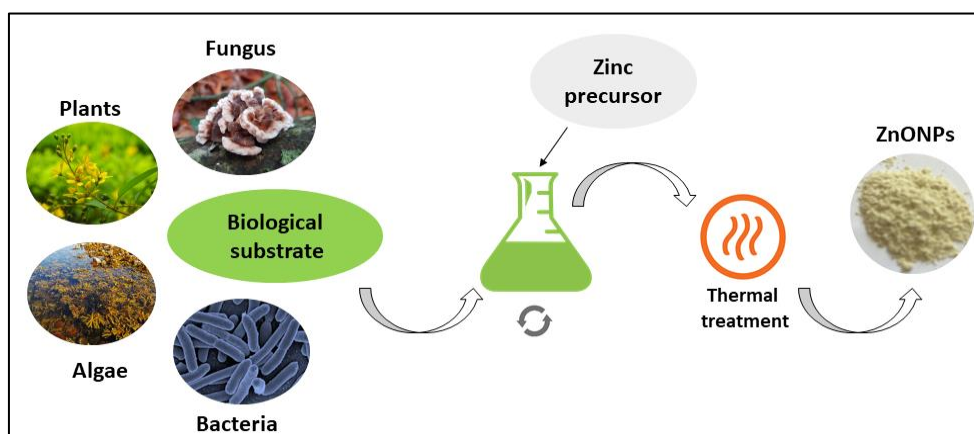
Figure 2.5: Green synthesis of ZnONPs

Nonetheless, published works indicate different methodologies for the green synthesis of ZnONPs. Table 2.1 summarizes several of the synthesis methods reported in the literature to date. Despite the fact that a wide variety of biological substrates with distinct composition have been applied for this purpose, the concentration of zinc salts, pH variations, reaction time and temperature vary considerably, resulting in particles with different sizes and morphologies.

Table 2.1: Reported methodologies of the green synthesis of ZnONPs

	Biological substrate	Zinc source[a]	pH	Reaction time and temperature	Thermal treatment	Average size (nm)	Shape	Reference
Algae	*Sargassum murticum (20 g L^{-1})*	Acetate (0.4 g L^{-1})	NS	3-4 h, 70 °C	4 h, 450 °C	30-57	Spheres	[97]
	C. peltata, H. Valencia and S. myriocystum (5 g L^{-1})	Nitrate (0.07-0.7 g L^{-1})	5-10	5-10 min, 50-100 °C	Not applied	Varied	Varied	[98]
Bacteria	*Acinetobacter schindleri* culture (NS)	Nitrate (0.9 g L^{-1})	NS	48 h, 37 °C	6 h, 60 °C	20-100	Spheres	[99]
	Bacillus licheniformis biomass (50 g L^{-1})	Acetate (43.9 g L^{-1})	NS	48 h, 37 °C	Not applied	620	Nanoflowers	[100]
	Lactobacillus plantarum culture (NS)	Sulphate (17.9 g L^{-1})	6	10 min, 80 °C – 12h, 37 °C	4 h, 40 °C	13	Spheres	[101]
	Pseudomonas aureginosa (0.05 g L^{-1})	Nitrate (0.19 g L^{-1})	NS	30 min, 80 °C	NS, 70 °C	35-80	Spheres	[102]
	Serratia ureilytica culture (NS)	Acetate (3.7 g L^{-1})	NS	30-90 min, 50 °C	Not applied	170-600	Varied	[94]
	Staphylococcus aureus culture (NS)	Acetate (0.18 g L^{-1})	NS	NS, 37 °C	Not applied	10-50	Acicular	[103]
Fungi	*Aspergillus fumigatus* biomass (NS)	Nitrate (0.02 g L^{-1})	NS	72 h, 28 °C	Not applied	3.8	Spheres	[104]
	Aspergillus niger biomass (NS)	Nitrate (0.02 g L^{-1})	6.2	48 h, 32 °C	Not applied	61	Spheres	[105]
Plants	*Aloe vera* leaves (NS)	Nitrate (NS)	NS	4-5 h, 150 °C	7-8 h, 80 °C	25	NS	[106]
	Aloe barbadensis miller leaves (50-500 g L^{-1})	Nitrate (NS)	NS	5 h, 150 °C	7-8 h, 80 °C	25-55	Spheres	[28]
	Camelia sinensis leaves (NS)	Nitrate (50 g L^{-1})	NS	NS, 60 °C	2 h, 400 °C	8	Spheres	[24]
	Citrus aurantifolia peel (20 g L^{-1})	Nitrate (20 g L^{-1})	NS	3 h, T$_a$	1 h, 60 °C	11	Polyhedron	[21]
	Citrus paradise peel (20 g L^{-1})	Nitrate (20 g L^{-1})	NS	3 h, T$_a$	1 h, 60 °C	19	Polyhedron	[21]
	Citrus sinensis peel (20 g L^{-1})	Nitrate (20 g L^{-1})	NS	3 h, T$_a$	1 h, 60 °C	12	Polyhedron	[21]
	Couroupita guianensis leaves (50 g L^{-1})	Acetate (5 g L^{-1})	NS	10 min, NS	Overnight, 60 °C	NS	Nanoflakes	[107]
	Costus woodsonii leaves (30-60 g L^{-1})	Nitrate (100 g L^{-1})	NS	60 °C, NS	2 h, 400 °C	20-25	Varied	[26]
	Eclipta alba leaves (100 g L^{-1})	Acetate (0.2-1.1 g L^{-1})	4-8	5-75 min, 20-100 °C	Not applied	3-9	Spheres	[108]
	Hibiscus subdariffa leaves (20 g L^{-1})	Acetate (14.3 g L^{-1})	NS	30 min, T$_a$	4 h, 30 -100 °C	190-400	Dumbbell	[25]
	Lycopersicon sculentus peel (20 g L^{-1})	Nitrate (20 g L^{-1})	NS	3 h, T$_a$	1 h, 60 °C	9	Polyhedron	[21]
	Lycopersicon esculentum fruit (NS)	Nitrate (NS)	NS	5 min, 80 °C or microwave	4-5 h, NS	40-100	Spheres	[109]
	Menta pulegium L. leaves (50 g L^{-1})	Nitrate (100 g L^{-1})	NS	NS	2 h, 400 °C	38-49	Spheres	[29]
	Moringa oleifera leaves (100 g L^{-1})	Nitrate (6 -206 g L^{-1})	5	18 h, T$_a$	1 h, 500 °C	12-30	Spheres and rods	[22]
	Oak fruit hull (jaft) (200 g L^{-1})	Acetate (33.4 g L^{-1})	NS	4 h, 60-80 °C	6 h, 80 °C; 4 h, 500 °C	34 nm	Spheres	[110]
	Stevia leaves (72.4 g L^{-1})	Acetate (18.3 g L^{-1})	NS	NS, 80 °C	2 h, 600 °C	50	Rectangular	[111]
	Peganum harmala seed (60 g L^{-1})	Nitrate (NS)	NS	1 h, NS	NS, 50 °C	40	Irregular	[112]
	Punica granatum leaves (NS)	Nitrate (18.9 g L^{-1})	NS	3-4 h, 60 °C	3-4 h 400 °C	10-30	Spheres	[27]

[a] Concentrations were approximated to be reported with the same unit; NS: Not specified; T$_a$: Ambient temperature

For instance, Bala *et al.* [25] observed that changing the temperature of the thermal treatment resulted in different morphologies and size of the ZnONPs. The thermal treatment at 30 °C showed irregular morphology and low crystallinity of the particles. In contrast, the nanoparticles obtained with thermal treatment at 60 °C and 100 °C presented high crystallinity and agglomerates of nanoparticles in morphologies such as cauliflower and dumbbell shape, respectively. These variations are probably related to the fact that higher temperatures increase the nucleation rate of crystal formation. In agreement, Parra and Haque [93] chemically synthesized ZnONPs. They observed that the higher the temperature, the faster will be the crystal growth and nucleation rate, which results in the agglomeration of nanoparticles and larger particle sizes.

Another feature related to the agglomeration is that the interval of time of the heat treatment may affect the formation of clusters. Dhadapani *et al.*[94] observed that increasing the time of the thermal treatment conducted at 50 °C from 30 to 90 min, increased agglomerates and particle growth. These findings corroborate with the results observed in different chemical synthesis process, where the increase of the time of nucleation led to the formation of larger particles of ZnONPs [95–96].

Although the pH condition poses a notable influence on the synthesis of inorganic nanoparticles, much of the available literature on the green synthesis of ZnONPs does not consider or report the pH of the solutions of the biological extracts used for obtaining this nanomaterial, as reported in Table 2.1 [21–24–25–28–100–104–106–107]. Thus, considering that each biological substrate has different compositions and pH values, the evaluation of the pH solutions would be of great

interest to better understand the differences in physical-chemical properties of the nanoparticles obtained through green synthesis.

Chinassamy *et al.* (2018) reported a further study on the green synthesis of ZnONPs by evaluating the effect of biological extract and zinc salt concentration, operating time and temperature, on the particle size and yield of the produced nanoparticles. From this work, the authors stated that using the minimum concentration of zinc precursor (~65 g L^{-1}) and maximum temperature (200 °C) and time (2 h) of reaction resulted in the highest yield. Furthermore, they concluded that the concentration of zinc nitrate is the factor that influences mostly the particle size among all the evaluated parameters.

Singh *et al.* [108] also reported the variation of the concentration of both plant extract and zinc precursor, incubation time and temperature of reaction in a study of the biosynthesis of ZnONPs using *Eclipta alba* leaves extract. The authors observed that increasing zinc acetate concentration (1.0 to 5.0 mM), particle formation became more uniform and smaller. Moreover, Singh *et al.* [108] state that these findings are in agreement with the ZnO synthesis performed using *Citrus aurantifolia* in which the increase of zinc acetate concentration enhanced the homogeneity of the particles and reduced their size [119].

Furthermore, it was observed that there was a direct correlation between the concentration of *Eclipta alba* extract and the intensity of the UV absorbance peaks observed, indicating a superior formation of ZnONPs [108]. These features may be related to a higher concentration of antioxidants, which are available during the synthesis when the plant extract concentration is increased. These compounds most

likely play an important role on the mechanism of formation of metal and metal oxides nanoparticles obtained by green synthesis [10–22–108–120].

Moreover, Singh *et al.* [108] investigated the influence of the variation of the temperature from 20 to 100 °C on the yield and size of ZnONPs. In their study, it was concluded that the higher the temperature, the greater the yield of ZnONPs. However, the increase of the temperature of reaction resulted in particles with a larger size, which corroborates with a similar study of the properties of ZnO synthesized *via* sol-gel synthesis [121]. Related to the time of reaction, it seems that rapid synthesis results in smaller particles, as the short reaction time will reduce the grain growth [108].

Although it is well understood that changing the parameters of the green synthesis will affect the physical-chemical properties of the ZnONPs, the mechanism route of the formation of these nanoparticles remains unclear. Several studies propose theoretical mechanistic routes for this biosynthesis [22–100–101–104]. Nonetheless, the composition complexity of the biological substrates poses a challenge for analytical evaluation and definition of the chemical reactions that take place during the green synthesis.

2.3.1 Mechanism of formation of zinc oxide nanoparticles via green synthesis

Although many studies indicate the effectiveness of the green synthesis for the production of metal and metal oxides nanoparticles, this process has only been demonstrated at a laboratory scale [12–58–69]. Hence, the determination of the mechanism route of the formation of green synthesis is of great interest for

establishing large-scale process. Thus, the recent advances found in the literature related to the mechanism of formation of ZnONPs using different types of biological substrates were summarized in this review.

2.3.1.1 Green synthesis using bacteria

The biosynthesis of metal and metal oxides nanoparticles using microbial culture or biomass may occur in an extra or intracellular environment [100–103–122–124]. In the case of the extracellular synthesis, studies suggest that the enzymes and proteins produced and released by the microorganisms can reduce the metal ions and stabilize the particles. Tripathi *et al.* [100] reported that ZnONPs can be stabilized by enzymes secreted by bacteria cells (*Bacillus licheniformis*). In their study, zinc acetate and sodium bicarbonate react to form $Zn(OH)_2$, which is thermally degraded to form the ZnO nuclei. The enzymes presented in the bacteria will then stabilize the ZnONPs to avoid agglomeration and particle growth guaranteeing the nanoscale size of the metal oxide.

In addition, the work developed by Selvajaran *et al.* [101] identifies that the enzymes produced by the microorganisms are responsible for the ZnONPs formation. However, authors state that the solution pH and the electrokinetic potential of the bacteria may play a role in the synthesis route by reducing the metal ions and, consequently, triggering the biosynthesis of the nanoparticles rather than forming $Zn(OH)_2$. The same concept was stated in a similar study using *Staphylococcus aureus* to obtain ZnONPs via extracellular biosynthesis [103].

Further work reports the successful utilization of activated ammonia from ureolytic bacteria (*Serratia ureilytica*) for ZnONPs production. The synthesis route

proposed in this study for the formation of nanoparticles is based on the reaction of zinc ions with the microorganism culture media, rich in ammonia producing $Zn(OH)_2$ and $[Zn(NH_3)_4]^{2+}$. These substances are then submitted to thermal decomposition at 50 °C to obtain the crystalline ZnONPs powder [94].

Regarding the intracellular synthesis, the mechanism of formation definition can be more challenging due to the complexity of the cell compositions and processes. However, various studies believe that the cells internalize the metallic ions, which will be reduced by the proteins and enzymes within the cell to form the nanoparticles [125–127]. Klaus *et al.* [127], for example, used *Pseudomonas stutzeri* to obtain silver nanoparticles with different shapes and identified their formation within the cell using transmission electronic microscopy (TEM). A recent study observed the formation of gold nanoparticles with sizes varying from 5-30 nm inside *Lactobacillus kimchicus* using the same analysis [128]. Rajeshkumar *et al.* [129], on the other hand, compared both intra and extracellular synthesis of silver nanoparticles and observed that it is more difficult to regulate particle morphology, dispersion and size when synthesizing the nanoparticles within the cells.

Similarly, it is also well known that microorganisms can internalize zinc (II) ions [65–129–131]. Therefore, the intracellular biosynthesis of ZnONPs could be a plausible mechanism route to obtain this nanomaterial. However, the literature indicates that the extracellular formation is the most common route to produce ZnONPs using bacteria cultures [94–99–101]. Figure 2.6 summarizes both extracellular and intracellular mechanism of the biosynthesis of nanoparticles using bacteria, based on the current literature. In contrast with the extracellular biosynthesis, the intracellular route requires an additional process of cell lysis to release the nanoparticles from

inside the microorganism [132]. Hence, this process becomes more time consuming and expensive than the extracellular synthesis in which the metal ions are directly reduced or chelated by the proteins and enzymes outside the cells.
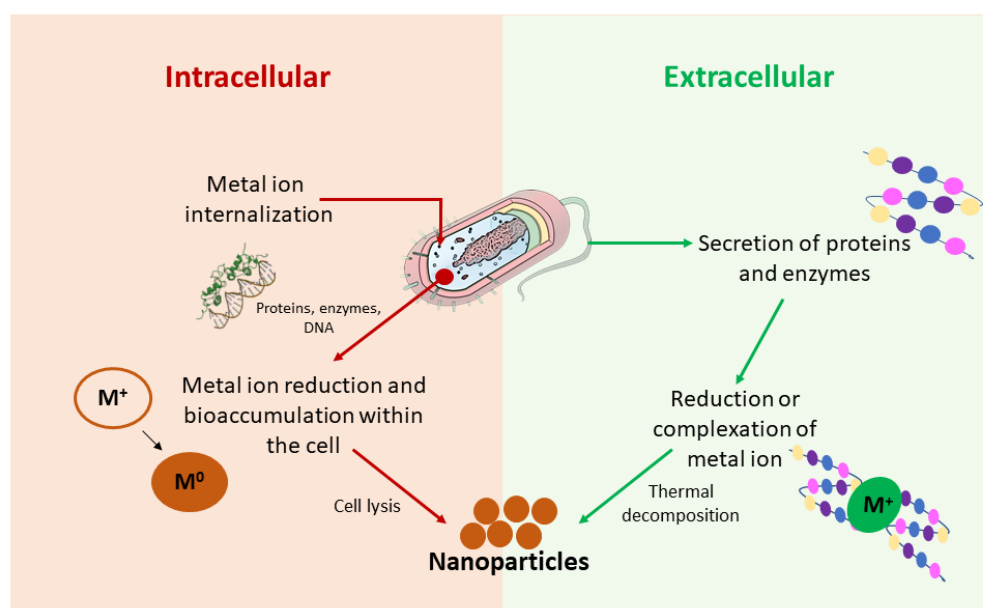
Figure 2.6: Green synthesis of nanoparticles using bacteria cultures

2.3.1.2   Green synthesis using fungi

The production of metal and metal oxides nanoparticles using fungal biomass or culture has a similar mechanistic route as the one described for the green synthesis using bacteria in Figure 2.6. Raliya *et al.* [104] successfully synthesized ZnONPs using *Aspergillus fumigatus* cell culture. They suggested that the proteins and enzymes secreted by this microorganism are responsible for the formation and encapsulation of the nanomaterial. In addition, Kalpana *et al.* [105] also reported the extracellular biosynthesis of ZnONPs using *Aspergillus niger* cell-free filtrate.

In comparison to the bacteria synthesis, it is believed that the fungus may have superior potential for the green synthesis of nanoparticles since it can release higher

concentrations of metabolites to the culture media than bacteria cells. Furthermore, fungus cells seem to be more resistant to process conditions and variations such as pressure, flow rate and stirring which enhance their potential use for large scale synthesis [133–135].

2.3.1.3 Green synthesis using plants

Plants are the most common biological substrate used for the green synthesis of nanoparticles with metallic ions [12–14]. This might be related to the fact that vegetal substrates are believed to be more cost-effective, easy to process and less toxic than microorganisms. Also, there is no exposure to health risks or concerns about safety issues related to hazardous microorganisms during the process when using plant-based substrates. In addition, plant extracts can be obtained in a straight forward manner by exposing the plant to a solvent, which is usually distilled water or ethanol [136]. Different parts of the plant have been applied to this purpose such as leaves, roots, seeds and fruits [22–24–28–112].

It is known that the plants have high concentrations of active compounds like methylxanthines, phenolic acids, flavonoids and saponins [137–140]. These compounds are more known as antioxidants as they can neutralize reactive oxygen species (ROS) and free radicals and chelate metals [141]. Hence, it is concluded that the antioxidants present in the plants are responsible for the green synthesis of metal or metal oxides nanoparticles due to their capability to bioreduce or chelate metal ions and to act as stabilizers of the produced nanoparticles [142–143].

Despite the knowledge of the phytochemical properties of the antioxidants, plant extracts are constituted of an enormous variety of these active compounds in

different concentrations [138–144–146]. This feature poses a problem to analytically determine the exact amount of all molecules that are extracted from the plant. Consequently, the definition of a precise mechanism route of the biosynthesis of metal and metal oxide nanoparticles using vegetal substrates is still a challenge to be surpassed.

Regarding the green synthesis of ZnONPs, published research suggest in theory that the compounds present in the plant extract react with a zinc salt to reduce or to form complexes with the metal [21–22–28–108–112]. Nava *et al.* [21] proposed a mechanism route based on the chemical characteristics of the flavonoids, limonoids and carotenoids that constitute the fruit peels used for obtaining the ZnONPs. In this work, these antioxidants are believed to chelate the zinc ions and form metal coordinated complexes that are further thermally treated to degrade the complex and form zinc oxide with an average size of 9.7 nm.

Matinise *et al.* [22] established a similar mechanism where the antioxidants of *Moringa oleiferea* leaves also chelate the zinc (II) ions which formed zinc oxide after a calcination process. In this work, the plant extract and ZnONPs obtained with different temperatures treatment (100 °C and 500 °C) were analyzed using Fourier transform infrared spectroscopy (FTIR). The vegetal extract exhibited absorption bands typical of bioactive compounds and the ZnO synthesized at 100 °C showed hydroxyl (–OH) stretching bands that might be an indication of the formation of zinc complexes with antioxidants during the synthesis. This result correlates with the findings of other research groups, where FTIR absorption bands characteristic of bioactive compounds were identified in the green synthesized ZnONPs [24–25–28–97–112].

Conversely, when *Eclipta alba* leaves are utilized to produce ZnONPs, studies have implied that zinc (II) ions are reduced by the plant active compounds to metallic zinc rather than forming coordinated complex with them. After the bioreduction of zinc, the metallic zinc reacts with dissolved oxygen present in the solution to form the ZnO nuclei. It is also proposed that the plant compounds act as stabilizers preventing agglomeration of particles and crystal growth [108]. Likewise, Sutradhar and Saha (2017b) proposed the bioreduction of zinc (II) ions by ascorbic acid when using *Lycopersicon esculentum* extract to obtain ZnONPs. Gupta *et al.* [147] biosynthesized ZnONPs using plant extract and suggested that the metabolites that compose the substrate are responsible for both the reduction of the metallic ions and particle stabilization.

Figure 2.7 illustrates the possible mechanism routes described in the literature for the green synthesis of ZnONPs using plant extracts, and some active compounds are cited as examples of the substances frequently found in plants. Also, two different mechanisms of ZnONPs formation are shown considering the ability of the active compounds in chelating and reducing the zinc (II) ions, as previously discussed. In addition, it is interesting to observe that, for metal oxide nanoparticles, the mechanism route of metal complexation requires a thermal treatment to obtain the nanoparticles. In contrast, the metal bioreduction produces the colloidal nanoparticle with the plant extract without further treatment.
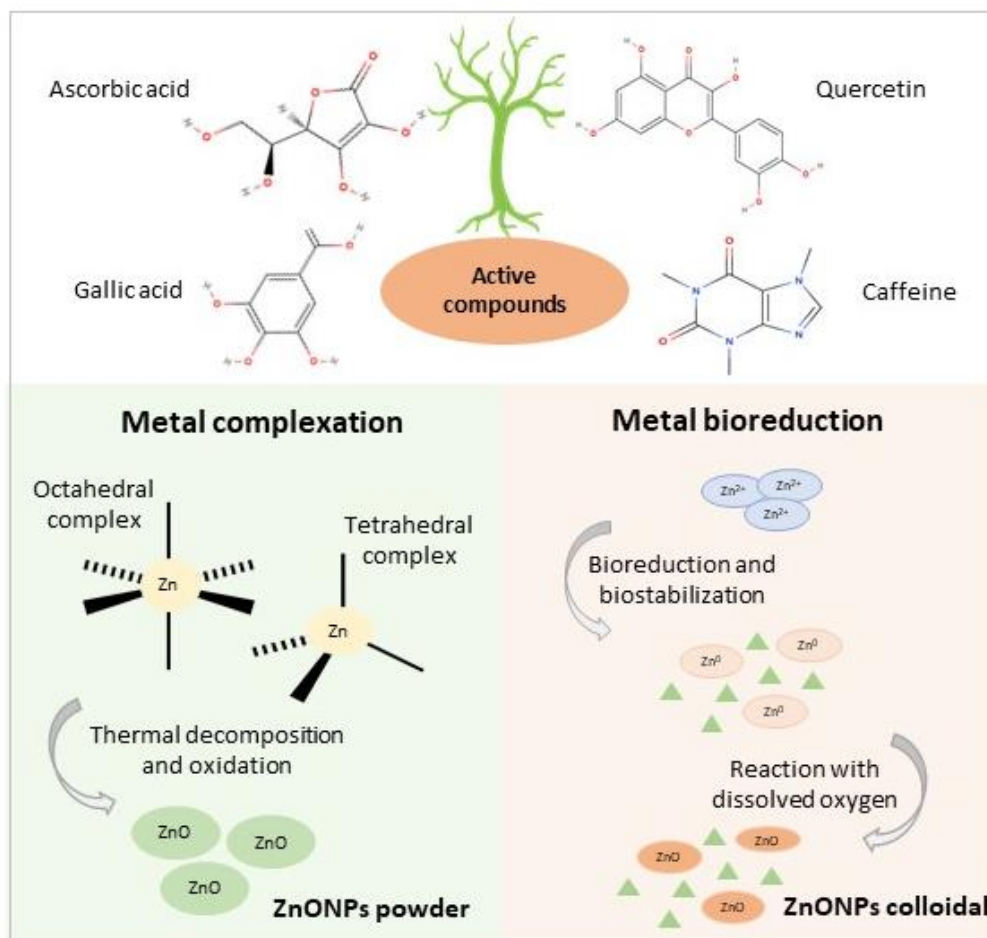
Figure 2.7: Green synthesis of ZnONPS using plants extracts

2.3.1.4 Green synthesis using algae

Although algae are simple organisms, the phytochemical composition of algae can be related to the composition of plant extracts. Active compounds containing functional groups such as hydroxyl and carboxyl groups can be found in different species of algae and their antioxidant activity has been reported [97–148–150]. In addition, different studies identified the presence of such active compounds by FTIR analysis in algae extracts when using them as substrates to green synthesize ZnONPs [97–98–151].

Therefore, the mechanism of formation of ZnONPs when using algae substrates for the biological synthesis can be related to the mechanism of plants already described and summarized in Figure 2.7, where active compounds such as polyphenols and flavonoids act as reducing and stabilizer agents and/or chelating substances.

2.3.2   Properties of ZnONPs green synthesized

The main advantages of using a green route to obtain nanoparticles are the environmentally friendly question, associated with the low cost and simple technique. Nonetheless, the green synthesis of nanoparticles can also enhance the properties of these nanomaterials due to the small size and shape obtained, and the specific properties of the biological substrates used [12–15–152].

In the case of ZnONPs, the green synthesis route has been shown to improve properties like antimicrobial activity [28], photocatalytic efficacy [153] and biocompatibility [69]. Therefore, the green synthesized ZnONPs have great potential to substitute conventional ZnONPs and to be applied on the development of nanocomposites. For example, biosynthesized ZnONPs can be utilized in the production of nanocomposites for anticancer and antimicrobial coatings in the biomedical field and to improve the degradation of dyes, to name but two applications [70–152–154–155].

Nanoparticles of similar metal oxides to ZnO were also obtained *via* biosynthesis. For instance, SnO_2 and CdO_2 nanoparticles were successful obtained using plant extract showing interesting properties, such as antimicrobial effect and potential to be applied in solar cells [156–157]. Moreover, recent studies observed the potential of producing binary composites based on ZnONPs using biological substrates. Rahmayeni *et al.*

(2019) synthesized ZnO-CoFe$_2$O$_4$ using *Nephelium lappaceum L.* peel extract to enhance the photocatalytic performance of ZnONPs. Honeycomb-like Ag-ZnO nanocomposite was also obtained for photocatalytic purposes with *Azadirachta indica* gum [159]. Likewise, Fuku *et al.* (2016) obtained ternary nanocomposites of CuO, Cu and ZnO, using pomegranate peels to produce a nanoplatelet structured electrode. Thus, the green synthesis has shown to be a promising alternative to easily obtain more complexes nanostructures.

Numerous studies report the possibility of obtaining ZnONPs through a green synthesis process using a variety of plants, fungus, bacteria and algae. Moreover, the studies cited here indicate that these substrates act as reducing and stabilising agents or as chelating substances despite its source. It is interesting to notice that besides the difference between the compositions found in biological extracts, parameters such as conditions of temperature, time of reaction, pH and concentrations, significantly alter the final properties of the synthesized nanoparticles. Among these parameters and according to the literature cited, the concentrations of both biological extract and zinc source and the pH of the solution play a major role on the final properties of ZnONPs obtained using green route.

Although the complexity of biological substrates still poses a challenge to evaluate the green synthesis of nanoparticles, further investigations on the mechanism of formation of the biological synthesis of ZnONPs are necessary to achieve a better understanding of the chemical processes and reactions that occur during the synthesis. It seems that with the designation of the mentioned mechanism, it will be possible to control and optimize the green synthesis process, which is essential for the large-scale production of ZnONPs. Hence, the rapidly advancing understanding of green synthesis

described herein, indicate the enormous potential of ZnONPs for industrial production using biological extracts in the near future.

2.4   Ilex paraguariensis

Yerba mate was firstly discovered by the indigenous in South America and was scientifically identified in 1820 by the botanist August Saint-Hilaire as *Ilex paraguariensis*, belonging to the *Aquifolaceae* family. This plant is widely used in the southern region of South America to prepare a tea called "chimarrão" or "mate", depending on the region, which is done by the infusion of the leaves in hot or cold water [161].

The habit of ingesting mate tea or "sacred leaf", as the indigenous people called it due to its stimulating activity, was cultivated by the Indians, who passed it on from generation to generation and which ended up attracting the attention of the first Spanish colonists who arrived in the region, and continued the tradition [162]. Figure 2.8 illustrates the *Ilex paraguariensis* tree.

Figure 2.8: a) *Ilex paraguariensis* tree b) Image magnified for visualization of the leaves [161]

With the increase in the consumption of *chimarrão*, *yerba mate* began to have economic value. Today, *Ilex paraguariensis* plantations are important in the agricultural sector in regions such as southern Brazil and part of Argentina, Uruguay and Paraguay [163]. According to IBGE data, approximately 350 000 t of the herb were produced only in Brazil in 2016 [164].

Yerba mate has been known since its discovery for its stimulating and invigorating action [162]. With the advancement of science, researchers identified that this resource was caused by the presence of methylxanthines, such as caffeine, one of the main constituents of this plant [165]. Also, several studies on the chemical composition of yerba mate and its benefits to human health have been performed in recent decades [30].
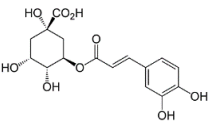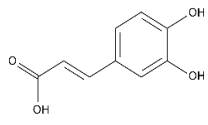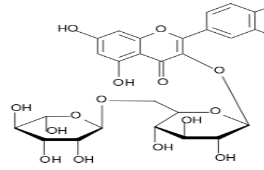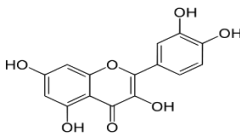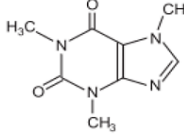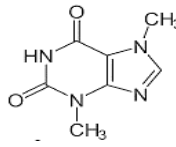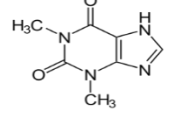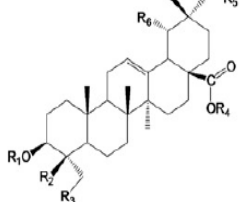
Literature proposes that *Ilex paraguariensis* has neuroprotective and anxiolytic properties [31], anti-inflammatory [32], antioxidants [30], helps to reduce obesity [166], among others. In addition, Filip *et al.* [167] reported fungicidal activity of this plant extract against *Malassezia furfur*, a fungus that causes damage to human skin.

In general, all the benefits above mentioned provided by *Ilex paraguariensis* to human health come from the phenols, flavonoids, methylxanthines and saponins present in this plant [30]. Table 2.2 shows the main chemical composition of *Ilex paraguariensis*. However, the concentration of each chemical substance can vary considerably according to the cultivation, climatic and soil conditions and extraction method of the plant [168].

The antioxidant substances present in greater quantity in yerba mate are chlorogenic acid, caffeic acid and rutin [169–170]. These compounds, together with the other phenols and flavonoids that are present in yerba mate, are responsible for

the high antioxidant property of this plant, which is already consolidated in the

literature [171–172].

Table 2.2: Main chemical composition of *Ilex paraguariensis* [30–33–169]

Group	Compound	Formula	Concentration (mg g^{-1})	Ref.
Phenolic acids	Chlorogenic acid[a]		18.4 – 67.5	[32–170–172]
	Caffeic acid		0.2 – 0.7	[170–172]
Flavonoids	Rutin		3.1 -12.4	[32–170–172]
	Quercetin		1	[173]
Methylxantines	Caffeine		5.6 – 29.3	[32–171–172]
	Theobromine		0.08 – 1.9	[171–174]
	Theophyilline		ND[c]	[174]
Saponins	Derivatives from oleanolic acid[b]		2.4[d]	[175]

[a] Chlorogenic acid have some isomers and derivatives with similar structural formula
[b] R is the carbon radical that determines each type of saponin
[c] Not detected
[d] Expressed in terms of ursolic acid

Thus, since *Ilex paraguariensis* has a high concentration of antioxidant substances, it is evident the potential of this plant to be used in the synthesis of metal nanoparticles and their oxides through a green chemistry approach. In this specific work, yerba mate extract will be used for the green synthesis of zinc oxide nanoparticles. To date, the use of yerba mate extract to produce zinc oxide nanoparticles by green synthesis has not been observed in the literature.

2.5   Biocompatible materials

Although biomaterials have been used in medicine for a long time, studies on the development of biocompatible materials have gained greater attention after World War II, when doctors observed that soldiers who were injured by plastic materials did not suffer serious illness or infection. After the 1950s, biomaterials began to be extensively studied, mainly in the area of implants at first [176–177]. Nowadays, in addition to implants [178], biomaterials are applied in several areas, such as contact lenses [179], dental surgery [180], drug release [181], tissue regeneration [182], among others.

In general, the term biocompatibility is defined as the ability of a material to be inert to the human body without causing any damage to it for a determined period [177]. However, with the advancement of technology and science, experts believe that this statement must be redefined, as the requirements necessary for a material to be applied to the human body vary according to its application and the reactions that can occur in a specific area [176]. For Ratner [183], biocompatibility may be better defined

as the ability of a material to create healing, reconstruction, and tissue integration at a specific site of the human body.

The investment in the research of biocompatible materials has resulted in several therapies and medical treatments, providing an important improvement in the quality of life and also helping to increase the life expectancy of people [184]. Different types of materials can be used in these treatments and therapies, such as metals, ceramics, and polymers. However, polymeric materials and their composites are gaining more visibility as biomaterials, as they have a variety of mechanical and chemical properties, enabling their application in the most diverse areas of medicine, such as tissue engineering, ophthalmology, dentistry, implants, among others [36].

Different polymers are considered to be biocompatible [185]. For instance, polyethylene glycol (PEG) and polycaprolactone (PCL) can be used to release drugs, since they are biodegradable [186]. On the other hand, composites containing polymethylmethacrylate (PMMA) were developed for use as bone cement, due to its high mechanical resistance [187]. Also, hydrogels of different polymers with at least 95% of light transmittance are used to produce contact lenses [188].

Thin films are another category of polymer material that is applied in the biomedical field. These films become interesting as their properties can be significantly changed to attend different requirements by modifying the combination of polymers used for their production, thickness, and incorporation of other materials, such as drugs or nanoparticles [189].

Polymer fibres scaffolds also play an important role in biomaterials development, especially for tissue regeneration improvement. Such materials are considered an excellent option for wound healing therapies, for example, as they provide a three-

dimensional structure that mimics the extracellular matrix of natural skin tissue [190–191].

2.6 Polyelectrolytes

Polyelectrolytes are polymers that have ionic or ionizable groups when in solution. When different oppositely charged polyelectrolytes are in contact, the formation of neutral polyelectrolyte complexes occurs through electrostatic interactions [192]. Like all polymers, polyelectrolytes can be classified according to their (1) origin, being natural or synthetic, (2) composition, called homopolymers when formed by only one monomer, or copolymers, when formed by two or more monomers, and (3) structure, being linear, branched or cross-linked [193].

Nonetheless, polyelectrolytes can also be classified according to their charge as polycation (formation of positive ions in solution), polyanion (formation of negative ions in solution), or polyanphoteros (formation of cationic and anionic groups simultaneously). Another classification of polyelectrolytes divides them into polyacids or polybasic. The determining characteristic of a polyacid is its ability to form a polyanion when dissociated, whereas that of the polybasic is the formation of a polycation [194]. The most common acid groups are carboxyl (-COOH) and sulfonic acid (-SO$_3$H) and the basic ones are amino groups (-NH$_2$) [192].

A polyelectrolyte is considered strong when its charge density is independent of the pH of the medium. Otherwise, a weak polyelectrolyte shows variations in the charge density when subjected to different pH conditions [193–194]. The charge density of polyacids and polybasic is related to the degree of ionization of the polyelectrolyte, which represents the dissociation of a substance in solution. The

greater the degree of ionization, the greater the formation of ions and, consequently, the greater the charge density [194].

Strong polyelectrolytes are fully ionized in aqueous solution. Conversely, the degree of ionization of weak polyelectrolytes depends on the balance of the reaction. Equation (1) represents the equilibrium reaction for a weak acid HA, which can dissociate to form an anion (conjugate base) and a hydronium ion [195].

$$HA_{(aq)} + H_2O_{(l)} \leftrightarrow H_3O^+_{(aq)} + A^-_{(aq)}$$

(1)
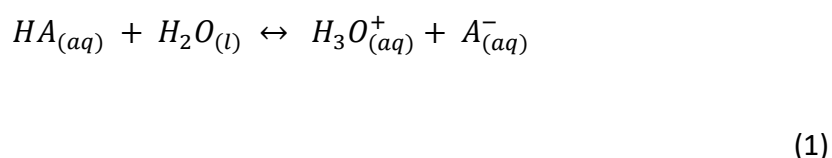
The equilibrium constant K_a of the reaction at equilibrium state can be determined using Equation (2), depending on the concentration of products and reagents in the reaction equilibrium. This constant is usually expressed as its negative cologarithm, called pK_a (Equation (3)) [195]. When the *pKa* of a substance is equal to the pH of the medium, the polyelectrolyte is 50% ionized. However, if the pH is different from the *pKa*, the substance will have its balance shifted, presenting a higher or lower degree of ionization [194].

$$K_a = \frac{[H_3O^+]\,[A^-]}{[HA]}$$

(2)

$$pK_a = -\log K_a$$

(3)

In this work, poly(acrylic acid) (PAA) and poly(allylamine hydrochloride) (PAH) were used for the development of biomaterials. PAA and PAH are classified as weak polyacid and weak polybasic, respectively, and their repetition units are shown in

Figure 2.9. Despite that strong polyelectrolytes are fully charged at any pH condition, the use of weak polyelectrolytes allows the manipulation of the charge density by changing the pH of the medium, enabling the achievement of versatile properties and, consequently, different applications, such as for the manufacture of sensors or the release of drugs [196].

PAA   **PAH**

Figure 2.9: Repetition unit of PAA and PAH polyelectrolytes [194]

PAA forms a polyanion when the functional group -COOH ionizes to form the carboxylate ion -COO⁻. The ionic form will predominate when the pH of the medium is higher than the pK_a, which varies between 5.5 and 6.5 for PAA under normal temperature conditions (25 ° C). On the other hand, if the pH is below the pK_a range, the PAA will be found in the protonated form, that is, in the non-ionized form. Furthermore, when submitted to a solution of pH equal to 10, the PAA will be fully ionized, while it will be fully protonated at pH below 4 [194].

PAH has a pK_a between 8.0 and 9.0, for solutions maintained at 25 ° C, and forms the ion - NH_3^+ when ionized. This polybasic is in the most ionized form when exposed to solutions with a pH below its pK_a. At pH lower than 5.0, PAH is fully protonated, while at pH greater than 11, this polybasic is found in a deprotonated form (-NH_2)[194].

2.7 Polymer thin films

In general, thin films have revolutionized several research areas, being used mainly for surface treatment to improve properties such as resistance to corrosion and abrasion, absorption, and permeability [197]. According to Web of Science, there has been a considerable number of publications and citations of thin films since the 1990s, which increased significantly since the year 2000. However, publications related to polymeric thin films for biomedical applications have started to become more significant since 2009 with a considerable increase since then, showing the potential and importance of these thin films as a biomaterial.

Thin polymeric films can be used in the biomedical area as implant and catheter coatings, preventing the formation of bacterial biofilms and, consequently, infections to the patient [198–199], for drug release [200], through the incorporation of drugs into the film, and for tissue engineering as they have versatile properties, such as elasticity and mechanical resistance [201].

These thin films can be obtained using different methods. For example, plasma polymerization is a complex method to obtain thin films as the monomers must be in the gas phase or carried by a gas. Conversely, solvent casting methods, like spin coating or dip coating are considered to be simpler, and require less energy consumption than plasma, using a solid substrate and a liquid solution of the polymer [202].

Thin polyelectrolyte films containing multilayers can be obtained by combining oppositely charged polyelectrolytes, forming nanometric layers of polycation and polyanion, which are combined by electrostatic interactions [203]. One of the most used techniques for obtaining these polyelectrolyte multilayer (PEM) thin films is the

layer-by-layer method (LbL) by dip-coating, which is based on the deposition of interleaved layers of a polycation and a polyanion [203–204].

This method is illustrated in Figure 2.10, in which (a) a substrate is immersed in a solution containing one of the polyelectrolytes, which will be deposited on the surface of that substrate. Then, (b) the substrate is immersed in a rinse solution to remove excess polyelectrolyte that has not been fully adsorbed. After, (c) this substrate containing the first layer of film is submerged in a solution containing a polyelectrolyte with an opposite charge, forming a bilayer of the film. Finally, (d) the substrate is immersed in another rinse solution to remove the non-adsorbed material. This procedure is then repeated sequentially until the desired number of layers is formed [203].
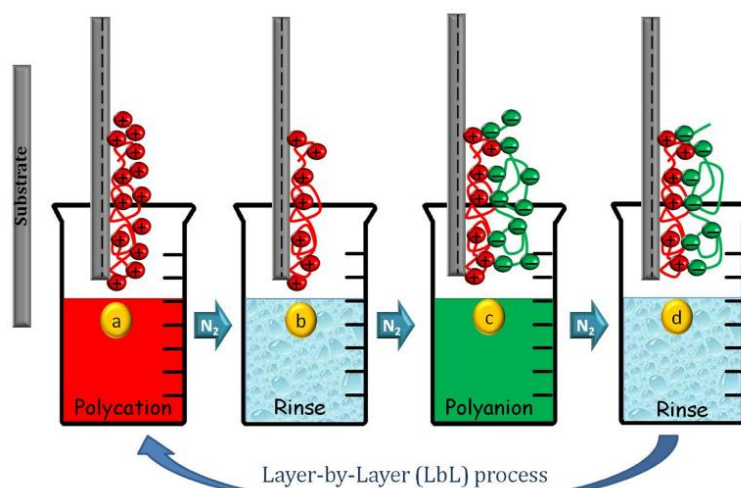
Figure 2.10: Deposition of thin films using the LbL process by dip coating. a) Substrate is immersed in a polyelectrolyte solution b) Substrate is rinsed to remove the excess of polyelectrolyte that did not adsorb c) Substrate containing the first layer of the film is submerged in a solution of an opposite charged polyelectrolyte d) Substrate is rinsed to remove excess of not adsorbed polyelectrolyte [203].

According to Choi and Rubner [194], the charge density of polyelectrolytes changes the growth of the film and its thickness. When the polyelectrolytes are in a more ionized state, the thickness of the layer will decrease as greater electrostatic interaction between the layers takes place. However, any change in the charge density in one of the polyelectrolytes can considerably increase the thickness of the film and, consequently, its physical-chemical properties. Thus, the pH of polyelectrolyte solutions is a determining factor for the synthesis of thin films.

In the biomedical field, thin films containing PAA and/or PAH in their composition have the potential to be used in different applications, such as, for example, drug release, bone tissue recovery, and antibacterial coatings [203]. For instance, Pallotta *et al.* developed PAA/PAH thin films containing gold nanoparticles (AuNP) at pH 7.4 with 3 polyelectrolyte bilayers and observed the potential application of this material as nanostructured medical devices [205].

Also, Pattabhi *et al.* [206] synthesized PAA and PAH films containing 29 and 30 layers at pH 7.4, being 29 with the last layer of PAH and 30 with the last layer of PAA. They verified in this work that the synthesized films have biocompatibility and can be used as a coating for implants. In addition, films containing PAA in the last layer presented lower cytotoxicity. Oppositely, Sailer *et al.* [207] observed that using a positive-charged polymer in the outer layer improved cell adhesion.

The number of bilayers of the polyelectrolyte film also influences the final properties of the films. Despite altering the mechanical properties, as expected, increasing the number of bilayers can alter the growth of cells on the surface of the film and, consequently, its biocompatibility. According to Chien *et al.* [208]*,* the minimum number of bilayers necessary for a PAH/PAA film to fully cover the substrate

are 4. However, with the increase of the bilayers, they observed a decrease in the proliferation of osteoblast cells on the surface of the film, thus decreasing its biocompatibility.

Similarly, Jaklenec *et al.* [209] evaluated the influence of the pH on cell attachment in PAA/PAH films. The findings showed a consistent fibroblast cell attachment when using PAA pH between 2.5 and 4.5 and PAH pH 5.5-9.0. However, the highest cell adhesion was found in films built with pH 2.5 for both PAA and PAH solutions. Conversely, a different study reported that using a combination of PAH pH 9.5 and PAA pH 3.0 resulted in a higher embryonic kidney cell attachment [207].

Although the mentioned studies have used different cell lines to assess the cytotoxicity of PEM films, the biocompatibility of these films was found to be directly associated and affected by the conditions used for film production, such as pH, number of layers, and thickness.

Tristán *et al.* [210] have studied the interactions of polyelectrolyte multilayers with proteins. According to the authors, the adsorption of glucose oxidase protein can be tunned by varying the pH of the polyelectrolytes solution and is related to the strength of electrostatic interaction between the PAA and PAH chains. This work highlights the promising properties of PEM for drug-release and biosensors applications.

Aiming for the improvement and the achievement of differentiated properties, nanoparticles have been incorporated into thin polymeric films. In addition to the work of Pallotta *et al.* [205], recent studies point to the use of silver nanoparticles to increase the bactericidal potential of films and silica nanoparticles to improve the performance of the film for drug release [211–212]. PAA/PAH thin films containing nanoparticles

were also successfully prepared for hydrogen production and drug degradation, for example, reporting new applications for PEM composite films [213–214].

2.8   Electrospun polymer fibres

A variety of techniques have been used to obtain polymer fibres. For instance, wet spinning is a common method, where a polymer solution is injected using a capillary tube into a chemical bath, precipitating the polymer through a chemical reaction. A single fibre is then formed and continuously collected, according to the flow rate of injection. Another common method is dry spinning, where a polymer solution is extruded into hot air, which evaporates the solvent. Conversely, the melt spinning is based on cooling molten extruded polymers. All these methods produce fibres with microscale diameters ranging from 10 to 100 μm [215–216].

Polymer fibres with smaller diameters, varying from nano to microscale, can be easily obtained using the electrospinning technique. This method is illustrated in Figure 2.11. Basically, a polymer solution is placed in a syringe-like vessel, where a high voltage is applied to the capillary tube or needle. The polymer droplet at the end of the tip becomes positively charged due to the power supply, forming a circular cone shape, also known as the Taylor cone. Consequently, the tip of the cone experiences an electrostatic repulsion, releasing a polymer jet at a controlled flow rate. Then, the solvent starts to evaporate forming the polymer fibre, which spins in the direction of the grounded collector (negatively charged) [215–217–218].
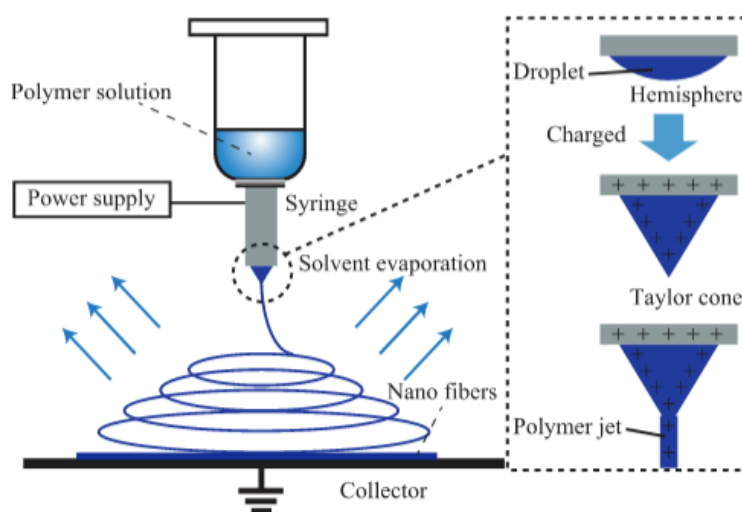
Figure 2.11: Electrospinning method illustration [218]

Despite being a simple and low-cost technique, the diameter and morphology of electrospun fibres can be modified by simply tunning the polymer solution viscosity and concentration, solvent, power supply, needle size, and pressure applied to the system. For example, polymer concentration directly affects the size and morphology of the fibre. Studies report that low concentration forms a mixture of beads and fibres, but uniform fibres can be achieved with the increase of this parameter. In addition, the increase of concentration leads to a larger fibre diameter [219–220]. Polymer concentration is also proportional to the viscosity of the solution. In extremely low concentrations or viscosity, no continuous fibre is formed. However, in high viscous solutions, no fibre is obtained, as the solution is not ejected from the needle. Figure 2.12 shows the photomicrographs of electrospun polyimide fibre in different concentrations, evidencing the variation of its morphology and size [221].
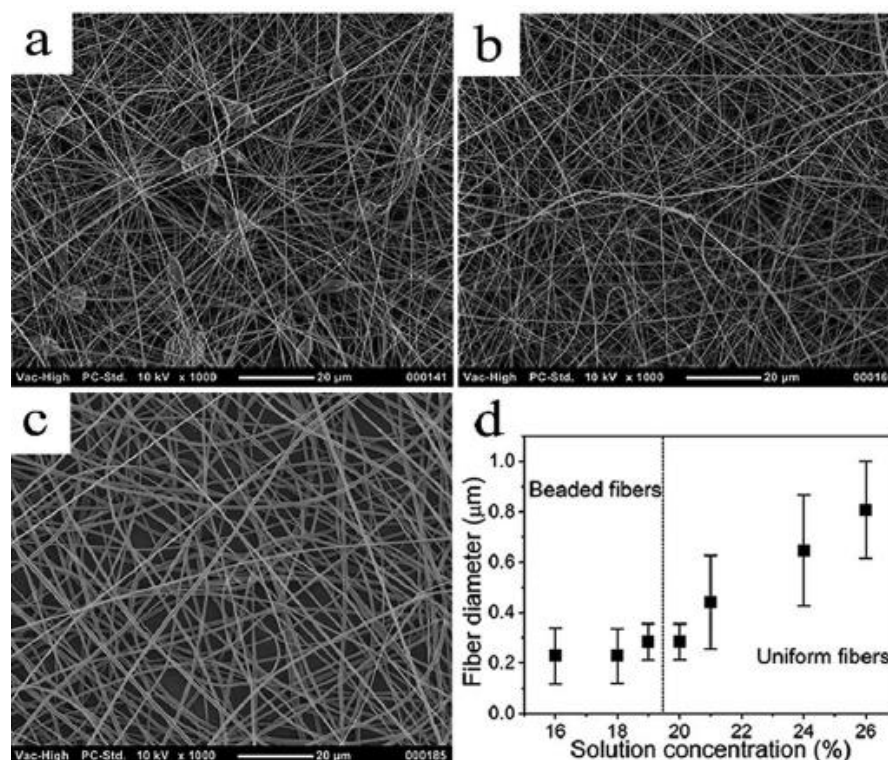
Figure 2.12: Photomicrographs of electrospun fibres produced with a poly(vinylidene fluoride) concentration of a)16%, b) 20%, and c) 26% and d) the effect on fibre diameter according to the polymer concentration [222]

The solvent to dissolve the polymer also plays an important role in the final electrospun polymer fibre. Boas *et al.* [223] observed, for example, that a concentration of 40% ethanol in water favoured the production of uniform polyelectrolyte fibres, while no fibre was formed when using only water as solvent. Conversely, electrospun polyvinyl alcohol (PVA) fibre dissolved in water results in high-uniform fibres [224]. Thus, despite being a simple technique, the electrospinning parameters must be carefully tuned to successfully achieve a uniform material.

Specific properties, like mechanical strength, hydrophobicity, biodegradability, among others, can also be achieved by using a different range of polymers, from synthetic to natural ones [215]. Regarding polyelectrolytes, they were reported to improve fibre length consistency and its mechanical properties due to the electrostatic

interaction of the charged polymer chains [223–225]. In addition, the combination of polyelectrolyte and the electrospinning technique is expected to be not only an alternative to the commonly LbL assembly used to obtain such complexes, as discussed in section 2.7, but also to obtain a novel material by combining the polyelectrolyte complexes and the electrospun fibre properties [226].

These features bring the electrospinning technique to applications in different areas [227–228]. In the biomedical field, biodegradable and biocompatible polymers are selected to produce electrospun scaffolds, and numerous studies report their promising performance in drug delivery, cancer therapies, tissue engineering, among others, as illustrated in Figure 2.13 [229–231]. In addition, electrospun fibres scaffolds have unique characteristics for tissue engineering, as it forms a porous film with a three-dimensional structure that mimics the natural extracellular matrix of tissues [230].

Recently, the electrospinning technique has been successfully used for the development of novel therapies for skin wound healing [191]. In general, electrospun fibre scaffolds have good breathability, due to their porous structure, cell adhesion, which is favoured by the similarity with natural skin tissue, and barrier properties against pathogens. This last characteristic can be easily enhanced by the incorporation of antimicrobial agents [232].

In fact, different substances can be incorporated into the electrospun fibre mats. Usually, those substances are added to the polymer solution before the electrospinning. However, if the substance affects the viscosity, homogeneity, or if they are large and insoluble particles, they must be incorporated after the

electrospinning process. In this case, the fibre is usually immersed in or sprayed with a solution containing the substance of interest [191–231–233].
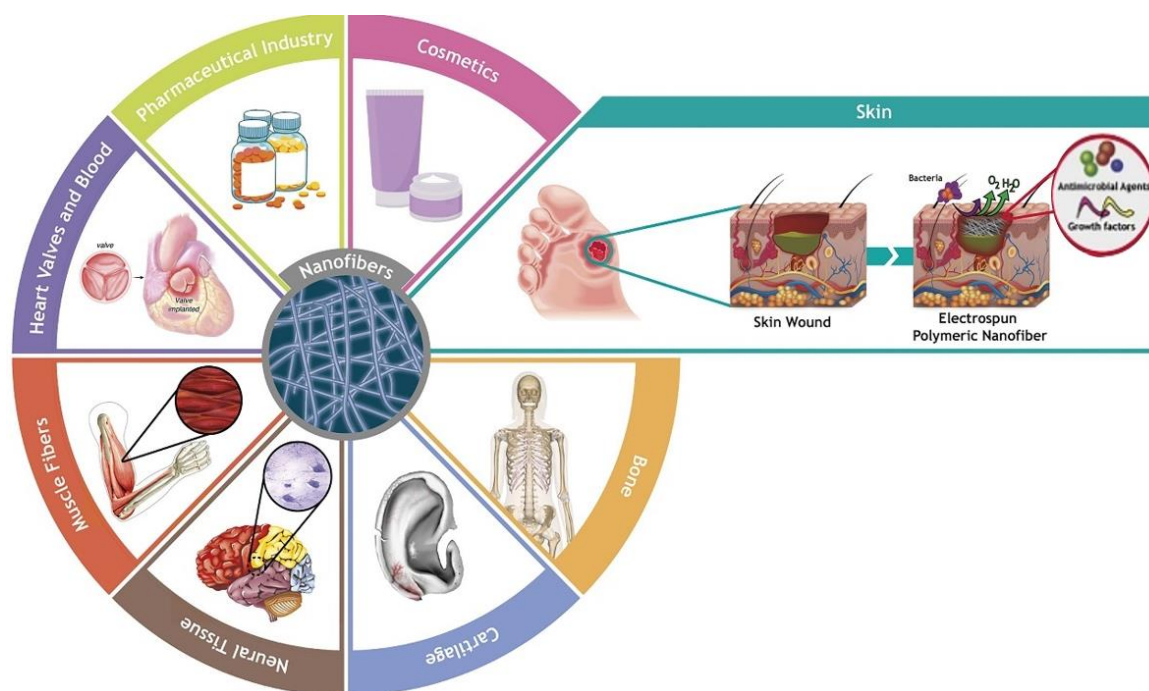
Figure 2.13: Biomedical applications of electrospun fibres with emphasis on wound healing [232]

For example, amoxicillin and hydroxyapatite have been incorporated into poly(lactic-co-glycolic acid) (PLGA) to obtain antimicrobial scaffolds to avoid wound infections [234]. Similarly, alternative substances to commonly used antimicrobial drugs have also been incorporated into fibres, aiming not only to achieve an antimicrobial scaffold but also to develop alternative solutions to drug-resistant bacteria. Currently, metal and metal oxide nanoparticles and natural antimicrobial substances extracted from plants have been incorporated in electrospun fibres with this purpose [235–239].

Methodology

CHAPTER 3:   Methodology

This chapter describes the materials and methods used to synthesize and characterize the biomaterials developed in this project and evaluate their potential for biomedical applications.

3.1   Materials

The materials used to perform the green synthesis included zinc nitrate hexahydrate (≥99.0%, Sigma-Aldrich), zinc acetate dihydrate (≥99.0%, Sigma-Aldrich) and ethanol 99% (Dinâmica Química Contemporânea Ltda.). The *Ilex paraguariensis* leaves were collected in the municipality of Caxias do Sul, RS, Brazil and identified at the Natural Science Museum of University of Caxias do Sul (registration number 46.334). For the characterization of the leaves extract Folin Ciocalteau 2N (Dinâmica Química Contemporânea Ltda), calcium carbonate P.A. (Dinâmica Química Contemporânea Ltda.), Tris-hydrochloride (≥99.0%, Sigma-Aldrich) and 1,1-diphenyl-2-picrylhydrazyl (DPPH, Sigma-Aldrich) were used.

Materials used to synthesize the fibres and the thin films include polyacrylic acid 25 % w/v solution (PAA, MW ~345,000, Polysciences) and polyallylamine hydrochloride (PAH, MW ~17,500, Sigma Aldrich).

For the cellular tests the following materials were used: mouse fibroblast L929 cells, cell medium Dulbecco´s Modified Eagle's Medium (DMEM, Sigma-Aldrich), fetal bovine serum (FBS, Sigma-Aldrich), penicillin-streptomycin (P/S, Gibco-BRL), 3-(4,5-dimethylthiazol-2-yl)-2,5-diphenyltetrazolium bromide (MTT, Sigma-Aldrich), dimethyl sulfoxide (DMSO, Sigma-Aldrich), GIEMSA staining (Sigma-Aldrich), rapamycin (Sigma-

Aldrich), methanol (99.8%, Sigma-Aldrich), monoclonal anti-LC3A/B antibody (Cell signaling – Autophagy kit), anti-mouse fluorescein isothiocyanate (FITC, Cell signaling – Autophagy kit) and bovine serum albumin (BSA, Sigma-Aldrich).

The antimicrobial activity was performed using bacterial strains of *Staphylococcus aureus* ATCC 25923 and *Escherichia coli* ATCC 35218. Bacteria cells were cultured using Mueller Hinton broth (MHB, Lab M Limited) and resazurin sodium salt (Sigma-Aldrich) was used to evaluate bacteria viability. Glutaraldehyde 50% w/v solution (Alfa Aesar), phosphate buffer solution (PBS, Sigma Aldrich), and ethanol 99% were used to prepare bacteria samples for microscopy analysis.

3.2 Green synthesis and characterization of zinc oxide nanoparticles

3.2.1 *Ilex paraguariensis* leaves extract preparation

The *Ilex paraguariensis* leaves were cleaned carefully with the following sequence of rinses to remove impurity particles: tap water, 50% (v/v) ethanol/water solution, and distilled water, respectively, at ambient temperature. At the end of this procedure, the leaves were dried at 60 °C for 1.5 h and were ground in a knife mill grinder in fine particles. The ground leaves were stored in an amber flask under refrigeration (4 °C) for further use.

To obtain the plant extract, 100 g L^{-1} of the ground *mate* leaves were heated and stirred with two different solvents: distilled water and a 50% (v/v) ethanol/water solution. Three ranges of temperature and time of extraction were evaluated, from 25 to 100 °C and 10 to 30 min, respectively. The extract was then filtered and centrifuged

for 20 min at 5000 rpm to remove particles of the medium and used on the same day

to avoid the degradation of the antioxidant substances.

3.2.2   Green synthesis of zinc oxide nanoparticles

Zinc salt (zinc nitrate or zinc acetate) in a Zn(II) concentration of 21.8 g L^{-1} was

added to 50 mL of the *mate* extract previously prepared. The solution was stirred for

1 h at room temperature and then heated for 4 h at 70 °C. After that, the mixture was

submitted to a hot air oven at 140 °C for 1 h, and finally calcinated at 400 °C for 1 h.

The resulting powder was collected for further characterization.

To evaluate the effect of the *mate* extract on the synthesis of ZnONPs, two

samples containing only zinc nitrate hexahydrate (named Nitrate) and zinc acetate

dihydrate (named Acetate) were calcinated under the same conditions used in the

green synthesis (400 °C, 1 h). Table 3.1 describes the samples synthesized and their

conditions. Only the sample prepared with zinc nitrate and ethanolic extract

(Nit_EtOHa) produced ZnONPs without the calcination process.

Table 3.1 Description of the ZnONPs samples synthesized

Sample	Zinc source	Plant extract solvent	Heat treatment
Nitrate		-	C
Nit_H$_2$O	Zinc nitrate	H$_2$O	O + C
Nit_EtOH		50% (v/v) EtOH$_{(aq)}$	O + C
NIt_EtOHa		50% (v/v) EtOH$_{(aq)}$	O
Acetate		-	C
Act_H$_2$O	Zinc acetate	H$_2$O	O + C
Act_EtOH		50% (v/v) EtOH$_{(aq)}$	O + C

C: calcination; O: hot air oven

3.2.3   Characterization of *Ilex paraguariensis* extract

3.2.3.1   Antioxidant activity

The antioxidant activity (AA) of the IP leaves extracts was evaluated through an oxidation-reduction reaction of the free radical 1,1-diphenyl-2-picrylhydrazyl (DPPH), following the method described by Yamaguchi *et al.* with slight modifications[240]. To perform the analysis, 100 µL of the plant extract was added to 400 µL of trishydrochloride 0.1 mol L^{-1} (pH 7.0) and 500 µL of a DPPH 0.5 mmol L^{-1} solution. The control sample was prepared with the substitution of the plant extract by its solvent (water or 50 % (v/v) ethanol/water solution). After 20 min of incubation in the absence of light, the absorbance was measured in a UV-Vis spectrophotometer (Thermo Scientific, model Evolution 60) at 517 nm. Results were expressed in percentual, following Equation 4.

$$\%AA = \frac{A_{control} - A_{extract}}{A_{extract}} \; x \; 100$$

(4)

where,

  AA = antioxidant activity (%);

  $A_{control}$ = control sample absorbance (arb. units);

  $A_{extract}$ = sample absorbance (arb. units).

3.2.3.2 Total polyphenol content

The total polyphenolic content was determined following the procedure of Singleton and Rossi with adaptations [241]. For this, 150 µL of the plant extract was added to 750 µL of Folin-Ciocalteau 10% (v/v) reagent and 600 µL of calcium carbonate 7.5% (w/v). The mixture was slightly hand-shaken until homogeneous and incubated at 55°C for 5 min. Then, at room temperature, the absorbance was measured in a UV-Vis spectrophotometer (Thermo Scientific, model Evolution 60) at 760 nm. Total phenolic content was performed in triplicate and determined by comparison with a standard curve of gallic acid (5, 25, 50, 75, and 100 µg mL^{-1}) and expressed in terms of micrograms of gallic acid per milliliter of plant extract (µgEAG mL^{-1}).

The statistical significance among the samples was evaluated using variance analysis (ANOVA) with Tukey test considering a confidence interval of 95%.

3.2.3.3 Determination of Ilex paraguariensis constituents by HPLC

The content of six main IP constituents was evaluated by high performance liquid chromatography (HPLC, HP model 1100, column Lichrospher RP18 5 µm) equipped with a UV detector operating at 272 nm and a quaternary pumping system. Prior to the analysis, IP extracts were filtered through a membrane (Millipore, 0.45 µm). The analysis in reverse phase mode was constituted of solvent A (Milli-Q water and 1% (v/v) acetic acid) and solvent B (methanol). The mobile phase was pumped with 75% of solvent A at 0.4 mL min^{-1} flux and the column was kept at 40 °C [171]. For the quantitative evaluation, a standard calibration curve was obtained using standard

solutions with a known concentration of the pure compounds (chlorogenic acid, caffeic acid, theophylline, theobromine, rutin, and caffeine).

3.2.4   Design of the green synthesis mechanism

3.2.4.1   Cyclic voltammetry

ZnONPs synthesis mechanism was investigated through cyclic voltammetry using a conventional three-electrode cell at room temperature and a potentiostat (Ivium Technologies, model Compactstat.h) operating with a potential range from -1.7 to 0.0 V, scan rate of 50 mV s^{-1} and 1.0 mV step. Cyclic voltammograms were obtained with a 3.0 mm glassy carbon working electrode, a platinum wire as a counter electrode, an Ag/AgCl reference electrode, and KCl 0.1 mol L^{-1} as the electrolyte solution. The concentration of Zn^{2+} ions and the plant extract was 0.1 mol L^{-1} and 50 g L^{-1}, respectively for all tests. The working electrode was polished with alumina powder and cleaned with acetone in a 5 min ultrasonic bath prior to each analysis.

The cyclic voltammetry technique is based on the analysis of electrochemical redox reactions, which generate an electric current due to the electron transfer that occurs between the substances involved in the reaction [242]. Thus, to carry out this experiment, a range of electric potential from -1.7 to 0 V was applied over the working electrode of the electrochemical cell (Figure 3.1a), generating an electric current. Then, when any electrochemical reaction occurs in this system, a change in this electric current generated by the oxidation or reduction reaction is observed. The peak current of the reduction or oxidation reaction for diffusional controlled process is given according to the Rendles-Sevcik equation (Equation (5)), considering a temperature of

25 °C [242]. Thus, voltammograms provide characteristic peaks of reduction and oxidation for each element studied, as shown in Figure 3.1b.

$$i_p = 2.69\text{x}10^5 n^{3/2} A D_0^{1/2} C_o v^{1/2}$$

(5)

where,

i_p = peak current (A);

n = number of electrons involved in the redox reaction;

A = electroactive area (cm^2);

D_0 = diffusional coefficient (cm^2 s^{-1});

C_o= analyte concentration (mol cm^{-3});
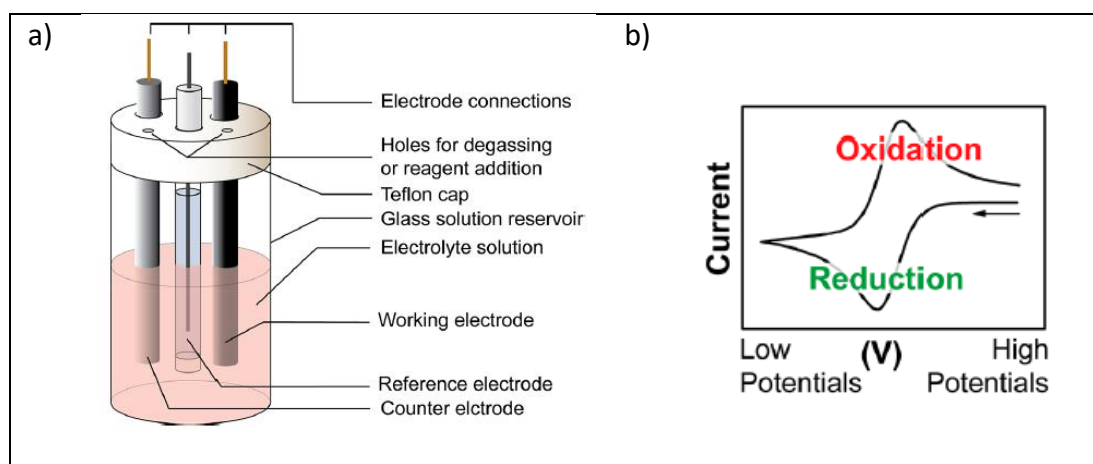
Figure 3.1: a) electrochemical cell b) cyclic voltammogram [243]

Standard solutions of caffeine were reacted with the zinc precursors for comparison with the green synthesis. It was used a concentration of 0.05 mol L^{-1} of zinc salt and the concentration of the antioxidants were determined considering a 1:4

molar ratio of Zn(II) to caffeine molecules. The first voltammetry cycle was runned in a single cycle.

3.2.4.2 Fourier Transform Infrared Spectroscopy (FTIR)

The functional groups present in the substance resulted from the reaction of caffeine and zinc acetate and pure caffeine were determined by FTIR spectroscopy (Thermo Scientific, model Nicolet iS10) using KBr pellets. The spectra were obtained in a range from 4000 to 400 cm^{-1} with a resolution of 1.0 cm^{-1}. Samples were vacuum dried at 60 °C for 24 h prior to the analysis to remove any possible adsorbed water.

3.2.5 Characterization of zinc oxide nanoparticles green synthesized

3.2.5.1 X Ray Diffraction (XRD)

XRD patterns of the ZnONPs synthesized were obtained using a powder diffractometer (Shimadzu, model XRD-6000) equipped with a Cu anode (Kα_1 = 1,5406 Angstrom) in a range of 2θ from 20° to 80°, with an acquisition time of 5s. The crystallite size was obtained using the Scherrer Equation [244] and with Match! Software.

3.2.5.2 Field Emission Scanning Electron Microscopy (FESEM)

ZnONPs morphology was examined with a field emission scanning electron microscope (TESCAN, model MIRA 3) equipped with an energy beam from 0.2 to 30 kV. All the samples were placed in an aluminum stub and were covered with a thin

layer of gold by the sputtering method (Denton Vacuum, Desk V) for 30 s at 0.13 mbar vacuum to perform the analysis.

3.2.5.3   Transmission Electron Microscopy (TEM)

The particle size of ZnONPs synthesized was investigated by the analysis of images obtained in a transmission electron microscope (Jeol, model JEM 1200 EX II) using a working voltage of 80 kV. The mean size of the particles was determined with Image J software based on 15 readings within a single field of view[245].

3.2.5.4   Ultraviolet and visible spectroscopy (UV-vis)

The surface plasma resonance (SPR) and the energy band gap (E_{bg}) of the green synthesized ZnONPs were evaluated by UV– Vis spectroscopy in a wavelength range of 250–600 nm. ZnONPs were suspended in distilled water (200 mg L^{-1}) and exposed to an ultrasonic bath for 30 min. The band gap energy was obtained using the Equation 6:

$$E_{bg} \;=\; \frac{h_c}{\lambda_{max}}$$

(6)

where,

h = Plank constant (6.63 $\times$ 10^{-34} J s);

c = velocity of light (2.99 $\times$ 10^{-8} m s^{-1});

λ_{max} = maximum absorption wavelength

3.2.5.5   Cell viability assay

Cellular cytotoxicity was evaluated by means of the MTT method. The L929 strain of mouse fibroblasts was used according to the standard method described by ISO 10993-5 [246]. Cells were cultured in DMEM, supplemented with 10% (v/v) of FBS and 1% (v/v) of P/S. The cultures were maintained in a humid atmosphere at 37 °C with 5% (v/v) CO_2. The study was performed as cells reached 70–80% confluence. Briefly, cells were seeded into the 96-well plates at a density of 5.0×10^4 cells mL^{-1}. After 24 h, cells were treated with different concentrations (1–80 µg mL^{-1}) of the compounds and incubated for 24 h. The compounds were solubilized in DMSO. Negative controls were treated with the same amounts of 0.5% (v/v) DMSO solution.

The medium was removed and 1.0 mg mL^{-1} MTT dye in serum-free medium was added to the wells. Plates were incubated at 37 °C for 2 h in a humidified controlled atmosphere with 5% (v/v) CO_2. Subsequently, the MTT solution was removed and the obtained formazan violet product was dissolved in 100 µL DMSO for 30 min. Absorbance was measured using a microplate reader (Molecular Devices -USA, model Spectra Max 190) at 570 nm. All readings were compared with the negative control, which represented 100% viability. The LC50 (concentration in µg mL^{-1} that inhibits cell growth by 50%) was also calculated. Each experiment was performed in triplicate and independently repeated at least four times.

3.2.5.6   Cellular morphological analysis

Mouse fibroblast cells (L929) were seeded into 24-well plates in similar conditions to the cell viability analysis. After 24 h of treatment with different

concentrations (1-25 µg mL^{-1}) of zinc oxide nanoparticles, the culture medium was then removed and cells prepared for FESEM and optical microscopy analysis. To perform the optical microscopy, the culture medium was removed after treatment, and cells were dyed with Giemsa staining 1% (v/v). To perform FESEM analysis, after removing the culture medium, cells were fixed with glutaraldehyde 2% (v/v) and dehydrated with ethanol.

3.2.5.7   Indirect immunofluorescence analysis

L929 cells were seeded into 24-well plates containing coverslips. After 24 h incubation, cells were treated with a range of different concentrations (5-15 µg mL^{-1}) of ZnONPs and incubated for 24h. Negative controls were treated with the same amount of growth medium. Positive control received rapamycin (100 nmol L^{-1}). Cells were fixed with methanol at − 20 °C, blocked with 2% BSA for 1 h, and incubated with the monoclonal anti-LC3A/B antibody (1:100 v/v) for 1h, followed by incubation with secondary anti-mouse fluorescein isothiocyanate (FITC) (1:150 v/v) for 1h. The slides were mounted with a coverslip and analyzed with a fluorescence light microscope (Olympus, model BX43).

3.2.5.8   Antibacterial assay of zinc oxide nanoparticles

Staphylococcus aureus ATCC 25923 and *Escherichia coli* ATCC 25922 were cultured and grown in an exponential phase in MHB medium at 37 °C. The viability of bacterial cells when exposed to different concentrations of ZnONPs and the electrospun fibre mats was analysed in a 96-well plate using the resazurin cell viability assay. Resazurin indicates cell viability by changing from a blue to a pink colour upon

chemical reduction resulting from aerobic respiration due to cell growth. Thus, the reduction of the dye is proportional to the viable cells present in the solution and the minimum inhibitory concentration is determined when no dye reduction occurs.

Overnight cultures of the two types of bacteria were diluted to a concentration of approximately 1.0×10^4 colony-forming units per millilitre (CFU mL^{-1}). An autoclaved aqueous suspension of ZnO nanoparticles (10 mg mL^{-1}) was diluted in MH broth in different concentrations (from 15 to 100 µg mL^{-1}). Then, 100 µL of different ZnONPs suspension and 5 µL of the diluted bacteria were added to each well. Two controls without nanoparticles were also included in each plate: a positive control (100 µL of MH broth with 5 µL of the diluted bacteria) and, a negative control (only 100 µL of MH broth). After overnight incubation at 37 °C, 15 µL of resazurin (0.15 mg mL^{-1}) was added to each well and mixed thoroughly for 2 h, and plates were then subjected to absorbance measurement at 600nm. The test was performed in two individual triplicates.

3.3 Thin films development

The thin films were developed on glass substrates which were carefully cleaned prior to the deposition of polymer layers according to the following sequence: Extran 10 % v/v solution under sonication for 10 min, immersion on a NaOH 0.1 mol L^{-1} solution for 10 min, immersion in acetone/ethanol 1:1 solution and carefully rinsed with dH$_2$O water.

Aqueous solutions of PAH and PAA were prepared in distilled water in a concentration of 0.05 mol L^{-1} regarding their monomer molecular weight. PAA solution

was set to pH 4.0, while the pH of the PAH solution was varied. NaOH 0.01 mol L^{-1} and

HCl 0.01 mol L^{-1} solutions were used to adjust the pH.

The deposition of each layer was done using the dip-coating method in automatic

equipment (Nanostrata, Stracto Sequence VI) following the method developed by Faria

et al. with adaptations. First, the glass substrate was immersed in a PAH 0.05 M

aqueous solution for 15 min, then it was rinsed three times in distilled water (dH_2O)

during 60s, 30 s, and 30 s, respectively. The second layer was then deposited by

submerging the substrate in a PAA 0.05 mol L^{-1} aqueous solution for 15 min and then,

rinsing in dH_2O as previously mentioned. This procedure was repeated consecutively

until obtaining 21 layers and is illustrated in Figure 3.2.
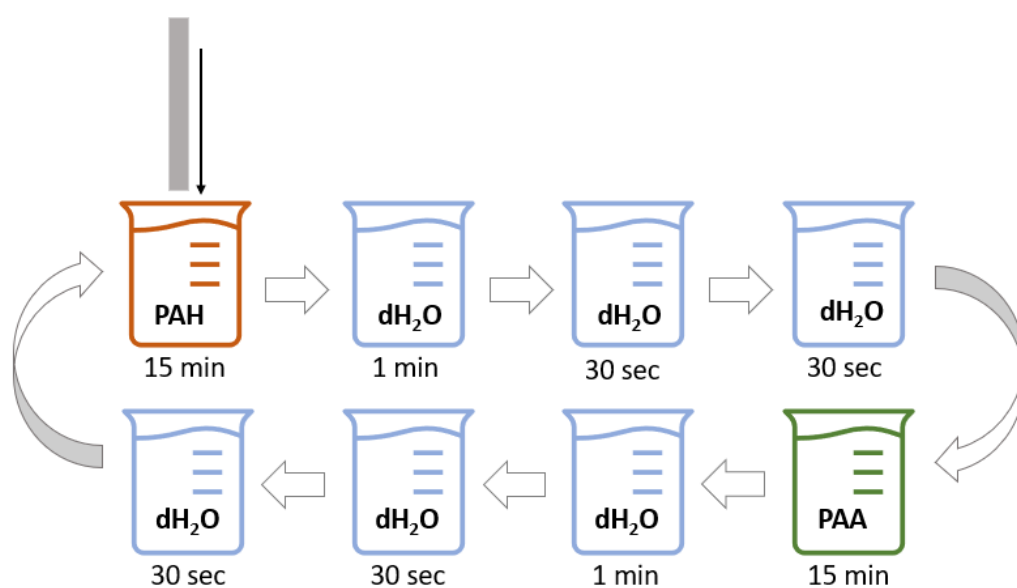
Figure 3.2: LbL process to obtain the thin films

To improve the antimicrobial activity of the thin films, the green synthesized

ZnONPs were added in the polycation solution (PAA) while aqueous plant extract was

added in the polyanion solution (PAA). To obtain a homogeneous suspension of

nanoparticles in the PAH solution, after the addition of ZnONPs the solution was sonicated for 15 min and then stirred for 30 min. The aqueous plant extract was added to the PAA solution and stirred for 30 min. A design of experiments was performed to evaluate the influence and interaction of 1) the presence of *Ilex paraguariensis*, 2) ZnONPs concentration, and 3) the pH solution of the polycation solution in the structure and properties of the thin films.

The use of experimental design based on statistical criteria allows us to evaluate the simultaneous influence, or interaction, between two or more independent variables. In addition, through the determination of these interactions, it is possible to optimize processes and build empirical models. The most well-known factorial design is 2^k, in which the number of factors (k, variables) is investigated at two levels (values), low (-1) or high (+1). To carry out a complete factorial design, all possible combinations of factor levels are tested. For example, for planning 2^2 (two levels and two factors) 4 experiments will be carried out [247].

However, a two-level factor implies that there is a linear correlation between the factors and the response. Thus, to evaluate the curvature of the independent variables and the response of the statistic model, a center point can be added to the design of the experiment. The center point is determined as the middle value between the lower and upper levels. This statistical model also allows replicating only the center point to report the experimental error of the model, as replicating every sample might be expensive and time-consuming [247].

In this work, a 2^3 design of experiment with a center point was performed, in which the factors and levels are reported in Table 3.2 while a detailed list of the samples prepared is presented in Table 3.3. All the experiments were performed in

random order to minimize the experimental errors and the analysis was performed using Statistica 64 software.

Table 3.2: Design of experiments for thin films production

Factors	Levels		
	-1	0	+1
PAH pH	5.5	7.0	8.5
ZnO (g L^{-1})	1	2	3
IP (g L^{-1})	0	25	50

Table 3.3: Thin films samples

Sample	PAH pH	ZnO (g L^{-1})	IP (g L^{-1})
TF1	5.5	1.0	0.0
TF2	8.5	1.0	0.0
TF3	5.5	3.0	0.0
TF4	8.5	3.0	0.0
TF5	5.5	1.0	50
TF6	8.5	1.0	50
TF7	5.5	3.0	50
TF8	8.5	3.0	50
TF9	7.0	2.0	25
TF10	7.0	2.0	25
TF11	7.0	2.0	25

3.3.1   Characterization of thin films

3.3.1.1   Dynamic light scattering (DLS)

The sizes of the ZnONPs agglomerates when varying their concentration and solution pH were determined in an aqueous suspension of 5 mmol L^{-1} PAH by the DLS technique in a 180° NANO-flex® Particle Metrix instrument with an acquisition time of 90s and considering a refractive index of 2.03. Each solution was sonicated for 15 min before the analysis.

3.3.1.2 Zinc quantification by inductively coupled plasma – optical emission spectrometry (ICP-OES)

The amount of ZnONPs absorbed in the thin films was quantified by means of zinc concentration using ICP-OES, according to Standard Methods EPA 3050b (1996) [248]. The test was performed using a sample with 30 cm^2 deposited in glass slide.

3.3.1.3 Antimicrobial activity

The viability of bacterial cells when exposed to the different thin films was evaluated against *Staphylococcus aureus* ATCC 25923, which was cultured and grown in an exponential phase in MH broth medium at 37 °C. For this, an overnight culture of the bacteria was diluted to a concentration of approximately $1.0×10^4$ colony forming units per milliliter (CFU mL^{-1}). Then, 0.5 cm^2 of the different thin films was incubated with 100 µL of MH broth and 5 µL of the diluted bacteria. Two controls without the thin film were also included in each plate: a positive control (100 µL of MH broth with 5 µL of the diluted bacteria) and, a negative control (only 100 µL of MH broth). After overnight incubation at 37 °C, the samples were serial diluted and 20 µL of the dilutions were spread in MH agar plates and incubated at 37°C. In the following day, the bacteria colonies were counted, and the results compared with the positive control.

For a faster evaluation, the antimicrobial activity of the thin films built with additional layers (81 and 121 layers) was assessed using the resazurin methodology. For this, after overnight incubation with the bacteria, 15 µL of resazurin (0.15 mg mL^{-1}) was added to each well and mixed thoroughly for 2 h. The thin films were then

removed from the solution and the plates were subjected to absorbance measurement at 600nm.

3.3.1.4   Field emission scanning electronic microscopy (FESEM)

The morphology of the thin films was examined with a field emission scanning electron microscope (TESCAN, model MIRA 3, Brno, Czech Republic) equipped with an energy beam of 10 kV. Prior the analysis, the samples were placed in an aluminium stub and were covered with a thin layer of gold by sputtering method (Denton Vacuum, Desk V, Moorestown, NJ, United States of America) for 30 s at 0.13 mbar vacuum to perform the analysis.

3.4   Electrospun fibres development

A polymer solution was prepared by first mixing 1.6 mL of PAA with 0.4 mL of ethanol/water 40% v/v. Then, 0.11g of PAH was added to the solution and mixed until homogeneous. The PAA/PAH solution was electrospun using a 0.9 needle and an electrical potential of 10 kV. A fixed working distance from the tip of the needle to the stainless-steel plate of 10 cm was used and the pressure was kept between 0.015 and 0.020 bar. A scheme of the electrospinning process is illustrated in Figure 3.3.
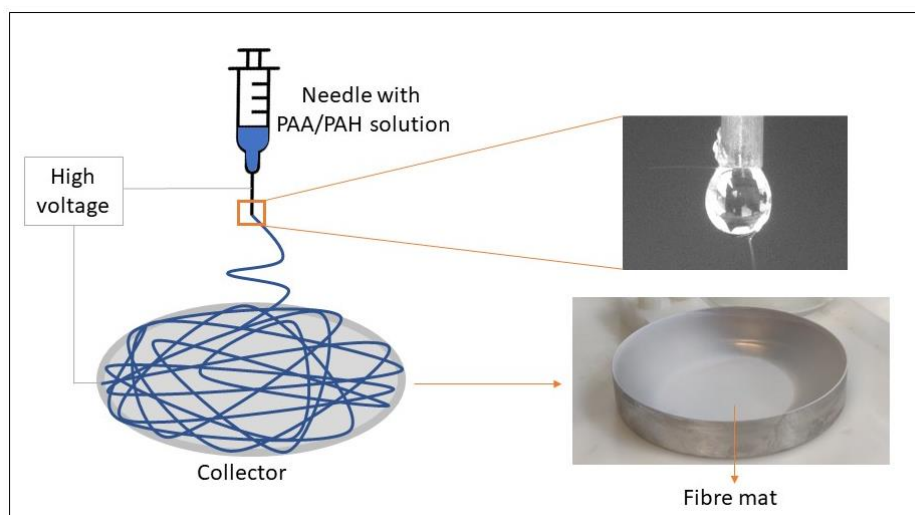
Figure 3.3: Production of electrospun PAA/PAH fibres

The fibre mat was then collected from the stainless-steel plate and annealed at 140 °C for 6h for polymer crosslinking [223]. After cooling to room temperature, the electrospun polymer blend was placed in 20 mL of a ZnONPs aqueous solution (1 g L^{-1}) for 40 min. The solution was then removed and the fibre mat dried for 2h at 37°C.

3.5   Characterization of electrospun fibres

3.5.1   Field emission scanning electron microscopy (FESEM) coupled with energy dispersive spectroscopy (EDS)

The morphology of the fibre was examined with a field emission scanning electron microscope (TESCAN, model MIRA 3, Brno, Czech Republic) equipped with an energy beam of 10 kV. Prior the analysis, the samples were placed in an aluminium stub and were covered with a thin layer of gold by sputtering method (Denton Vacuum, Desk V, Moorestown, NJ, United States of America) for 30 s at 0.13 mbar vacuum to perform the analysis. EDS analysis of Zn was performed coupled with FESEM using a silicon drift detector (SDD). The mean diameter of the fibres were determined using

the Image J software [245], considering the measurements of 15 fibres within a single field of view.

3.5.2 Zinc quantification by inductively coupled plasma – optical emission spectrometry (ICP-OES)

The amount of ZnONPs absorbed in the fibres was quantified by means of zinc concentration using ICP-OES, according to Standard Methods EPA 3050b (1996) [248].

3.5.3 Fourier transform infrared spectroscopy (FTIR)

The interaction of the electrospun PAA and PAH polymers was addressed by FTIR spectroscopy (Perkin Elmer, Waltham, MA, USA). Cast films of pure PAA and PLA were also analysed for comparison. The spectra were registered in a range of 4000 to 650 cm^{-1} and a resolution of 1 cm^{-1} was employed.

3.5.4 Antimicrobial assay of electrospun fibres

To evaluate the antimicrobial activity of the fibre mats, where 0.5 cm^2 of PAA/PAH/ZnONPs and PAA/PAH fibres were incubated in a 96-well plate with 50 µL of MH broth and 2.5 µL of bacteria solution ($1x10^4$ CFU mL^{-1}) prepared as previously described (item 3.2.5.8). After overnight incubation at 37°C, 7.5 µL of resazurin was added to each well and incubated for a further 2h. Then, the fibres were removed, and the absorbance was measured at 600 nm. A positive control (50 µL of MH broth and 2.5 µL of bacteria solution) and negative control (50 µL of MH broth) were included in each plate and the tests were performed in two individual triplicates.

Microbial adhesion to the fibres was evaluated using SEM analysis. For this, the antimicrobial test was performed as described above, but without the addition of resazurin. Thus, after overnight incubation, the media was removed from the wells and bacteria cells were fixed with 3% glutaraldehyde solution in PBS (v/v) for 15 min at 4 °C, following a sequence of dehydration with 30, 50, 70, 90, and 100% (v/v) ethanol aqueous solutions for 10 min. The fibre mats were then kept in a desiccator until the analysis was performed. The samples were gold-coated in sputtering equipment (Baltec model SCD 005, USA) for 110 sec at 0.1 mbar before the SEM analysis in high vacuum mode with a maximum beam voltage of 9 kV and back-scattered electron mode.

Green synthesis

CHAPTER 4:   Green synthesis and characterization of zinc oxide nanoparticles

4.1   Introduction

Nanotechnology is a growing field of science and researchers believe that the use of nanomaterials will increase considerably in a variety of new areas [1–4]. Within this context, zinc oxide nanoparticles (ZnONPs) have been widely investigated due to their unique physical, chemical, and optical properties that enable them to be utilized in a variety of technological applications, including novel biomedical devices and therapies [5–8]. More specifically, ZnONPs enhanced the efficacy of bone regeneration when incorporated into polymer scaffolds by inducing early mineralization and preventing infections due to their antibacterial activity [34]. This nanomaterial has also been investigated for its wound healing performance. The incorporation of ZnONPs on polymeric beads, for example, led to faster wound closure and avoided the formation of microbial biofilms on the skin [249]. This characteristics corroborates with the findings of related studies [70–152–206–250–251].

The toxicity of ZnONPs for use in human health applications is still a subject of discussion, as nanomaterials have different toxicity mechanism routes, such as reactive oxygen species (ROS) production, cell internalization, and metal ions release, among others, which can affect human cells in different manners compared to the bulk material form [252]. Recent developments on this topic have been made, and the cytotoxicity of oxide nanoparticles is now known to be not only dose-dependent but also associated with properties like size, morphology, and surface characteristics [253–255].

Several methods are applied to obtain these nanomaterials through chemical, physical, or biological synthesis [9–10]. However, the biological approach has gained much attention as it is more environmentally friendly than conventional methods, considering that it substitutes hazardous solvents with plant extracts, and can improve the properties of the nanomaterials. Commonly known as green synthesis, many plant extracts have been used to synthesize metal and metal oxides nanoparticles with enhanced properties [12–20]. Although the mechanism of formation of nanoparticles through green synthesis is not completely understood, it is believed that antioxidant compounds present in the plant, such as flavonoids and polyphenols, reduce or form coordinated complexes with the targeted metal [21–23].

Many plant extracts have been applied to the green synthesis of ZnONPs [16–22–24–27]. Gunalan *et al.* [28], for example, used *Aloe vera* extract and obtained ZnONPs with enhanced antibacterial effect in comparison to ZnONPs synthesized by chemical method. Shahriyari Rad *et al.* [29] also confirmed the antimicrobial activity of ZnONPs obtained using *Menta pulegium L.* leaves. Nava *et al.* [21] obtained ZnONPs using fruit peel extract for photocatalytic degradation of dyes with enhanced degradation rate than ZnONPs commercially available.

In this work, we report the green synthesis of ZnONPs and its optimization using *Ilex paraguariensis* leaves extract. This plant, also called *mate*, is commonly found in the south of Brazil, Uruguay, and Argentina, where it is used to prepare a traditional tea [30]. Anxiolytic, neuroprotective, and anti-inflammatory properties have been described in m*ate* tea and have been associated with a variety of antioxidant compounds found in the plant, which include chlorogenic acid, caffeic acid, and caffeine [31–33].

Although many tea extracts have been used for synthesizing ZnONPs [256–258], this is the pioneer work where Ilex paraguariensis leaves was used to obtain ZnONPs . In addition, even though much research has designed a probable mechanism route for the green synthesis, none have used cyclic voltammetry to evaluate and confirm it. In this sense, this work contributes to a better understanding of the green synthesis of ZnONPs at a molecular level, which is essential to develop and implement a sustainable large-scale production of nanoparticles. Moreover, a careful study on the cytotoxicity and cell internalization of ZnONPs was performed to evaluate their application in the biomedical field.

4.2   Characterization of *Ilex paraguariensis* leaves extract

4.2.1   Antioxidant activity (AA)

In this method, the antioxidant substances present in the IP extract reduce the DPPH radical, according to the reaction shown in Figure 4.1, causing a colour change of the solution from violet to yellow.
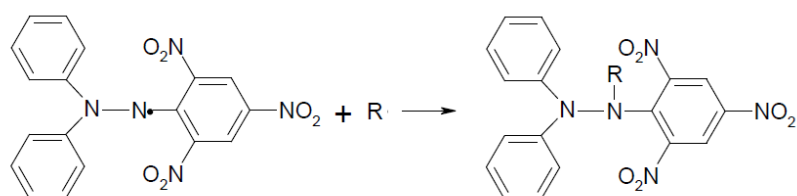
Figure 4.1: Reduction reaction of the DPPH radical

Initially, the AA was examined for three different conditions of temperature extraction: 25 °C, 50 °C, and boiling point, approximately 80 °C for the 50% (v/v) ethanol/water extraction, and 100 °C for water. Extraction time was set as 30 min to perform this analysis, and the results are shown in Table 4.1. According to this test,

both extracts examined have high AA, scavenging 70-80% of the free radical used in this analysis (DPPH), which goes in agreement with other studies previously reported [171–172].

In relation to the aqueous extract, increasing the temperature of extraction resulted in a slight increase in AA. However, the AA of the ethanolic extract enhanced significantly from 25 °C to 50 °C, while not showing variation from 50 °C to the boiling point. In this sense, a temperature of 50 °C was selected to prepare the plant extract for green synthesis.

Table 4.1: *Ilex paraguariensis* extract antioxidant activity for different extraction temperatures

Temperature	Antioxidant activity (%)	
(°C)	H_2O	50% (v/v) EtOH$_{(aq)}$
25	[a]75.4 ± 0.1	[a]69.1 ± 2.0
50	[b]78.3 ± 0.3	[b]80.0 ± 0.7
Boiling point	[c]82.1 ± 0.5	[b]80.4 ± 0.7

*Means with different letters in the same column are significantly different ($p < 0.05$)

Subsequently, the influence of extraction time was investigated using extraction times of 10, 20, and 30 min, keeping the temperature at 50 °C. Table 4.2 shows the results of the AA of the IP extract with variations on the extraction time. Most of the antioxidant compounds were extracted during the first 10 min. The increase in the time of extraction slightly enhanced the antioxidant activity of the plant extract, except when augmenting the extraction time from 20 to 30 minutes for the 50% (v/v) EtOH$_{(aq)}$ solution, in which no significant changes in AA were observed.

Table 4.2: *Ilex paraguariensis* extract antioxidant activity for different extraction time intervals

Time (min)	Antioxidant Activity (%)	
	H₂O	50% (v/v) EtOH
10	[a]73.4 ± 0.7	[a]77.8 ± 0.3
20	[b]75.9 ± 0.9	[b]80.0 ± 0.7
30	[c]78.3 ± 0.3	[b]80.1 ± 0.7

*Means with different letters in the same column are significantly different ($p < 0.05$)

4.2.2   Total polyphenolic content

The polyphenols present in the plant extract reduce the molybdenum found in the reagent Folin-Ciocalteu, which causes a colour change, through the formation of coordination compounds, from yellow to blue. Figure 4.2 shows this reaction with gallic acid.
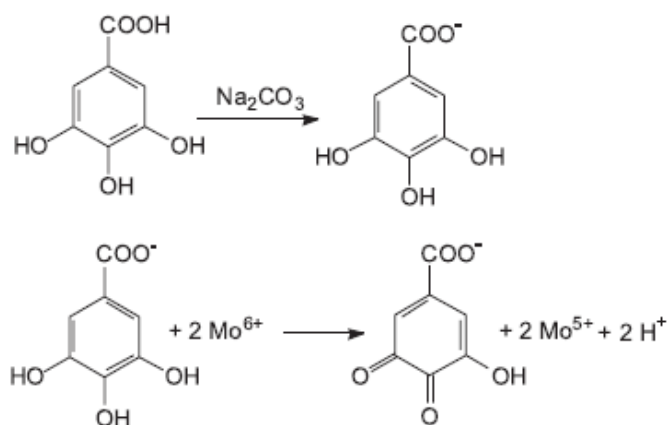
Figure 4.2: Reaction between Folin-Ciocalteu reagent and gallic acid

Total polyphenolic content was evaluated at the same conditions used in the AA test. The results of total phenolic content present in the IP extracts in each extraction temperature examined are shown in Table 4.2 in terms of equivalent acid gallic concentration (EAG). The increment in temperature from 25 °C to 50 °C enhanced the total polyphenolic content significantly for both aqueous and 50% (v/v) ethanol aqueous extracts. On the contrary, the change in temperature from 50 °C to the boiling

point did not result in a considerable enhancement of the total phenolic content. These results agree with the AA test, where the temperature of 50 °C showed to be most efficient, extracting almost the same amount of antioxidant compounds as in the extraction performed in the boiling point temperature.

Table 4.3 Total phenolic content of *Ilex paraguariensis* extract varying the extraction temperature

Temperature (°C)	Total polyphenolic content (μg EAG mL^{-1})	
	H_2O	50% (v/v) EtOH$_{(aq)}$
25	[a]204.5 ± 3.4	[a]161.6 ± 1.4
50	[b]309.8 ± 2.7	[b]316.6 ± 6.0
Boiling point	[b]318.6 ± 6.9	[c]338.1 ± 3.2

*Means with different letters in the same column are significantly different ($p<0.05$)

Subsequently, the total phenolic content of IP extracts was assessed at different extraction times (Table 4.4). As observed in the AA test, the majority of polyphenolic substances were extracted during the first 10 min of extraction.

To the aqueous extraction, the phenolic content yielding was optimized by approximately 6% by increasing the extraction time from 10 to 20 min. However, a longer extraction time (30 min) promoted a reduction of the total polyphenolic content, indicating polyphenolic decomposition. Conversely, the 50% (v/v) ethanol solution enhanced the total polyphenolic content to ca. 9.5% when expanding the extraction time from 10 to 20 min and 8% from 20 to 30 min.

Table 4.4 *Ilex paraguariensis* extract total polyphenolic content for different extraction time intervals

Time (min)	Total polyphenolic content (μg EAG mL^{-1})	
	H_2O	50% (v/v) EtOH
10	[a]300.2 ± 8.3	[a]266.5 ± 8.8
20	[b]319.7 ± 4.3	[b]292.1 ± 4.4
30	[a,b]309.8 ± 2.7	[c]316.6 ± 5.9

*Means with different letters in the same column are significantly different ($p<0.05$)

Therefore, considering the results of the AA and total polyphenolic content, the extraction time of 20 min was chosen to be optimal to prepare the IP extract for the green synthesis of ZnONPs.

4.2.3 Determination of selected *Ilex paraguariensis* constituents by HPLC

The concentration of six main compounds present in IP leaves was quantified by HPLC in both aqueous and ethanolic extracts (Table 4.5). Plant extracts were prepared following an extraction time of 20 min at 50 °C.

Table 4.5: Concentration of the main *Ilex paraguariensis* compounds determined by HPLC

Substance	Concentration (μg mL^{-1})	
	H$_2$O	50% (v/v) EtOH
Chlorogenic acid	42.86 ± 0.68	47.96 ± 1.27
Caffeic acid	7.18 ± 0.02	7.53 ± 0.09
Caffeine	541.39 ± 0.72	654.22 ± 0.99
Theophylline	13.22 ± 0.35	28.26 ± 0.64
Theobromine	111.00 ± 0.92	125.44 ± 0.72
Rutin	n.d.	n.d.

n.d. = not detected

In comparison to the aqueous extract, the 50% (v/v) ethanol extract exhibited a higher concentration of the substances evaluated, mainly for caffeine, theophylline, and theobromine. This result agrees with the work of Vieira *et al.* [259], where ethanol increased the extraction of antioxidants substances compared with the extraction performed exclusively with water. The substance rutin, commonly found in IP leaves was not detected in either of the extracts with the applied methodology. Converse to our findings, Berté *et al.* [171] reported that chlorogenic acid was the main antioxidant

present in the *mate* leaves, followed by caffeine and theobromine. Anesini *et al.* [172] have also found a major state for chlorogenic acid in commercial IP leaves; however, the rutin content showed to be higher than caffeine. Nonetheless, the concentration of antioxidants is significantly affected by climate, leaves age, soil characteristics, extract conditions, and others [260–261].

4.3 Evaluation of the green synthesis mechanism

4.3.1 Cyclic voltammetry

Cyclic voltammetry was performed in the samples Nit_EtOH, Nit_H$_2$O, Act_EtOH, and Act_H$_2$O (before heat treatment) to evaluate the mechanism of formation of ZnONPs. This analysis observes a change in the current when reduction or oxidation reactions occur in a system due to the transference of electrons. The cyclic voltammetry test was performed from the highest to the lowest potential, i.e., from the reduction to oxidation potential. Equation (6) illustrates the oxidation-reduction reactions for zinc:

$$Zn^0 \rightarrow Zn^{2+} + 2e^- \text{ (oxidation)}$$

$$Zn^{2+} + 2e^- \rightarrow Zn^0 \text{ (reduction)}$$
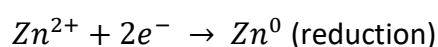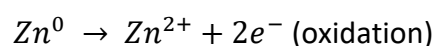
$$(6)$$

Several studies support the idea that antioxidant compounds present in plants have the capacity of forming complexes with or reducing metal ions [12–21–108]. Thus, if the Zn(II) ions were reduced by the *mate* extract, only an oxidation peak will be visualized. Conversely, if the Zn(II) ions are free in solution, both reduction and

oxidation peaks will be observed, and if the Zn(II) ions were complexed by the plant extract, no peak will be observed as no redox reaction will take place.

Figure 4.3 shows the voltammograms of the 50% (v/v) ethanol and aqueous extracts with a concentration of 50 mg L^{-1} in KCl 0.05 mol L^{-1}. Oxidation and reduction peaks were not observed for the IP extract solutions in comparison to the electrolyte voltammogram, which indicates that no electrochemical reaction occurred.
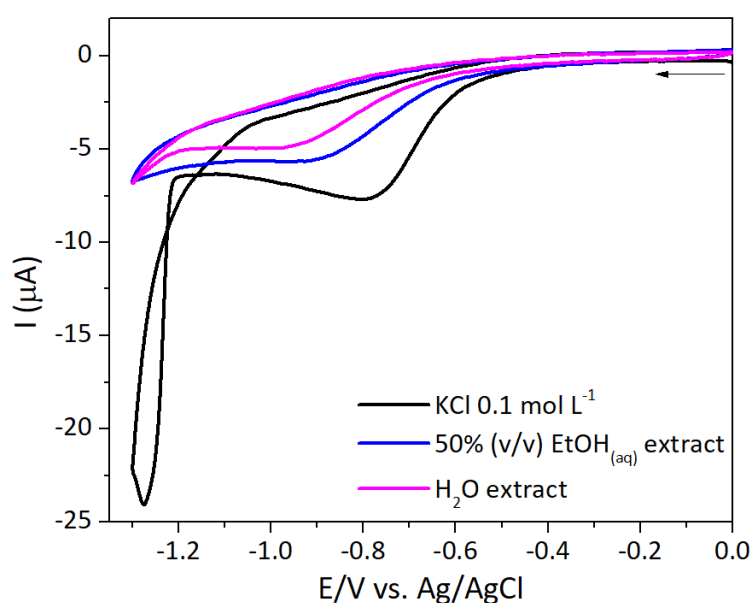
Figure 4.3: Voltammograms of *Ilex paraguariensis* extracts

Figure 4.4a shows a typical zinc nitrate voltammogram where the peaks between −0.7 V and −1.0 V are related to the oxidation-reduction reaction of Zn(II), and the peaks between −1.0 and −1.25 V are related to the redox reaction of the nitrate ion, corroborating with the literature [262–263]. The cyclic voltammograms of Nit_EtOH and Nit_H$_2$O (Figure 4.4b) suggest that Zn(II) were complexed by both *mate* extracts as no peak was observed in comparison to the electrolyte (KCl 0.1 mol L^{-1}).
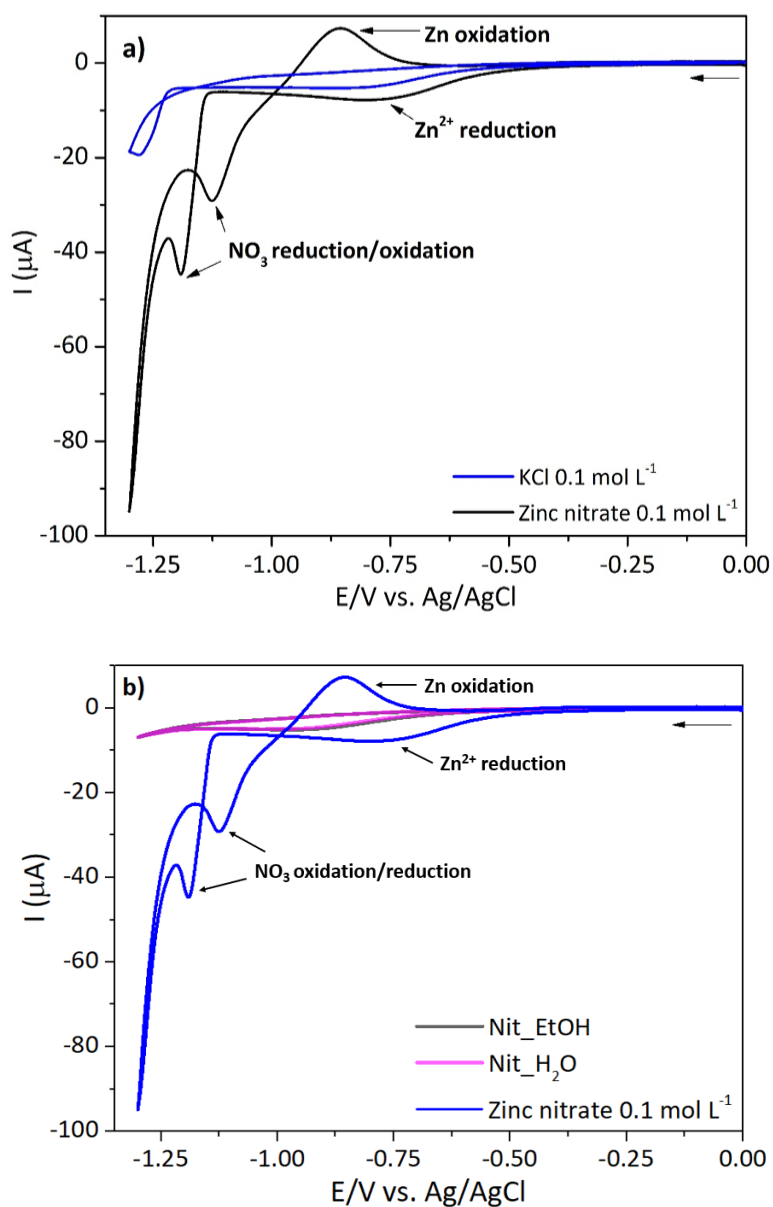
Figure 4.4: Cyclic voltammograms: (a) zinc nitrate 0.1 mol L^{-1}; (b) Nit_EtOH and Nit_H_2O containing 0.1 mol L^{-1} of zinc nitrate in 100 g L^{-1} mate extract

Different from the samples with zinc nitrate, the samples Act_EtOH and Act_H_2O (Figure 4.5a and Figure 4.5b) displayed peaks of reduction and oxidation, but with a lower current than the pure zinc acetate solution. The peak current is linearly proportional to the concentration of the targeted substance (Zn(II) in this case) [242]. Figure 4.5c indicates the linearity relation between the peak current and zinc acetate concentration of the standard solution.
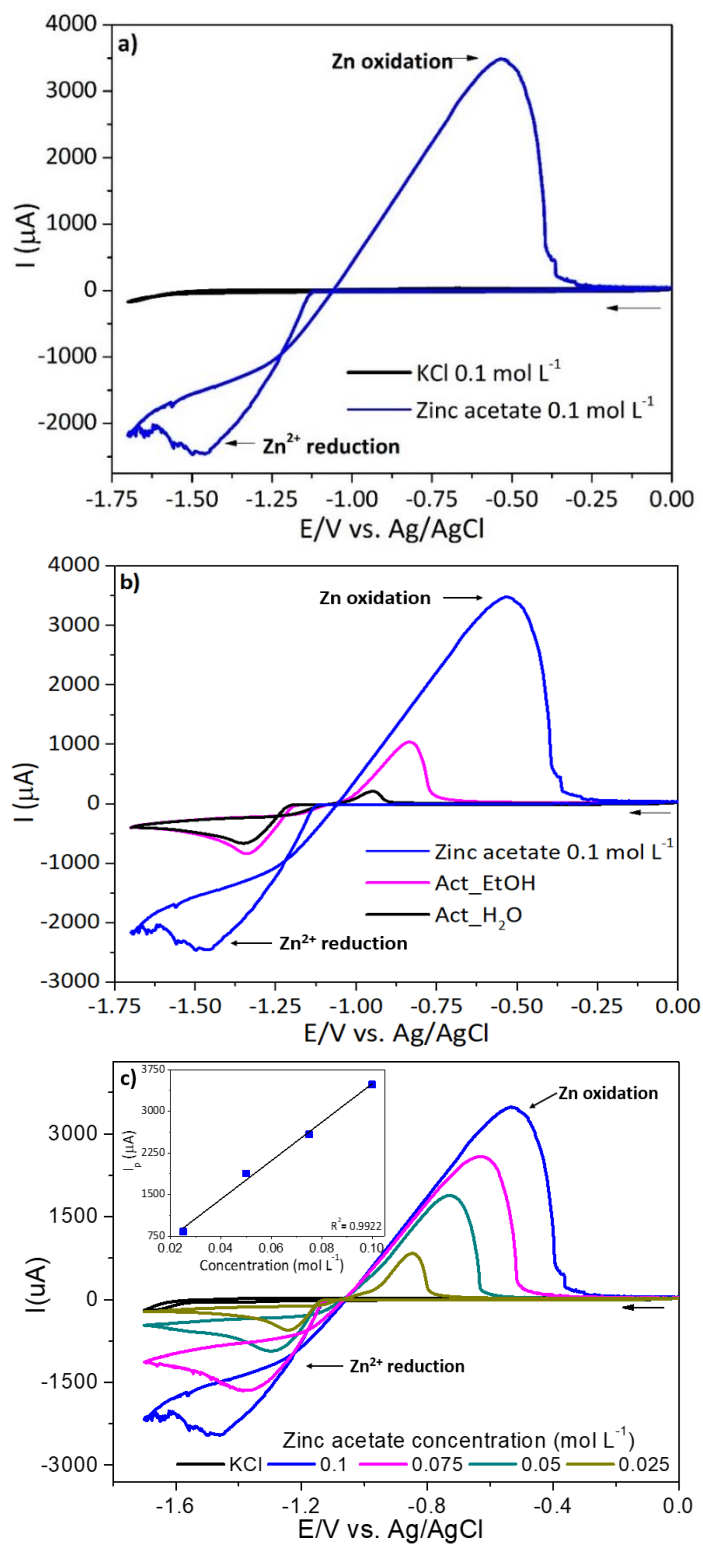
Figure 4.5: Cyclic voltammogram: (a) zinc acetate 0.1 mol L^{-1}; (b) Act_EtOH and Act_H$_2$O containing 0.1 mol L^{-1} of zinc acetate in 100 g L^{-1} mate extract; (c) linear relation between peak current and zinc acetate concentration

From this relation, the concentration of zinc acetate that was reduced in the Act_EtOH and Act_H$_2$O samples was determined as 0.041 mol L^{-1} and 0.008 mol L^{-1}, respectively, with the remainder complexed by the antioxidants of the *mate* extract. Thus, considering the concentration of zinc that did not undergo the redox reaction, only 71% of zinc available in the sample Act_EtOH and 95% in sample Act_H$_2$O was possibly complexed by the *mate* extract.

In general, Zn(II) can form coordinated complexes with nitrogen, sulfur, halogens, and oxygen ligands, resulting in complexes with tetrahedral (sp^3 hybridization) or octahedral (sp^{3}d^2 hybridization) geometry, being the octahedral the less thermodynamically stable form [264]. Antioxidant compounds available in plant extracts usually have hydroxyl groups (from phenolic compounds) in their composition or atoms with lone electron pairs, such as nitrogen and oxygen (methylxanthines) that will form metal complexes by originating an anion or by the element with a lone electron pair.

Methylxanthines are found in high concentrations in *mate* extracts [171–259–265]. Thus, the mechanism of formation of the green synthesis of ZnONPs here developed is based on the molecular structure of this group of active compounds and is shown in more detail in Figure 4.6. According to the HPLC results, caffeine is the methylxanthines with the highest concentration in the plant extract used in this study. This substance has one dissociation site, where a lone pair of electrons in the nitrogen reacts to form the respective conjugated acid of caffeine as indicated in Figure 4.6 [266]. Besides, several studies report the formation of complexes of Zn(II) and caffeine and Zn(II) and theophylline, supporting the mechanism proposed here [266–270].
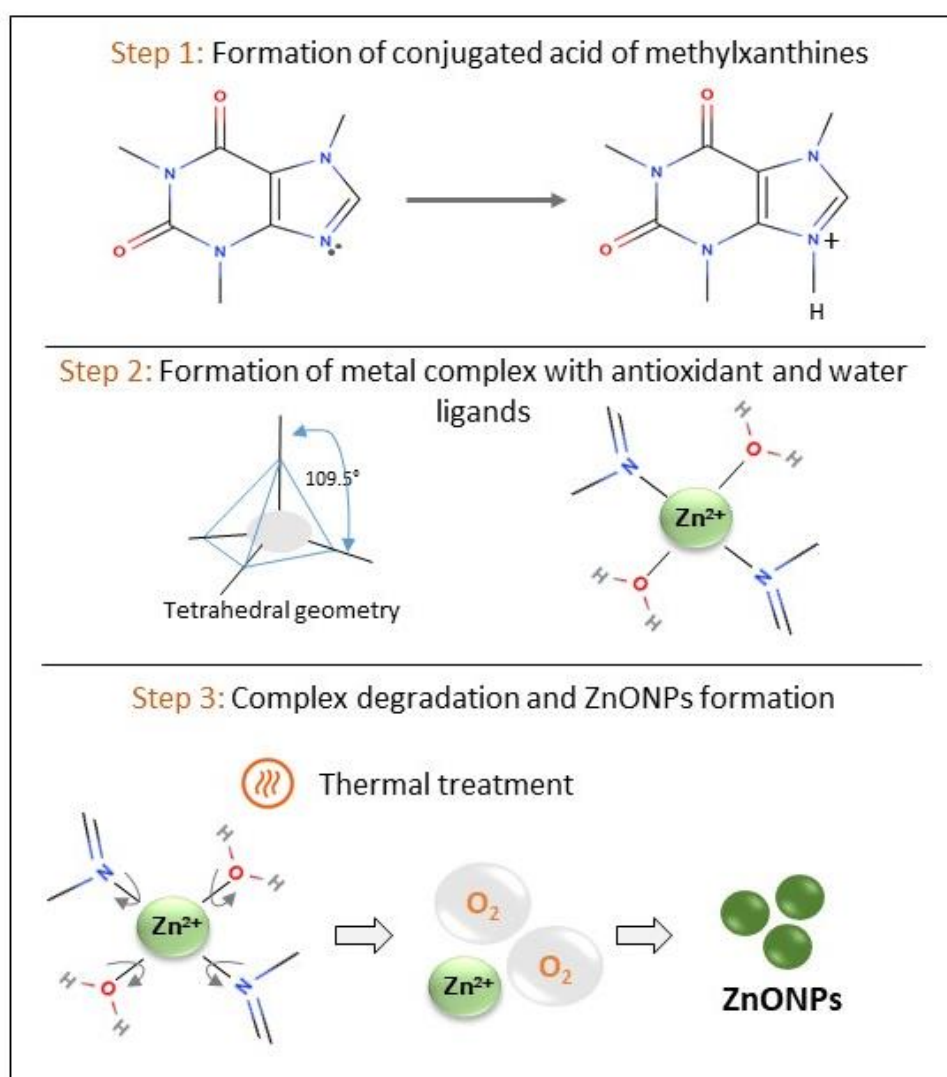
Figure 4.6: ZnONPs mechanism of formation via green synthesis

The formation of these complexes was further evaluated using pure solutions of caffeine. Figure 4.7 shows that the cyclic voltammograms of caffeine with zinc nitrate and zinc acetate have the same pattern of the solutions prepared with the *mate* extracts, confirming the involvement of this methylxanthine compound on the green synthesis of ZnONPs. In addition, the analysis with zinc acetate (Figure 4.7b) also indicates that zinc salt did not react completely with the antioxidant, corroborating with the results observed in Figure 4.5b.
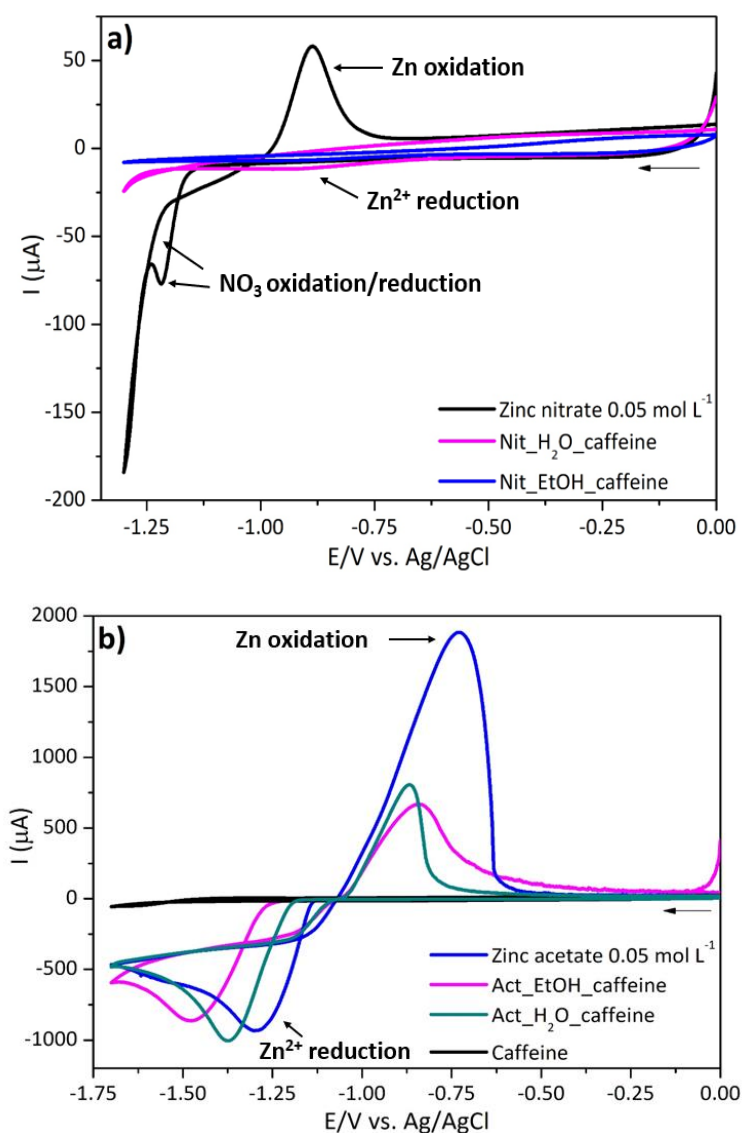
Figure 4.7 Cyclic voltammetry of caffeine solutions reacted with (a) zinc nitrate and (b) zinc acetate

According to the calibration curve of zinc acetate (Figure 4.5c) approximately 60% of the Zn(II) in the Act_EtOH_caffeine and 70% in the Act_H₂O_caffeine were complexed by caffeine, which is lower than the concentration obtained in the analysis of the green synthesis. However, the *mate* extract has different types of active compounds, which might have improved the formation of complexes when using the plant extract instead of the pure caffeine solution.

4.3.2 Fourier transform infrared spectroscopy

Figure 4.8 shows the FTIR spectra of Act_EtOH_caffeine in comparison to pure caffeine. Caffeine illustrates a broad and weak peak at 3460 cm^{-1} related to the OH stretching and two weak peaks at 3115 cm^{-1} and 2950 cm^{-1} associated with the vibration of CH and CH$_3$ bonds. The peaks at 1700 cm^{-1} and 1655 cm^{-1} represent the symmetric and asymmetric vibration of C=O of ketones, respectively, and a strong peak at 1550 cm^{-1} indicates the presence of C=C and C=N groups. At 1240 cm^{-1}, a strong and narrow peak indicates the vibration of CH bend and CN stretching. The peaks at 973 cm^{-1} and 645 cm^{-1} are associated with ring deformation while the weak peak at 860 cm^{-1} is related to the wagging of CH bonds [270–272].
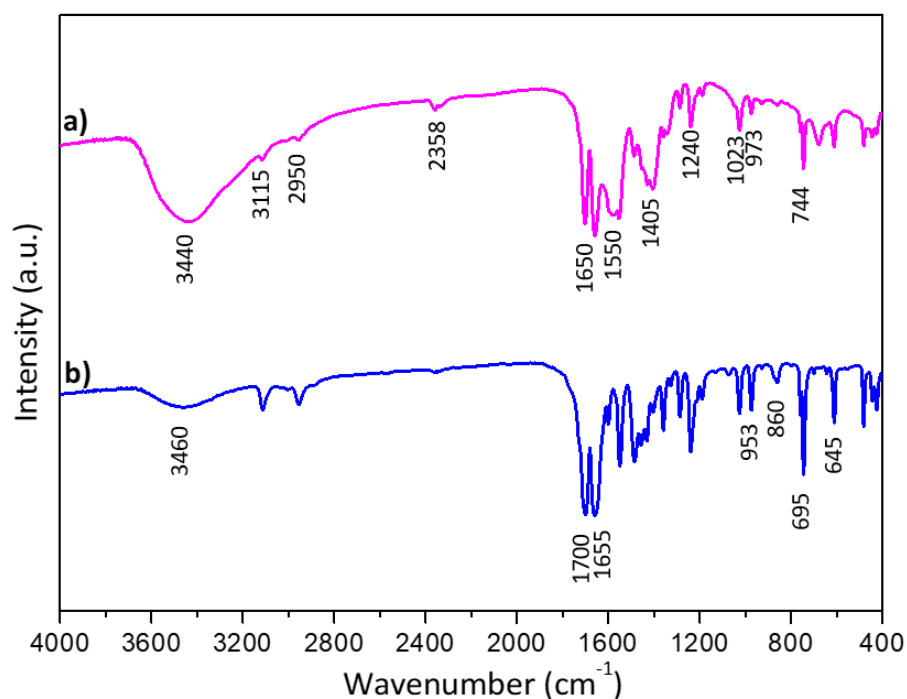
Figure 4.8: FTIR spectra: (a) Act_EtOH_caffeine; (b) caffeine

Regarding the Act_EtOH_caffeine, a broad and strong peak at 3440 cm^{-1} is related to the vibration of OH indicate the presence of water in the complex structure. Also, the appearance of both peaks associated with the vibration of –C=O groups (1700

cm^{-1} and 1650 cm^{-1}) indicates that complexation of Zn(II) did not occur via the oxygen atom. The weak band at 2358 cm^{-1} is associated with atmospheric carbon dioxide.

An analysis of specific peak areas was developed to evaluate the difference associated with the transmittance and presence of functional groups between the two substances (Table 4.6)**.** The vibration of CH$_3$ (1405 cm^{-1}) was taken as a reference as the methyl groups should not be affected by the Zn(II) complexation, once they are radicals attached to the main structure of the caffeine molecule. Peak areas were taken considering the same wavenumber interval.

Table 4.6: Ratio of peak areas of FTIR spectra of caffeine and Act_EtOH_caffeine samples

Wavenumber (cm^{-1})	Peak area (P$_a$)		Ratio P$_a$/P$_a$ (1405 cm^{-1})	
	Caffeine	Act_EtOH_caffeine	Caffeine	Act_EtOH_caffeine
1405 (-CH$_3$)	2551.54	2819.11	-	-
3460 (-OH)	2666.18	13493.57	1.04	4.79
1240 (-CH/-CN)	1434.47	689.36	0.56	0.24
1023 (-CN)	434.98	283.82	0.17	0.10
973 (rd)	379.94	125.44	0.15	0.04
645 (rd)	448.36	263.46	0.18	0.09

rd = ring deformation

A higher Act_EtOH_caffeine ratio for the OH stretching and H$_2$O vibration peaks in relation to the caffeine confirms the presence of water bonded to the complex. A decrease in the peaks related to the CN group (1240 cm^{-1} and 1023 cm^{-1}) was observed for the Act_EtOH_caffeine, indicating the complexation of the nitrogen with the Zn(II) due to a lower vibration of CN bonds. A lower ratio of ring deformation (973 cm^{-1} and 645 cm^{-1}) for the Act_EtOH_caffeine sample indicates a reduced vibration of the ring due to the formation of complexes [267]. All these findings corroborate with the complexation of the Zn (II) ions and the mechanism route for the green synthesis here proposed.

The mechanism of formation was designed specifically for ZnONPs synthesized with *Ilex paraguariensis* extract. However, the green synthesis of other metal oxides obtained from plant extract reported in the literature probably follows the same mechanistic route [258–273–275]. Likewise, the *Ilex paraguariensis* extract used in this study has great potential to be applied in the production of metal and metal oxides nanoparticles other the zinc oxide.

4.4   Characterization of zinc oxide nanoparticles

4.4.1   X-Ray diffraction (XRD)

XRD patterns of all samples synthesized are shown in Figure 4.9. All the peaks observed correspond to *zincite* (JCPDS nº 36-1451), a hexagonal form of ZnO, confirming the formation of this oxide [78]. Patterns of other crystalline structures were not observed, suggesting that the nanomaterial synthesized has high purity. The average crystallite size was estimated to be 19 nm for Nit_EtOH, 37 nm for Nit_H_2O, 24 nm for Nit_EtOHa, 61 nm for Act_H_2O, 59 nm for Act_EtOH, and 31 nm and 65 nm for Acetate and Nitrate, respectively, according to the Scherrer Equation [244] . The lattice parameters were determined according to the Bragg equation and considering all the identified planes of the hexagonal structure. The parameters were found to be a = 3.2518 Å and c = 5.2162 Å for samples obtained from zinc nitrate, and a = 3.2564 Å and c = 5.2166 Å for samples obtained from zinc acetate, corroborating with the literature [276–277].
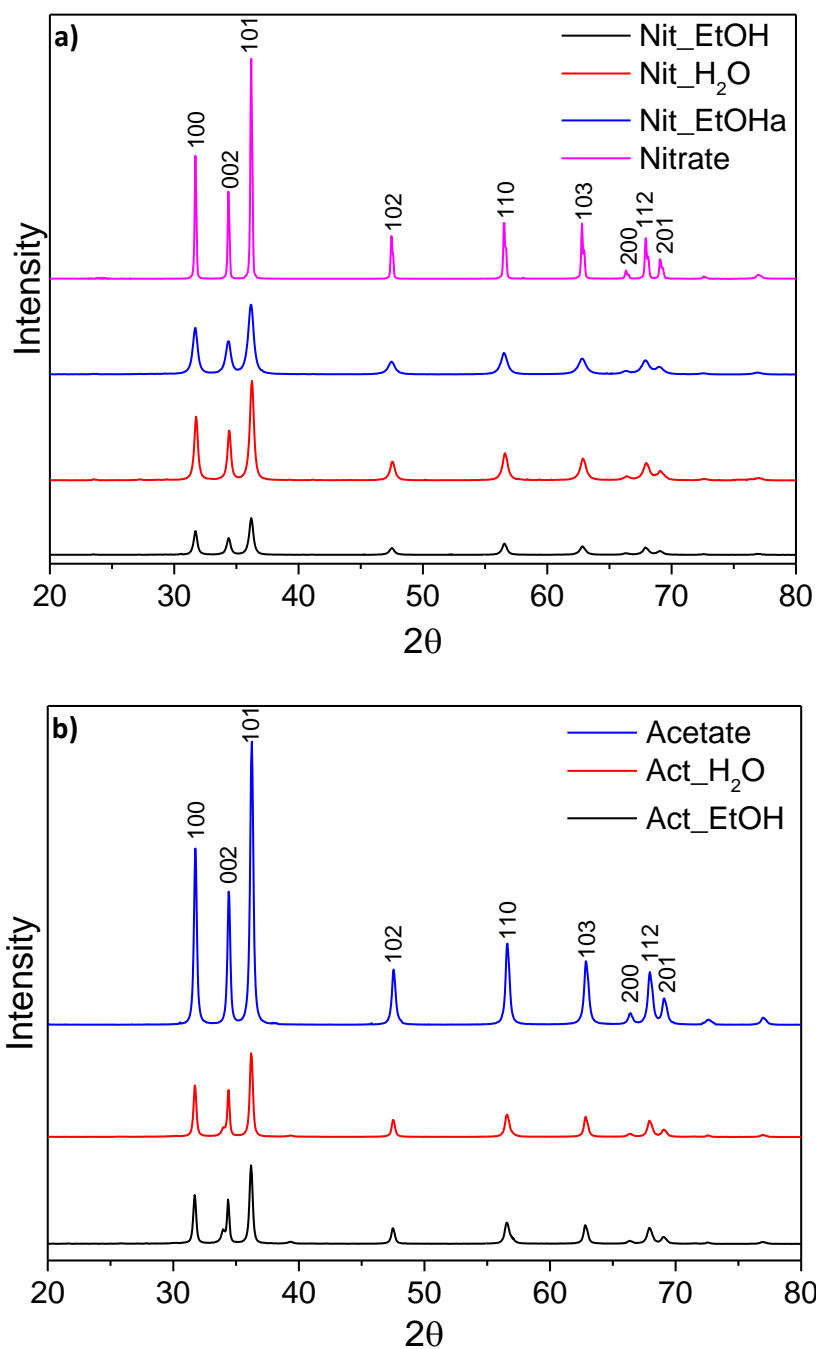
Figure 4.9: XRD pattern of ZnONPs synthesized with (a) zinc nitrate and (b) zinc acetate

4.4.2   Field emission scanning electron microscopy (FESEM) coupled with energy dispersive energy (EDS)

The surface morphology of all samples was studied by FESEM micrographs (Figure 4.10 and Figure 4.11). The samples produced from calcination of zinc nitrate

and zinc acetate (Nitrate and Acetate) showed triangular and rod particle morphology, respectively (Figure 4.10a-b and Figure 4.11a-b). Samples synthesized with the green route and zinc nitrate showed spherical shape (Figure 4.10c-h), while those synthesized with the green route and zinc acetate have irregular shapes and sizes (Figure 4.11c-f).

Samples obtained with *mate* extracts and zinc nitrate have the smallest particle size (Figure 4.10c-h). In addition, the synthesis with 50% (v/v) ethanol extract (Figure 4.10e-h) resulted in more uniform shape and size particles than the sample obtained with an aqueous extract (Figure 4.10c-d). According to the HPLC analysis, the ethanolic extract has a higher concentration of antioxidants compounds, favoring the complexation of Zn(II), which results in more uniform particles. The influence of calcination can be evaluated from Figure 4.10e-h, where the sample Nit_EtOH (calcinated) presented more homogeneous particles than the sample Nit_EtOHa (without calcination). However, depending on the applciatioin, the sample without calcination can be employed as it requires less energy for production.

Different morphologies were observed for ZnONPs obtained by the biological method using a variety of plant extracts. For instance, Nava *et al.* [21] obtained ZnONPs from fruit peel extract and zinc nitrate with a polyhedral shape. Bala *et al.* [25] used *Hibiscus subdariffa* and zinc acetate to produce spherical ZnONPs that formed agglomerates with a cauliflower shape. On the contrary, Anbuvannan *et al.* [5] produced ZnONPs from *Phyllantus niruri* leaves extract and zinc nitrate with irregular morphology. However, the methodologies applied in each synthesis were different and a comparison among the morphologies obtained is not plausible.
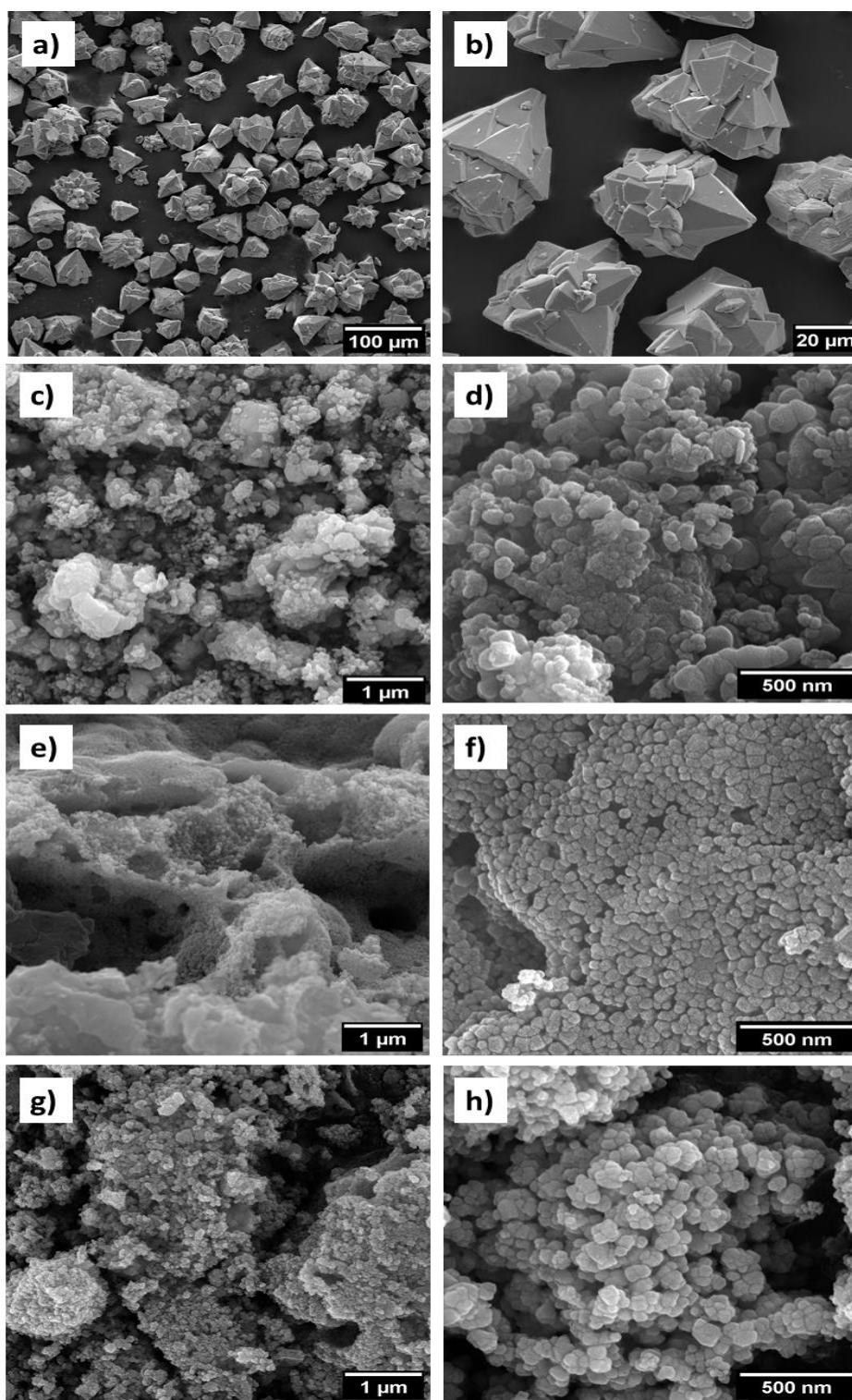
Figure 4.10: FESEM micrographs of ZnO synthesized from zinc nitrate: (a-b) Nitrate (control); (c-d) Nit_H$_2$O; (e-f) Nit_EtOH; (g-h) Nit_EtOHa
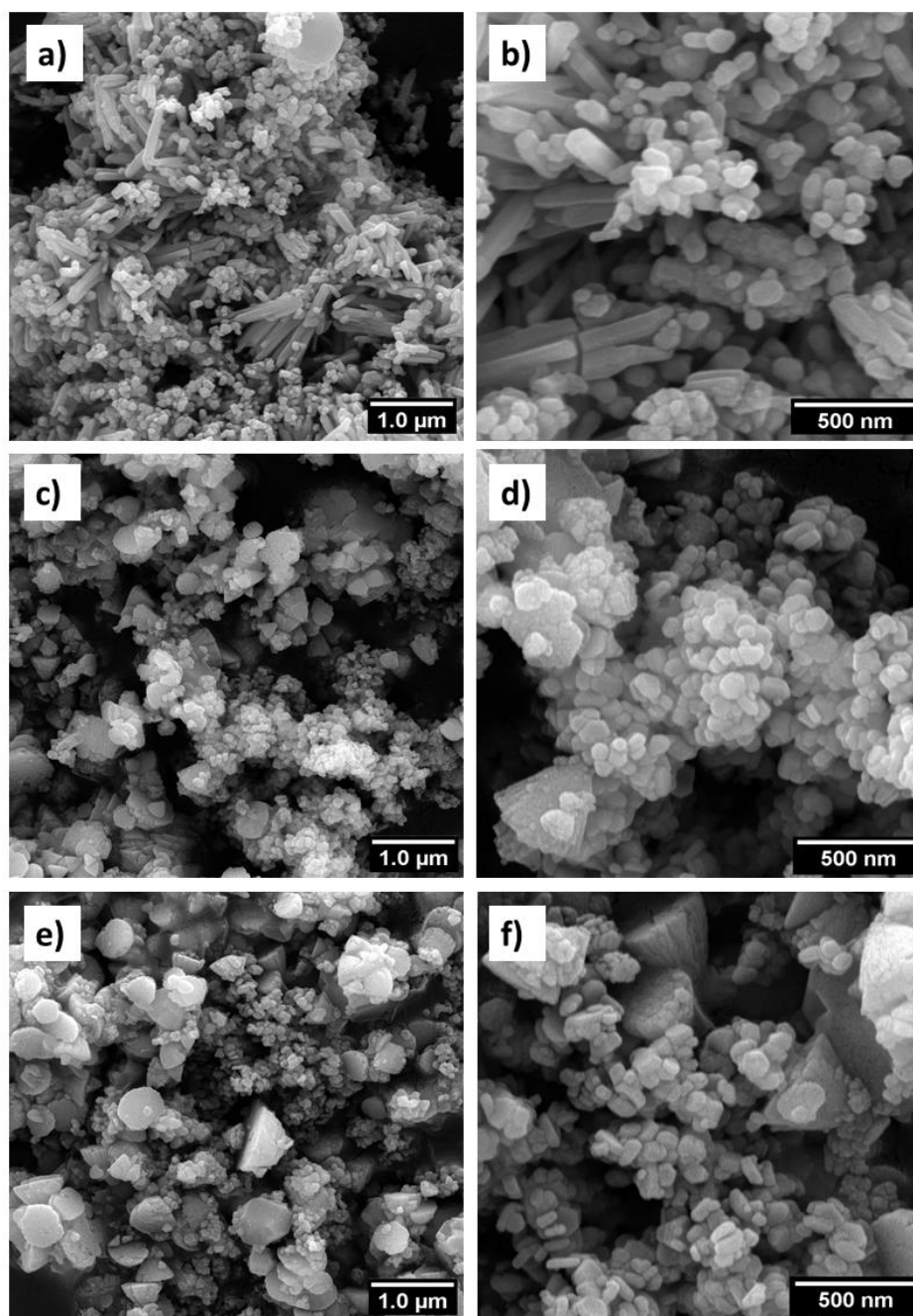
Figure 4.11: FESEM micrographs of zinc oxide synthesized from zinc acetate: (a-b) Acetate (control); (c-d) Act_H_2O; (e-f) Act_EtOH

EDS results of all green synthesized ZnONPs are shown in Figure 4.12**.** In theory, ZnO has 80.3% of Zn content. Thus, the ZnONPs synthesized from *Ilex paraguariensis* extract have shown high purity with approximately 70-80% of Zn content, with exception of the sample Act_H_2O that presented a lower Zn content (67%). The presence of C, O, and a small peak related to K may be originated from the plant

compounds. Similar results were observed for ZnONPs obtained from other plant extracts [22–25].
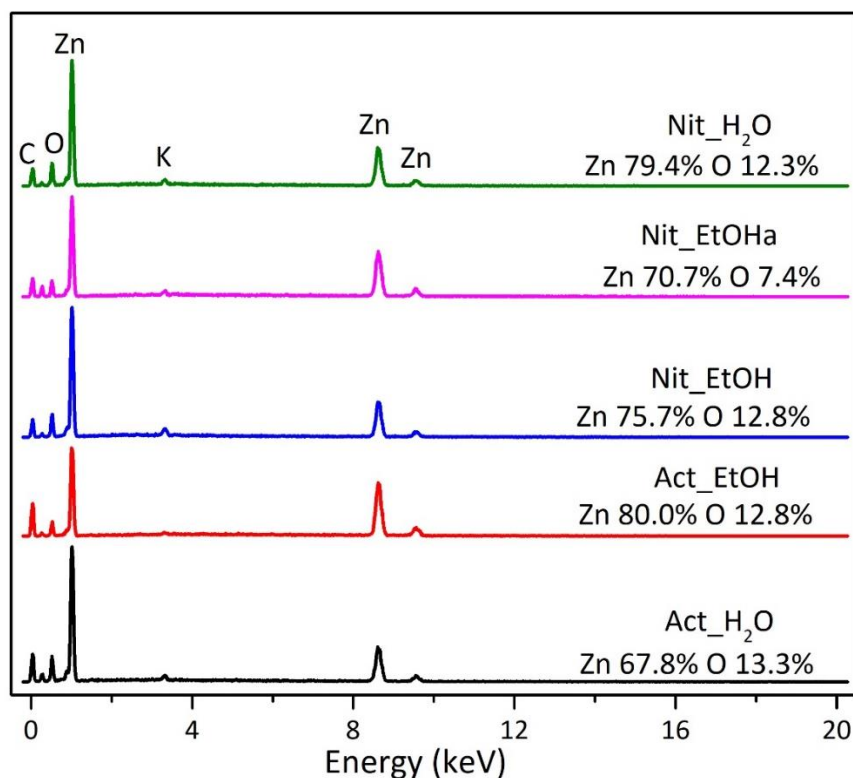
Figure 4.12 EDS spectra of green synthesized ZnONPs

4.4.3 Transmission electron microscopy (TEM)

Particle size was determined by TEM micrographs (Figure 4.13), except for the sample Nitrate because its size is greater than the size limit of analysis of a transmission electron microscope (~1μm) and was determined by FESEM. Table 4.7 shows the mean particle size for each sample. Samples green synthesized with zinc nitrate are formed by a single crystal, as the particle sizes are similar to the crystallite size determined by XRD, while the other samples are formed by several crystallites.
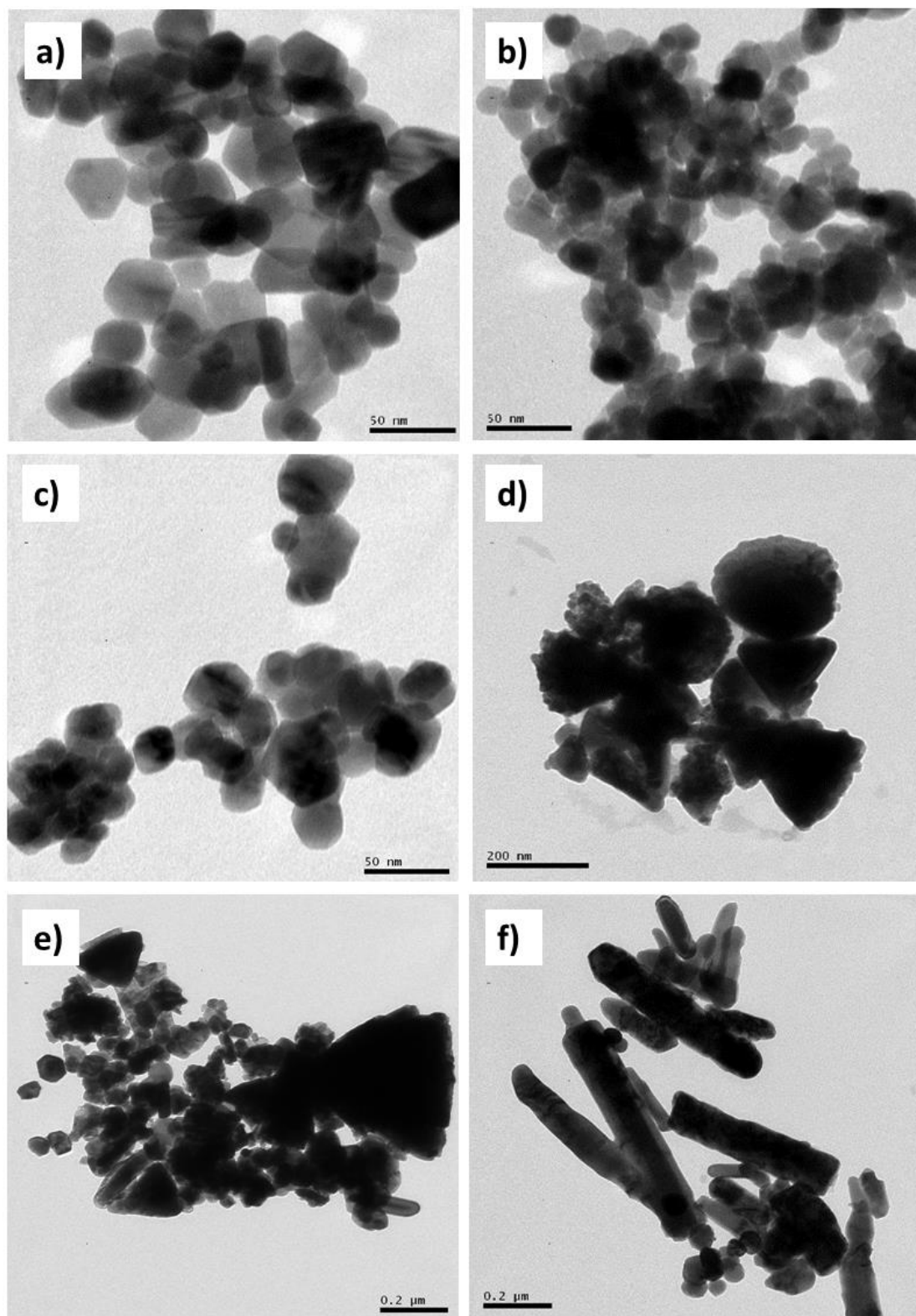
Figure 4.13: TEM micrographs of (a) Nit_H_2O; (b) Nit_EtOH; (c) Nit_EtOHa; (d) Act_H_2O; (e) Act_EtOH; (f) Acetate (control)

Table 4.7: Mean size of the ZnONPs samples

Sample	Mean size (nm)
Nitrate	53 ± 8 µm*
Nit_H$_2$O	33 ± 9
Nit_EtOH	18 ± 5
Nit_EtOHa	29 ± 10
Acetate	389 ± 249
Act_H$_2$O	176 ± 50
Act_EtOH	116 ± 103

*Result is given in micrometers (µm)

Samples synthesized by green synthesis showed reduced particle size in comparison to the samples obtained only from the calcination of zinc salts (Nitrate and Acetate), confirming the influence of *mate* extract to obtain ZnONPs in nanometric size. It was observed that using zinc nitrate (Figure 4.13a-c) in the green synthesis route resulted in particle sizes in the approximate range of 18 to 33 nm, which exhibited a reduction of particle size in comparison to using zinc acetate (Figure 4.13d-e). This difference in the particle size possibly occurred due to the number of nucleation sites that were formed during the synthesis.

The nucleation process is the first stage of a crystal formation in which the atoms organize in a crystal structure thermodynamically stable forming the crystal nucleus from where the particle grows [278]. In the case of Nitrate and Acetate, Zn(II) ions were very close, resulting in fewer nucleation sites and consequently larger particle sizes. Conversely, the samples Nit_EtOH, Nit_EtOHa, and Nit_H$_2$O were complexed by the antioxidants present in the *mate* extracts that kept the Zn(II) separated, originating more nucleation sites and smaller particle sizes.

The samples Act_EtOH and Act_H$_2$O showed increased particle size and more irregular shape than the samples Nit_EtOH, Nit_EtOHa, and Nit_H$_2$O. This may have

occurred because the Zn(II) of the samples containing zinc acetate were not completely complexed by the *mate* compounds as shown in the cyclic voltammetry analysis, resulting in fewer nucleation sites. Also, Krezel and Maret [279] evaluated the inorganic chemistry of zinc ions and reported that acetate anions have a stronger coordination binding to zinc (II) ions in comparison to nitrate anions. The authors also observed that the fraction of free Zn(II) ions from a nitrate solution is nearly 100% while from an acetate salt solution is about only 50%. Moreover, when zinc acetate is dissolved in water, the acetate anion reacts with water, forming hydroxyls that increase the pH solution. In more basic solutions, the formation of $Zn(OH)_2$ species occurs, decreasing the concentration of free Zn(II) ions [279]. Therefore, fewer Zn(II) ions were free in solution to coordinate with the active compounds of the plant extract when using zinc acetate compared to zinc nitrate, which might have resulted in the varied particle size.

ZnONPs obtained by plant extracts and zinc nitrate have exhibited particle sizes of approximately 10 to 50 nm [5–21–25]. Nonetheless, when using zinc acetate as the metal precursor, research studies have presented a contrast on the ZnONPs size that varied from *quantum dots* of only 3-9 nm to clusters of 500 nm [107–108]. However, the extract composition and synthesis method differ among these works and cannot be directly compared.

4.4.4   Ultraviolet and visible spectroscopy (UV-vis)

Figure 4.14 shows the UV-Vis spectra of all green synthesized ZnONPs and their respective E_{bg}. All samples showed absorption peaks between 360 and 380 nm and E_{bg} around 3.3 eV characteristic of ZnONPs [280–282]. The difference between the

samples corroborates with the findings of Goh et al., where a decrease in particle size

led to a shift of the maximum absorbance to lower wavelengths and E_{bg} [283].
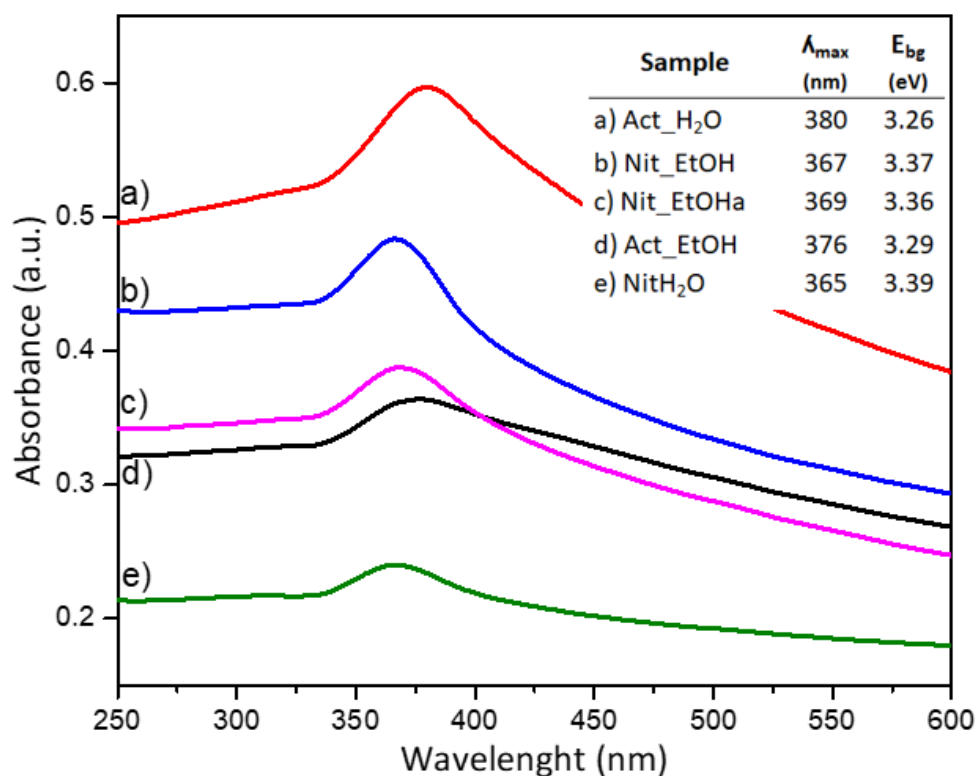
Figure 4.14: UV- vis spectra of the green synthesized ZnONPs

4.4.5 Cell viability assay

The cytotoxicity of ZnONPs was evaluated with L929 cells for the samples

Nit_ETOH, Nit_EtOHa e Nit_H$_2$O, as they showed reduced size and regular shape, and

for the sample Act_EtOH to compare the cytotoxicity of both zinc sources. Cell viability

for ZnONPs concentrations varying from 1-25 µg mL^{-1} is shown in Figure 4.15.

Cell viability decreased with the increase of ZnONPs concentration in all samples.

However, the samples Nit_EtOH exhibited low cytotoxicity for concentrations varying

from 1 to 10 µg mL^{-1}, as cell viability was not affected in this range of concentration.

Syama *et al.* [284] also observed no cytotoxicity up to a concentration of 10 µg mL^{-1} when treating L929 cells with spherical ZnONPs ranging from 20 to 40 nm. Different from our findings, the authors found that cell viability decreased only around 20% for samples treated with 20 µg mL^{-1} while cells treated with Nit_EtOH resulted in a decrease of around 50%. Paino *et al.* [285] reported low levels of necrosis and apoptosis when treating the same type of cells with ZnONPs in concentrations lower than 10 µg mL^{-1}.
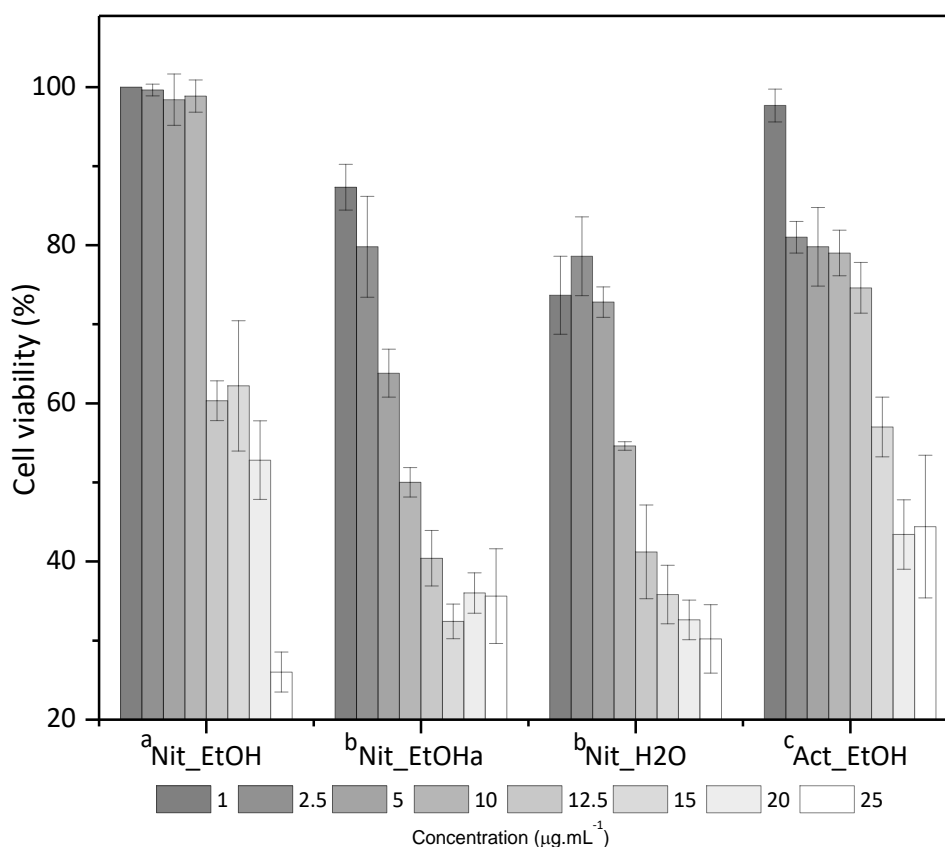
Figure 4.15: L929 cell viability after treatment with ZnONPs. Samples with different letters represent significant difference (p < 0.05)

The LC50 (concentration to reduce cell viability by 50%) was determined as 18 µg mL^{-1} for Nit_EtOH and Act_EtOH, 9 µg mL^{-1} for Nit_H$_2$O, and 7 µg mL^{-1} for Nit_EtOHa. These results suggest that the samples Nit_EtOH and Act_EtOH have lower cytotoxicity

in comparison to the other samples. Hence, a higher concentration of nanoparticles was required to reduce cell viability by 50%. On the contrary, the sample Nit_EtOHa was the most cytotoxic. This sample was not calcinated which may have resulted in the presence of Zn(II) species, NO_2^- and $-COO^-$ that may affect cell viability. Therefore, as the sample Nit_EtOH exhibited the least cytotoxic, further analysis was performed to evaluate the difference of cell viability through the different concentrations.

4.4.6   Morphological analysis of L929 cells

Morphological tests in L929 cells were developed with the samples (Nit_EtOH, Act_EtOH, Nit_EtOHa, and Nit_H$_2$O) to evaluate the morphological parameters with Giemsa staining through optical microscopy (Figure 4.16 a, d, g, j, m) and FESEM (Figure 4.16 b, e, h, k, n).

Micrographs of both methods show similarities with elongated cytoplasm in control samples (Figure 4.16 a, b, c) and cytoplasmic retraction and chromatin condensation points for the sample treated with Nit_EtOH (Figure 4.16 d, e, f). Other treatment conditions with Act_EtOH, Nit_EtOHa, and Nit_H$_2$O showed cellular morphology with intermediary nuclear and cytoplasmatic condensation when compared to the control and Nit_EtOH samples. These results may have been related to the reduced size and regular morphology of Nit_EtOH nanoparticles which can facilitate the internalization of this nanomaterial into the cell, altering its biochemical and morphological structure [286]. It is relevant to observe that samples exposed to Nit_EtOH exhibited a cell survival *plateau* up to a maximum concentration of ~10 µg mL^{-1}, displaying cytotoxicity in higher concentrations.

These findings corroborate with similar reports related to the cytotoxicity of ZnONPs nanostructures. Syama *et al.* [284] observed a change from elongated to round shape after treating L929 cells with ZnONPs at 50 µg mL^{-1}. Satimano *et al.* [287] report morphological changes in human A549 cells from polygonal to granules appearance after treatment with different concentrations of ZnONPs.
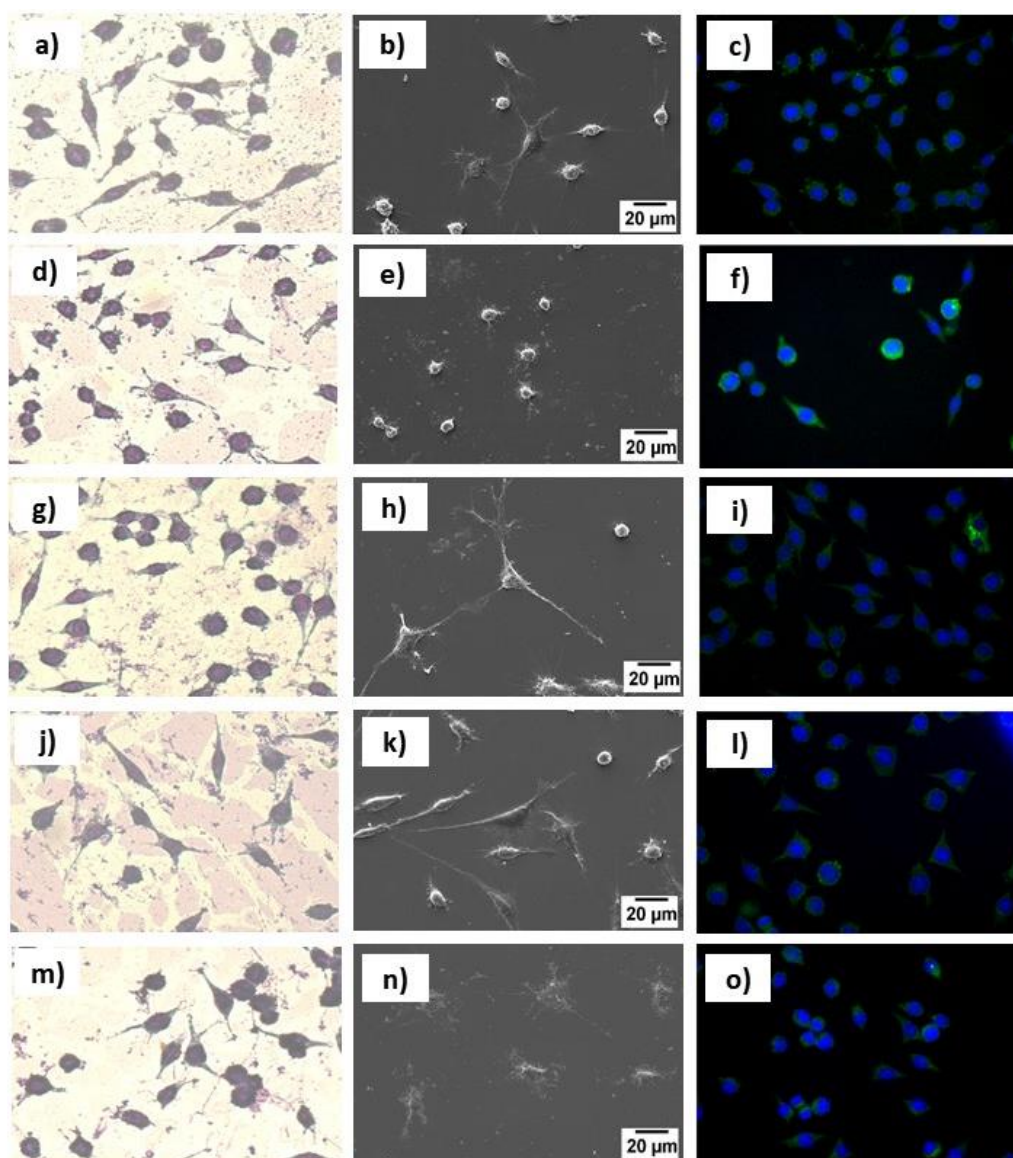
Figure 4.16: LC3A/B expression in cells L929 after 24h of exposure to ZnONPs (Nit_EtOH, Act_EtOH, Nit_EtOHa, and Nit_H$_2$O) with concentrations related to each IC50. a, b, c – control samples; d, e, f – samples exposed to NitEtOH; g, h, i – samples exposed to Act_EtOH; j, k, l – samples exposed to Nit_EtOHa; m, n, o – samples exposed to Nit_H$_2$O.

4.4.7   Indirect immunofluorescence analysis

Indirect immunofluorescence tests were developed in L929 cells to evaluate if the morphological alterations in treated cells observed using Giemsa staining and FESEM were related to autophagosome effects due to internalization and deposition of ZnONPs on this vesicle. Cells were exposed to the ZnONPs (Nit_EtOH, Act_EtOH, Nit_EtOHa e Nit_H$_2$O) for 24h with concentrations related to the LC50. An increase of LC3A/B expression in cells exposed to Nit_EtOH (Figure 4.16f) was verified in comparison to negative control and cells exposed to other samples (Figure 4.16 c, i, l, o). Expression parameters of LC3A/B are evaluated with topographic qualitative reading in the cell cytoplasm, more specifically in phagocytic regions, evidencing more intense green staining for the sample treated with Nit_EtOH (LC50 concentration). All conditions exhibited blue staining on the nuclear region to locate cellular structures.

To evaluate the LC3A/B protein expression in L929 cells exclusively to the sample Nit_EtOH, a second investigation was developed with a crescent concentration gradient treatment (5-15 µg mL^{-1}) with an exposure period of 24 h. This analysis showed an evident increase in the LC3A/B expression after exposure to Nit_EtOH in concentrations higher than 10 µg mL^{-1} (Figure 4.17 e and f). For comparison, cells were exposed to a positive control (rapamycin 100 nmol L^{-1}) that exhibited LC3A/B expression compatible with cells treated with high concentrations of Nit_EtOH (Figure 4.17 e, f, g). Topographical distribution using indirect immunofluorescence analysis revealed that cells treated with different ZnONPs progressively increased LC3A/B expression, confirming the affinity of this protein in the autophagosome of cellular structures.
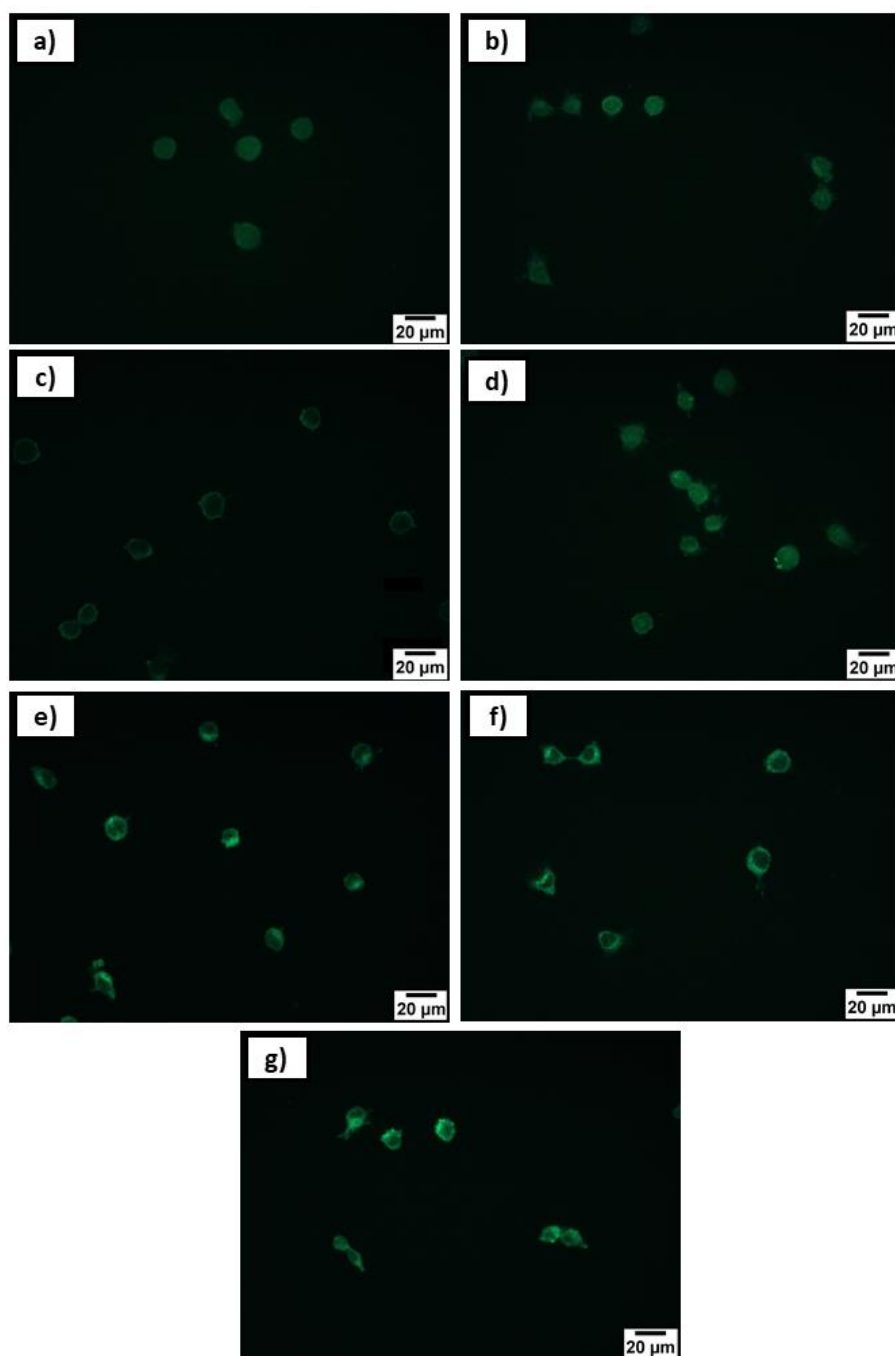
Figure 4.17: LC3A/B expression in L929 cells after 24 h of exposure to Nit_EtOH in a crescent gradient of concentration (b- 5 µg mL^{-1}; c-7,5 µg mL^{-1}; d- 10 µg mL^{-1}; e-12,5 µg mL^{-1}; f- 15 µg mL^{-1}). a – negative control, without treatment; g – positive control, treated with autophagy inducer rapamycin (100 nmol L^{-1}), with a cellular marker pattern of LC3A/B similar to elevated concentrations of Nit_EtOH (e, f)

4.4.8   Antimicrobial activity

An antibacterial assay was performed to evaluate the antimicrobial potential of the sample Nit_EtOH, exclusively, in different concentrations (15 to 55 µg mL^{-1}). The results are shown in Figure 4.18. Overall, ZnONPs showed antimicrobial activity in a dose-dependent manner to both bacteria strains. However, higher antimicrobial activity was observed in Gram-positive (*S. aureus)* compared to Gram-negative (*E. coli*) bacteria. The minimum inhibitory concentration (MIC) is determined as the lower concentration where no resazurin reduction occurred. Therefore, the MIC of ZnONPS for the Gram-positive *S. aureus* was 35 µg mL^{-1}, while the Gram-negative *E. coli* showed higher resistance with 70% viability in the highest concentration tested (100 µg mL^{-1}).
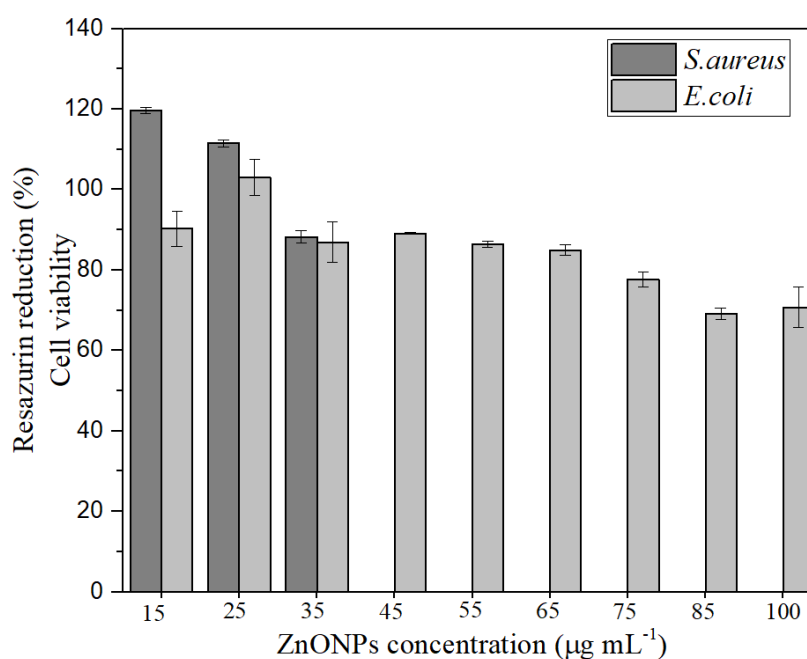
Figure 4.18: Antimicrobial activity of eco-friendly ZnONPs

Previews works have also reported higher toxicity of ZnONPs to Gram-positive bacteria than Gram-negative [65–288–290]. This feature is related to the different cell structures of Gram-positive and Gram-negative bacteria. The antimicrobial activity

mechanism of metal and metal oxide nanoparticles involves membrane damage, nanoparticle internalization, metal ions, and ROS that affect cell metabolism [21–106]. For instance, Gram-positive cells have a thicker peptidoglycan layer than Gram-negative bacteria. Nonetheless, Gram-negative bacteria have an outer membrane surrounded by lipids and proteins, which can result in higher resistance to nanoparticle and metal ions penetration into the cell. Moreover, Gram-positive bacteria have a more negatively charged surface, which facilitates the attraction of positive ions, such as Zn(II) ions that can be released from the dissolution of ZnONPs [66–291].

4.4.9   Summary

ZnONPs were synthesized using *Ilex paraguariensis* leaves extract. A mechanism route for the green synthesis of this nanomaterial was designed, in which the antioxidants of the plant extract form coordinated complexes with Zn(II) and nanoscale particles of ZnO were formed via thermal degradation of these complexes. Samples obtained with zinc nitrate exhibited reduced particle size and a more regular shape than those synthesized with zinc acetate. These findings might be related to the fact that Zn(II) present in the synthesis with zinc acetate did not react with the plant compounds in total, as observed in the cyclic voltammograms.

Ethanol increased the extraction of active compounds from the plant resulting in more uniform particles. Therefore, the sample obtained with zinc nitrate and 50% (v/v) ethanol extract showed the smallest and more uniform size, which can be effective for photocatalytic and biological applications.

Cell viability decreased with increasing of ZnONPs concentration to all samples. However, sample Nit_EtOH showed no cytotoxic effects for concentrations up to a

limit of 10 µg mL^{-1}. Morphological analysis showed a degree of the nucleus and cytoplasmic condensation for cells treated with all ZnONPs samples. Small and uniform ZnONPs were able to internalize cells and form deposits in the phagosome, which can initiate metabolic processes of cell death in elevated concentrations. Finally, the ZnONPs synthesized here can be applied in biocompatible materials in low concentrations and for the development of novel therapies within the cells.

The antimicrobial assay showed a higher antimicrobial activity to *S. aureus* than *E. coli* strains, which is probably related to the difference in the cell structure of Gram-negative and Gram-positive bacteria strains. While no bacteria growth was observed for *S. aureus* strain in concentrations higher than 35 µg mL^{-1}, only 30% of *E. coli* inhibition was observed at a concentration of 100 µg mL^{-1}.

Considering that the sample Nit_EtOH presented the lower cytotoxicity and uniform morphology and size, this sample was further tested in the biomaterials developed in this work and will be addressed as solely ZnONPs in the following chapters.

Thin films

CHAPTER 5:   **Development of biocompatible PAA/PAH thin films containing green synthesized zinc oxide nanoparticles and *Ilex paraguariensis* extract**

5.1   Introduction

A wide range of composites has been developed to enhance the performance of biomedical devices, mainly to avoid infections and to improve the biocompatibility of the device [292–294]. Polymeric thin films have shown to be a promising coating material to solve these issues, once they can be loaded with antimicrobial substances or substances that improve cell adhesion and proliferation [295]. Moreover, polymeric films have a low thickness and flexibility, thus not interfering in the physical and mechanical characteristics of the coated device [201]. A variety of thin films has been investigated for implant and catheter coating [198–296], drug-release [297], infection prevention [198], among other biomedical applications.

Among the materials used to obtain these thin films, polyelectrolyte systems were found to be extremely attractive due to their tuneable properties. These types of polymers become ionized when in solution, forming a polycation or polyanion, depending on their charge. In addition, when oppositely charged polyelectrolytes are in contact, they can easily form polymer complexes through electrostatic interaction [193].

A simple technique to obtain polyelectrolyte thin films is the layer-by-layer (LbL) method by dip-coating, where a substrate is dipped in a sequence of solutions containing a polycation and a polyanion, resulting in a multilayer thin film [203]. One of the main advantages of this method is that the final properties of the thin films can be easily modified by varying the polyelectrolyte solution pH, concentration, and the

number of layers. Moreover, functional substances can be added to the polymer solutions to obtain a composite thin film with specific properties [193–203–297].

In this work, a multilayer thin film was obtained using polyacrylic acid (PAA) and polyallylamine hydrochloride (PAH) polyelectrolytes using the LbL approach. These polyelectrolytes form stable thin films and were shown to have biocompatibility [205–206]. Moreover, the incorporation of nanomaterials in PAH/PAA systems has also been reported to successfully achieve specific characteristics, like antimicrobial activity, hydrogen production, and drug degradation [43–213–214].

The thin film developed in this study was loaded with green synthesized ZnONPs and *Ilex paraguariensis* extract, aiming to obtain a thin film coating with antimicrobial activity and biocompatibility to enhance the performance of biomedical devices by preventing infections. ZnONPs presents good antimicrobial activity towards different microorganisms. Besides, this nanomaterial is a promising substitute for antibiotics that are now resistant to bacteria [298–299].

The ZnONPs were green synthesized with *Ilex paraguariensis* (IP) leaves extract, using a more eco-friendly and less cytotoxic approach to obtain this nanomaterial as no toxic solvent is used in the process [13–300]. The IP extract used in the synthesis holds important properties for biomedical applications, such as anticancer and antimicrobial properties [32–167]. This feature is related to the high concentration of polyphenols, flavonoids, and methylxanthines present in the plant composition [30]. Moreover, a synergistic effect between ZnONPs and plant extract active compounds was found to improve the antimicrobial activity of a composite material built with cellulose, ZnONPs, and propolis extract [301].

To the best of my knowledge, no polyelectrolyte thin film has been produced using metal oxide nanoparticles and natural plant extract. Therefore, this study aims to investigate the synthesis of a PAH/PAA composite biomaterial containing ZnONPs and IP extract to be used as an antimicrobial coating in biomedical applications.

To evaluate the thin film synthesis, a design of experiments was carried out by varying the PAH pH solution, the concentration of ZnONPs, and the addition of IP extract. Then, the thin films were characterized according to their ZnONPs content by ICP-OES and antimicrobial activity against *S.aureus* bacteria strain.

5.2   Dynamic light scattering (DLS)

The particle size distribution of ZnONPs agglomerates in solution was evaluated using DLS analysis for every combination of PAH pH solution and ZnONPs concentration used for synthesizing the thin films. The results are shown in Figure 5.1, including the intensity (MI) and number (MN) hydrodynamic particle size means for each test condition. All ZnONPs solutions presented a unimodal distribution and similar hydrodynamic diameter. The average intensity diameter was 260 nm and 95 nm for the number diameter. The hydrodynamic particle diameter is higher than the actual size (~18 nm determined by TEM in Chapter 3) as particle aggregates are commonly formed in solution and the DLS technique accounts not only for the core particle size but also the solvent and polymer adsorbed in the particle [302–303].

The DLS results indicate a stable and uniform distribution of the ZnONPs in PAH solutions, despite the solution pH. In addition, the increase in ZnONPs concentration did not affect particle dispersion, as the distribution continued unimodal, and the hydrodynamic diameter was comparable for the three concentrations. These findings

corroborate with the findings of Liufu *et al.* [303], where the adsorption layer did not change significantly when dispersing ZnONPs in a low concentration of polyelectrolyte aqueous solution despite the pH media. However, the adsorption layer was found to be dependent on the pH solution when dispersing the ZnONPs in higher concentrations of polyelectrolytes (> 8 mmol L^{-1}).
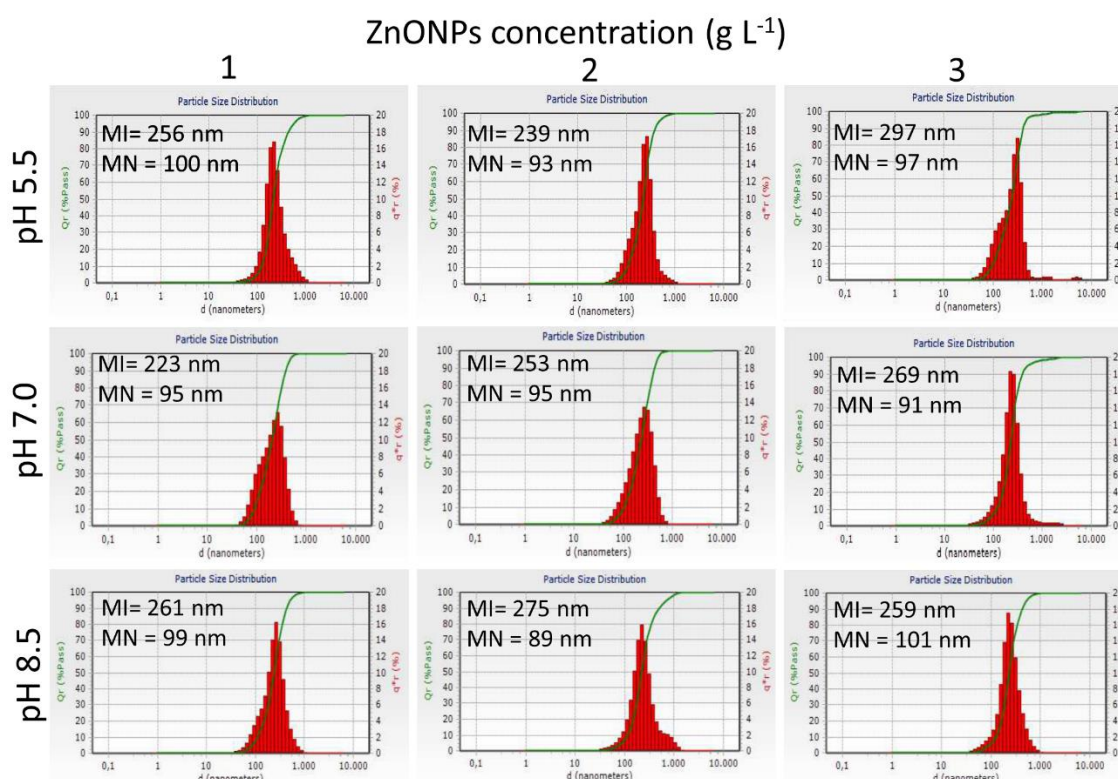
Figure 5.1: Particle size distribution of ZnONPs in PAH 5mM solutions.
MI= Intensity mean; MN= Number mean

5.3 Zinc quantification by inductively coupled plasma – optical emission spectrometry (ICP-OES)

ZnONPs concentration was determined by means of Zn(II) ions quantification using ICP-OES analysis and is described in Table 5.1. The ZnONPs concentration in each film was determined considering that ZnO contains 80.3% of Zn(II). In general, the

concentration of ZnONPs adsorbed in the thin films varied from 0.72 to a maximum of 1.25 µg cm^2. These results are further discussed according to the full factorial DOE in the next section.

Table 5.1: ZnONPs concentration in the different thin films formulations

Sample	PAH pH	ZnO (g L^{-1})	IP (g L^{-1})	ZnO (µg cm^2)
TF1	5.5	1.0	0.0	0.85
TF2	8.5	1.0	0.0	1.18
TF3	5.5	3.0	0.0	0.99
TF4	8.5	3.0	0.0	1.25
TF5	5.5	1.0	50	0.75
TF6	8.5	1.0	50	0.88
TF7	5.5	3.0	50	0.72
TF8	8.5	3.0	50	1.12
TF9	7.0	2.0	25	0.92
TF10	7.0	2.0	25	1.03
TF11	7.0	2.0	25	0.86

5.4 Design of experiment (DOE)

The DOE was developed to evaluate the influence of the PAH solution pH and the concentration of ZnONPs and IP extract on the synthesis of the LbL thin films. The PAH pH range of 5.5 to 8.5 was chosen considering the stability of ZnONPs in the solution. This stability was evaluated in terms of the isoelectric point and the solubility of ZnO.

Literature reports that the isoelectric point of ZnO in solution is around pH 9.0-10 [255–304]. The consideration of this parameter is essential as at the isoelectric point the particles have no electric charge and, therefore, are unstable in solution. Thus, the maximum pH was set below the isoelectric point, at 8.5. The minimum pH used was 5.5, considering that ZnO dissolves completely in more acidic solutions.

Even though using a low range of pH, the protonation of PAH changes considerably, as shown in Table: 5.2, affecting the linearity of the polymer chains. The higher the degree of ionization, the more linear is the polymer chains due to charge repulsion. The PAA pH was kept constant at 4.0, as it resulted in more uniform and stable films, according to preliminary tests (data not shown). At this pH, PAA is only 10% ionized [194–305].

Table: 5.2: Degree of ionization of PAH in different pH solutions

pH	Degree of ionization
5.5	90%
7.0	80%
8.5	50%

The plant extract was prepared in an aqueous solution and its composition was discussed in Chapter 4. For this variable, the concentrations were varied from 0 to 50 g L^{-1} and added to the PAA solution. To the best of our knowledge, no polymer thin film developed by the LbL method containing plant extracts has been reported in the literature.

A statistical analysis of the DOE was carried out to evaluate the effect of the three factors on the adsorption of ZnONPs in the thin films, using the results obtained in the ICP-OES analysis. Table 5.3 presents the ANOVA results, where the significant parameters are highlighted in red, considering a 90% confidence interval. Only the pH of PAH solution and the concentration of IP extract significantly affected the deposition of ZnONPs in the thin films ($p < 0.1$).

Table 5.3: ANOVA results for the DOE according to the adsorption of ZnONPs using a 90% confidence interval (p<0.1)

Factor	Effect	Coefficient	*t*	p
Curvature	-0.062	-0.031	-0.456	0.679
(1) pH PAH	0.286	0.143	4.038	0.027
(2) ZnONPs (g L^{-1})	0.105	0.052	1.483	0.235
(3) IP (g L^{-1})	-0.198	-0.099	-2.795	0.068
1 by 2	0.054	0.027	0.756	0.505
1 by 3	-0.015	-0.008	-0.217	0.842
2 by 3	-0.002	-0.001	-0.029	0.978

R^2= 0.900; R^2_{adj}= 0.668

Studies report the influence of the polyelectrolyte solution pH on the synthesis and properties of thin films, such as the surface area, thickness, and roughness [194–305]. Therefore, it was expected that the pH solution also controlled the incorporation of ZnONPs.

Even though many studies report the incorporation of nanoparticles in PEM films, no study has investigated the relation between ZnONPs adsorption and the pH solution so far [43–213–214]. However, Liufu *et al.* [303] examined the adsorption of polyelectrolytes on the surface of ZnONPs. The polymer adsorption was found to be dependent on the polymer concentration, ionic strength, and solution pH. More specifically, the increase of pH from 5.4 to 10 led to higher adsorption of polyelectrolyte, evidencing a higher interaction of the nanomaterial with the polyelectrolyte in more basic pH conditions.

In addition, Tang *et al.* [306] evaluated the interaction of polyelectrolytes and semiconductor nanoparticles. The authors observed a higher nanoparticle density on polydiallydimethylammonium chloride (PDDA) film surface when increasing the pH solution of the polyelectrolyte. Nonetheless, the mentioned studies are punctual works, where the nanoparticles were investigated against other types of polyelectrolytes than those used in this work. Thus, a strong comparison with these

studies cannot be stated as the polymers have different compositions, ionic charges, and behaviour in solution.

Regarding the IP extract concentration, it was observed in Chapter 3 that it is constituted by different active compounds, which contain hydroxyl (-OH) and carboxyl (-COOH) groups. Therefore, the higher the degree of ionization of the polycation, the stronger the electrostatic interaction between the polymer and the plant extract will be. Likewise, a study involving the complexation of quercetin (flavonoid) and chitosan (polycation) has reported the interaction of both materials through the ionic interaction of the hydroxyls groups of the flavonoid with the amino groups of chitosan [307].

The concentration of ZnONPs in the solution showed no significant changes in the final concentration of ZnONPs present in the thin film. This fact may be related to the high concentration of nanoparticles used in the synthesis solution (1-3 g L^{-1}), in comparison to the amount that was adsorbed in the multilayer film (approximately 1 µg cm^{-2}). Moreover, no significant nanoparticle distribution in solution was visualized when altering the pH or concentration of ZnONPs in solution, as discussed in the DLS analysis (item 5.2). The curvature effect was also not significant, which implies that the surface response of the DOE follows a linear mathematical model [247].

The surface response of the ZnONPs adsorption as a function of the IP extract and the PAH pH is shown in Figure 5.2. The response was determined considering the lowest level of ZnONPs solution (1 g L^{-1}), as this factor was not significant (p>0.1). The higher the PAH pH and the lower the IP extract, the more nanoparticles are adsorbed in the thin films.

According to Liufu *et al.* [303], polyelectrolytes stabilize ZnONPs through electrosteric interaction, and this stabilization increases in more basic pH conditions, which might have contributed to higher adsorption of nanoparticles on the thin films. In addition, in higher pH conditions, PAH charge density decreases, resulting in less linear polymer chains, due to a lower repulsion of the amino groups. A folded conformation of the polymer chains results in an increase of film rugosity and thickness, which is reported to improve particle incorporation [214].
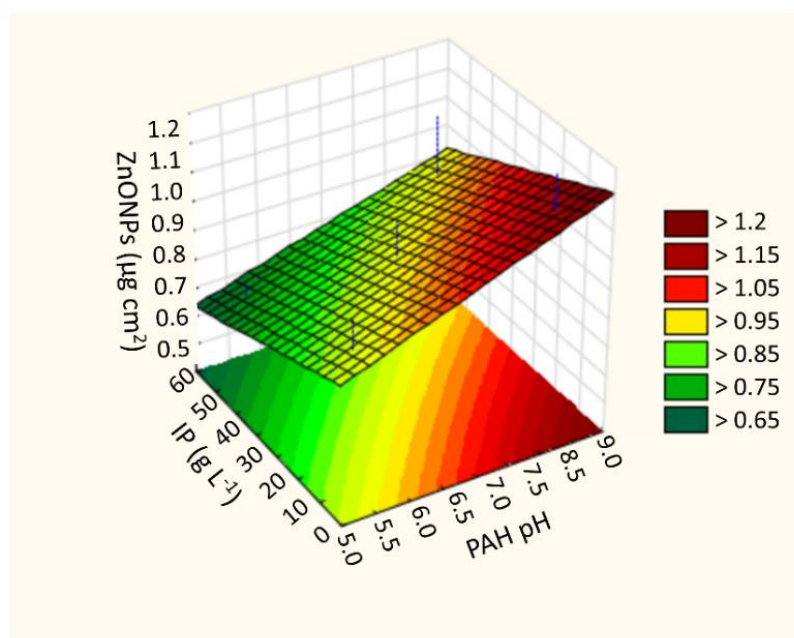
Figure 5.2: Response surface of the PAH solution pH and IP extract concentration factors maintaining the concentration of ZnONPs solution at 1 g L^{-1}

Conversely, the addition of IP extract decreased the adsorption of the ZnONPs. As the IP extract is also constituted by negatively charged groups like the PAA, when the plant extract is added to the polyanion solution, it might cause an electrostatic repulsion from the polyanion chains. Also, the active compounds might interact with the PAH, affecting the deposition of the polyanion and, consequently, the deposition of nanoparticles.

5.5   Antimicrobial activity of thin films

The antimicrobial activity of the thin films was performed only for *S. aureus* bacteria strain, as this type of bacteria showed to be more susceptible to the ZnONPs than *E. coli* strain (see Chapter 3). No significant antimicrobial activity was observed for any of the thin films developed within the DOE.

Figure 5.3 shows the results for samples TF1, TF 2, TF5, TF6, and TF 9, which are the extreme and central points of the DOE as illustrated. Even though samples 6 and 9 showed around 40% reduction in relation to a positive control (PAA/PAH thin film without ZnONPs or IP extract), the materials did not successfully inhibit bacteria growth.
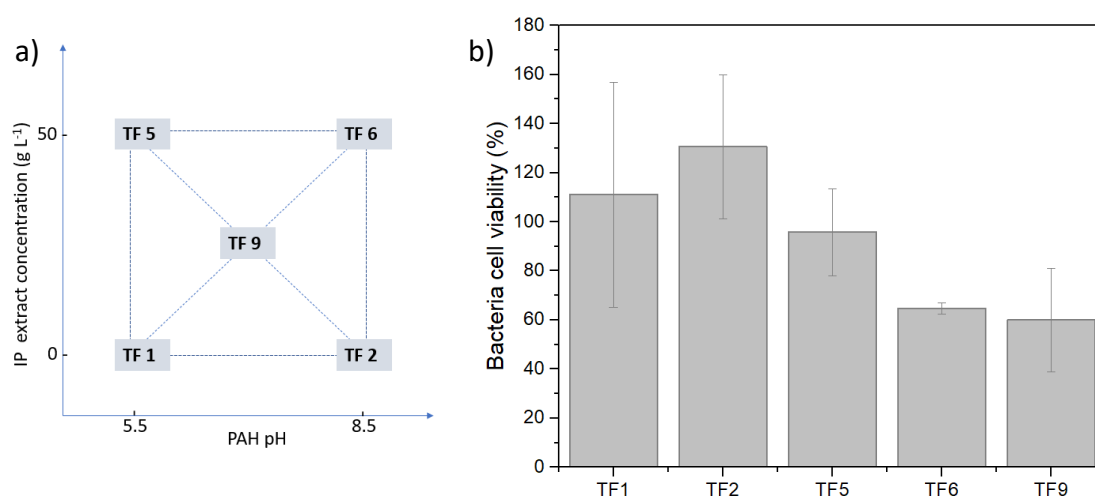
Figure 5.3: a) Extreme and central points of the DOE and b) *S. aureus* bacteria cell viability after 24h incubation with the thin films

Many factors may have contributed to these results. Firstly, the antimicrobial assay should be performed in a short time after its synthesis to avoid any degradation both of the film and the antioxidants compounds of the plant extract. In addition, the samples were stored under the dark but at room temperature. Thus, in future work,

the samples should be kept under refrigeration to maintain the properties of the plant extract. In fact, the active compounds present in the IP extract can easily degrade due to oxidation and lose their antimicrobial action [308]. Moreover, the amount of ZnONPs incorporated in the thin films was very low. Therefore, in an attempt to increase the incorporation of the ZnONPs in the thin films, and consequently their antimicrobial activity, new samples were developed by increasing the number of layers from 21 to 81 and 121 layers.

5.6   Development of thin films with additional layers

To evaluate the possibility of increasing the concentration of ZnONPs in the thin films, the sample TF2 was chosen to repeat the synthesis with 81 and 121 layers, considering the result of the DOE for zinc adsorption (high PAH pH and no IP extract).

The deposition of a thicker and more opaque film was observed with the increase of the number of layers (Figure 5.4). Their respective concentration of ZnONPs was verified by ICP-OES and is presented in Table 5.4. The increase of layers enhanced the ZnONPs adsorption. More specifically, when the number of layers was increased approximately 4 times (81 layers), the concentration of ZnONPs increased by approximately 2times, and with 6 times more layers (121 layers), the ZnONPs concentration was increased by approximately 4 times.
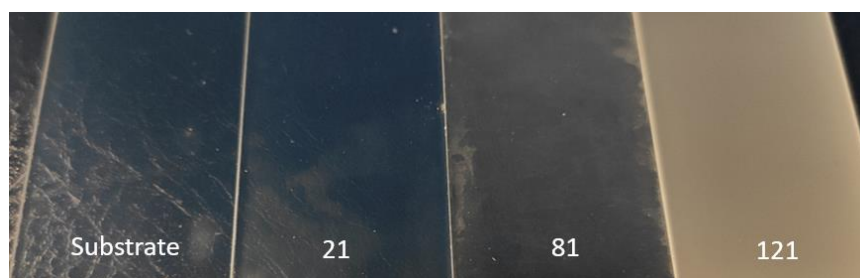
Figure 5.4: Thin film TF2 containing 21, 81 and 121 layers

Table 5.4: Concentration of ZnONPs adsorbed on the thin films according to the number of layers deposited

Sample TF2 (number of layers)	ZnONPs ($\mu g\ cm^2$)
21	1.17
81	2.71
121	4.40

The antimicrobial activity against *S. aureus* bacteria strain was then repeated for these two samples and compared to a control sample (PAA/PAH film with 121 layers). **Figure 5.5** presents the results of three independent antimicrobial assay tests. In test 1, there is a discrepancy in the bacteria cell viability for the sample TF2_121, where two replicates (A and B) showed only 40% viability, while C showed 80%, similar to the film control. On test 2, this sample showed no bacteria growth in replicate A, while replicates B and C presented higher viability than the control film.

Sample TF_81 showed a drop in cell viability in replicate B, for test 1, in comparison to the control (TF_control). In the second test, a more uniform result was obtained, as no significant bacteria inhibition was observed for the three replicates. Therefore, it was concluded that sample 81 did not present antimicrobial activity.

However, as sample TF2_121 did not show a reproducible result in the first 2 tests, a third test was performed for this sample. In test 3, complete inhibition of bacteria growth was observed for the three replicates of the sample built with 121 layers, as shown in Figure 5.3, where no resazurin reduction occurred for any of the replicates, where resazurin dye maintained the blue colour.
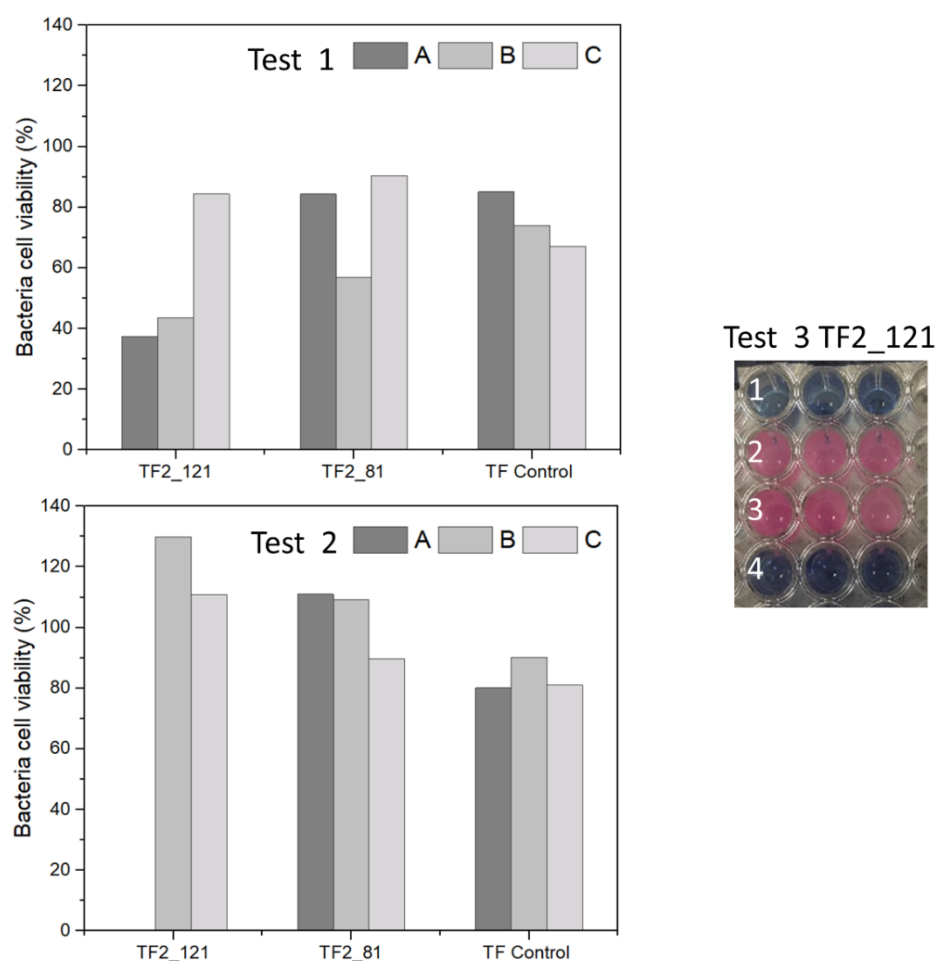
Figure 5.5: Antimicrobial assay for thin films containing 81 and 121 layers. A, B, and C represent each replicate inside a test. 1) TF2_121, 2) Film control 3) positive control, and 4) negative control

To further evaluate the inconsistent antimicrobial activity results observed for sample TF2_121, the morphology and dispersion of ZnONPs for this sample were investigated by FESEM and EDS analysis. The photomicrographs are shown in Figure 5.6. Even though there is a good dispersion of ZnONPs, according to EDS analysis, the thin film is not evenly deposited, exhibiting some cracks that leave the substrate exposed. Moreover, Figure 5.6B shows that the thin film is detaching from the substrate. This fact explains the lack of reproducibility of the antimicrobial activity, as the thin films are not stable, probably due to the high amount of layers.
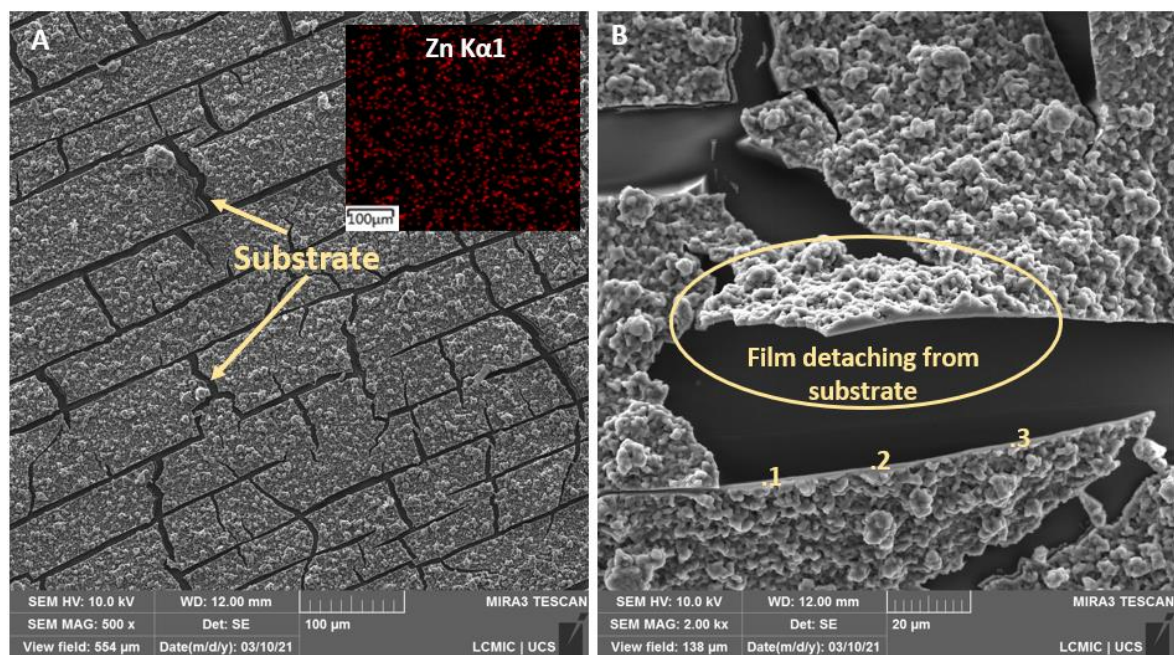
Figure 5.6: photomicrographs of A) thin film TF2 built with 121 layers and EDS elemental analysis of Zn, and B) amplification of TF2 121, where 1 = 2.0 μm, 2= 3.0 μm, and 3= 2.2 μm are the thickness of the thin film.

5.7   Summary

Multilayer thin films were produced with the incorporation of ZnONPs green synthesized and IP extract. A DOE followed by statistical analysis showed that the polycation solution pH and the concentration of plant extract affect the incorporation of ZnONPs in the thin films. Moreover, the adsorption of ZnONPs followed a linear model, where it increases as the PAH pH increases and the IP extract concentration decreases.

These results are related to the higher stability and interaction of the polyelectrolytes with ZnONPs in more basic conditions. Also, the IP extract is believed to reduce the incorporation of ZnONPs due to an interaction between the active compounds and the positively charged amino groups, and an electrostatic repulsion

with the carboxyl groups of the polyanion, which may have affected the deposition of both polyanion and ZnONPs on the substrate.

To the best of our knowledge, no previous study has reported the addition of plant extracts in the deposition solution of multilayer films by dip-coating approach. Therefore, this work shows the possibility of adding natural extracts in thin coatings, which can open a new range of applications for these composite materials, considering the many interesting properties of plant extracts, such as antimicrobial activity, biocompatibility, anticancer activity, among others.

Even though the thin films here developed showed no significant antimicrobial activity, this work gives an important direction for future work. First of all, the thin films should be characterized in terms of antimicrobial activity in a short time after being synthesized to avoid any plant compound degradation. Moreover, the plant extract could be added after the deposition of all layers, aiming for higher adsorption of ZnONPs.

Also, another approach would be the deposition of a more concentrated layer of ZnONPs only on the surface of the material. This methodology could enhance the attachment of ZnONPs to the substrate, as it has been reported to be an issue in previous work.

If successful, a composite of polyelectrolytes containing ZnONPs and plant extract active compounds could enhance the performance of different biomedical devices, like implant and catheter coatings. The two main advantages of these materials would be the easy deposition, independent of the shape of the substrate, and the flexibility given by the polyelectrolytes combined with the properties of nanomaterials and natural active compounds.

The next chapter examines the use of the PAA and PAH polyelectrolytes to produce electrospun fibres, which can be easily loaded with higher concentrations of ZnONPs, in comparison to the thin films. Also, this material presents a stable three-dimensional structure that favours the wound healing process.

Electrospun fibres

CHAPTER 6:   Development of electrospun PAA/PAH fibres containing green

synthesized zinc oxide nanoparticles

6.1   Introduction

Skin wounds are a common condition caused by burns, surgery, skin diseases, traumas, among others, causing physical and psychological stress to the patient. Thus, the development of biomaterials to improve wound closure has been addressed [309–310]. The addition of antimicrobial agents to these biomaterials is also essential, as infections are reported to be the main reason of wound complications [311–312].

Zinc oxide nanoparticles (ZnONPs) have been studied for antimicrobial purposes due to their efficacy against a range of microorganisms [298]. In addition, this nanomaterial has shown antimicrobial activity against drug-resistant bacteria strains and is considered to be a potential coadjutant in therapy [299]. In the biomedical field, ZnONPs are applied in drug delivery systems, cancer and tissue regeneration therapies, among others [69–70]. Zinc is also a natural component of the human body, being present in bones, muscles, and skin tissue, for example, and is vital for many metabolic processes[313].

Literature have reported the role of ZnONPs in tissue regeneration [74], where it has been successfully employed for wound healing [249–314]. For instance, Gong *et al.* [315] and Khalid *et al.* [72] observed wound healing improvement when applying a polymer material loaded with ZnONPs into the wounds. Both studies showed not only the antimicrobial efficacy of ZnONPs but also its importance for faster tissue regeneration and wound closure.

Electrospinning is a low-cost and facile approach to obtain micro and nanofibrous material that is comparable to the extracellular matrices of skin tissue. For instance, scaffolds obtained using this technique have three-dimensional structures formed by thin fibres, and presents porosity, flexibility and mechanical resistance [190]. Several works report the advantages of electrospun fibres for wound healing, such as cell adhesion and proliferation, flexibility, breathability, and facility for drug release [190–191–316].

Different approaches have been used to incorporate zinc oxide into electrospun fibres varying the polymer or the incorporation of particles. In general, electrospun polymer/zinc oxide fibres were obtained by mixing the particles in the polymer solution before the electrospinning, by adding a zinc precursor in the polymer solution and exposing the electrospun fibre to a calcination process, by incorporating the particles after obtaining the fibres, and by performing an in situ synthesis in the electrospun mat [317–318]. In the field of wound healing, electrospun gelatine/ZnONPs were successfully applied as wound dressing [319–320]. Chitosan, polyvinyl alcohol, and sodium alginate are also examples of polymers used to prepare electrospun composites with ZnONPs for tissue engineering [321–322].

PAA and PAH are weak polyelectrolytes that present negative and positive charges when in solution, respectively. These materials form polymeric complexes due to their opposite charges and their biocompatibility has been reported for a range of applications, like tissue engineering, drug delivery, and implant coatings [205–206–223]. These polyelectrolytes are water-soluble and require no chemical crosslinking agent as the amino groups of PAH react with the carboxyl groups of the PAA molecules, providing moisture stability and mechanical resistance [223].

The ZnONPs were synthesized using *Ilex paraguariensis* leaves *via* a sustainable process [323]. This green synthesis is beneficial not only regarding environmental preservation but also to obtain a product with promising low cytotoxicity and side effects, as no hazardous material is used in the process [142]. Literature reports the synthesis of ZnONPs using different plants [22–24–25–106]. For example, ZnONPs obtained with *Aloe vera* extract and *Stevia* leaves showed enhanced antibacterial effect against different pathogens [106–111]. Another study used *Hibiscus subdarifa* leaves and achieved ZnONPs with antidiabetic properties [25]. Here, ZnONPs were biosynthesized using *Ilex paraguariensis* leaves extract. This plant is found in South America and is reported to have high concentrations of active compounds, such as chlorogenic acid and caffeine, which are essential for the green synthesis of metal and metal oxide nanoparticles [12–30]35–37].

In this chapter, a novel antimicrobial material for wound healing applications was developed by combining the antimicrobial activity of green synthesized ZnONPs with a biocompatible electrospun PAA/PAH polyelectrolyte fibre mat, that resembles the extracellular matrix morphology of the skin tissue.

6.2   Characterization of electrospun fibres

The morphology and size of the polymer electrospun fibres was examined using SEM analysis as shown in Figure 6.1. The thermal treatment of the fibres (Figure 6.1A) resulted in an increase in the uniformity of the fibres, resulting in an average diameter of ~230 nm, while the non-thermal treated sample (Figure 6.1B) presented irregular morphology showing a mix of beads with a diameter up to 4 μm and fibres with a diameter of ~240 nm. PAA and PAH are polyelectrolytes that form electrostatic

complexes due to the opposite charges of carboxylate (-COO⁻) and amine (-NH₃⁺)

groups present in the PAA and PAH molecules, respectively [223]. The thermal

treatment results in the crosslinking of the polyelectrolytes through these carboxylate

and amine groups, which improves the uniformity of the fibres and moisture stability

[223]. The morphology of the electrospun scaffold is also found to be suitable for

wound dressing as it mimics the extracellular matrix of skin tissue, having a fibrous

three-dimensional structure, which provides mechanical support for cell attachment

and growth and benefits wound healing [230–324].

Figure 6.1C presents the morphology of the fibre after the incorporation of

ZnONPs with an elemental analysis of Zn identified by EDS analysis. The incorporation

process of ZnONPs did not affect the morphology and size of the fibre mat, as it

maintained its characteristics. The green synthesized ZnONPs were characterized in

Chapter 3 and have a spherical shape and an average size of 18 nm.

However, even though EDS analysis shows a homogeneous dispersion of ZnONPs

in the fibre mat, different sizes of agglomerates of nanoparticles were formed. This

result might be related to the high concentration of the ZnONPs solution. Considering

that it is now known that the fibres can absorb a considerable amount of ZnONPs, more

diluted nanoparticle solutions could be used to decrease the particle agglomerates.

Different studies have produced electrospun fibres containing zinc oxide but usually by

incorporating the ZnONPs into the polymer solution, which resulted in a more uniform

dispersion of nanoparticles without particle agglomeration [321–322]. Nonetheless,

this approach was not possible in this study due to the non-homogeneous solution

formed when mixing the polyelectrolytes with the ZnONPs.

The concentration of zinc oxide incorporated in the fibres was measured using ICP-OES. The analysis resulted in a concentration of 9.01% wt. of Zn(II). Considering that ZnO is constituted of 80.3% of Zn(II), the amount of ZnONPs in the fibre mat is 11.2 % wt. The fibre mats presented a thickness of 30 ± 3 µm and a grammage of 0.83 ± 0.20 mg cm^2. There was no significant difference between the fibres with and without ZnONPs in these aspects. Therefore, the concentration of ZnONPs per area of the fibre mat is approximately 0.09 mg cm^2.
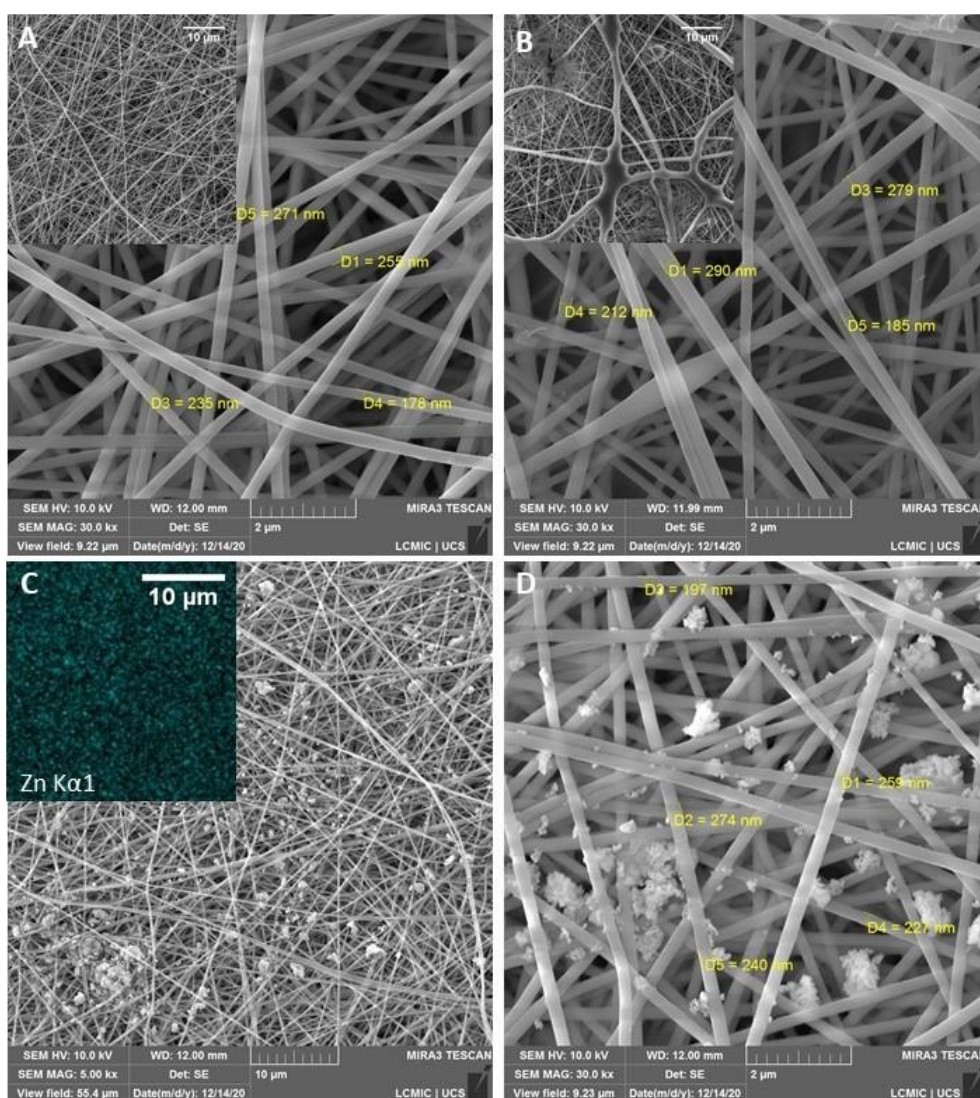
Figure 6.1: Photomicrograph of a) PAA/PAH fibre mat thermally treated, b) PAA/PAH fibre without thermal treatment, c) PAA/PAH fibre containing ZnONPS and EDS analysis of elemental zinc and, d) Amplification of PAA/PAH fibres containing ZnONPs

6.3   Fourier transform infrared spectroscopy (FTIR)

FTIR spectra of the different fibre mat in comparison to the cast film of pure PAA and PAH are shown in Figure 6.2. The main peaks are reported and assigned to their respective groups in Table 6.1. Peaks 1450 and 1410 cm^{-1} were seen in every sample and are assigned to C-H vibration of the carbon chain of the polymers. PAH shows the characteristic peaks of primary amines (3400 and 1600 cm^{-1}) while the PAA presents a strong peak at 1695 cm^{-1} related to the C=O stretching of carboxylic acid [223]. The peak at 1260 cm^{-1} is also related to the carboxylic acid group but it is associated with the C-O stretching and is seen in both PAA and PAA/PAH_nt (without thermal treatment) samples. These peaks related to the carboxylic acid groups are also presented in both non-thermal treated and thermally treated PAA/PAH samples. However, it is absent in the PAA/PAH/ZnONPs spectrum. The peaks between 1580 and 1550 cm^{-1} in the fibre samples are related to the amide groups, which are formed by the reaction of the carboxylic acid with the amine groups during polymer cross-linking [325].
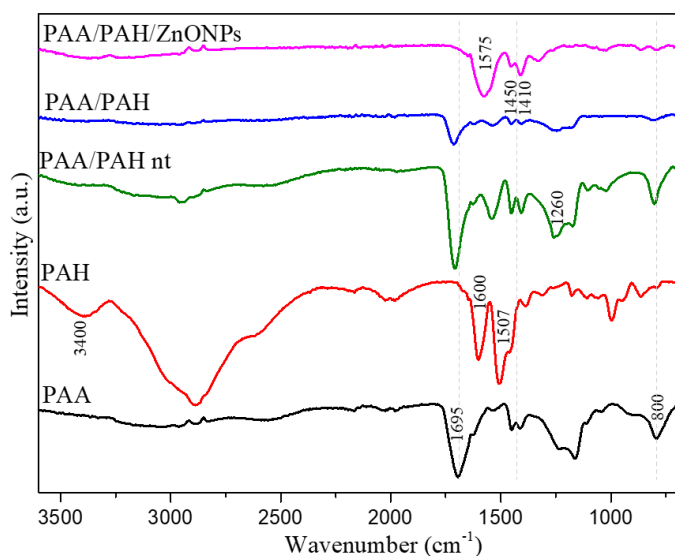
Figure 6.2: FTIR spectra of fibre mats and PAA and PLA cast films

Table 6.1: Description of FTIR peaks

Wavenumber (cm^{-1})	Group
3400	N-H stretching (amine)
1695	C=O stretching (carboxylic acid)
1600	N-H bending (amine)
1575	-NH bending (amide)
1450, 1410	C-H bending
1260	C-O stretching

6.4   Antimicrobial activity of electrospun fibres

The antimicrobial activity of the electrospun fibres is presented in Figure 6.3. The PAA/PAH fibre decreased the *S. aureus* cell viability to around 40%. Conversely, the *E. coli* showed higher resistance to the fibre mat with only a 10% drop of cell viability in comparison to the positive control.
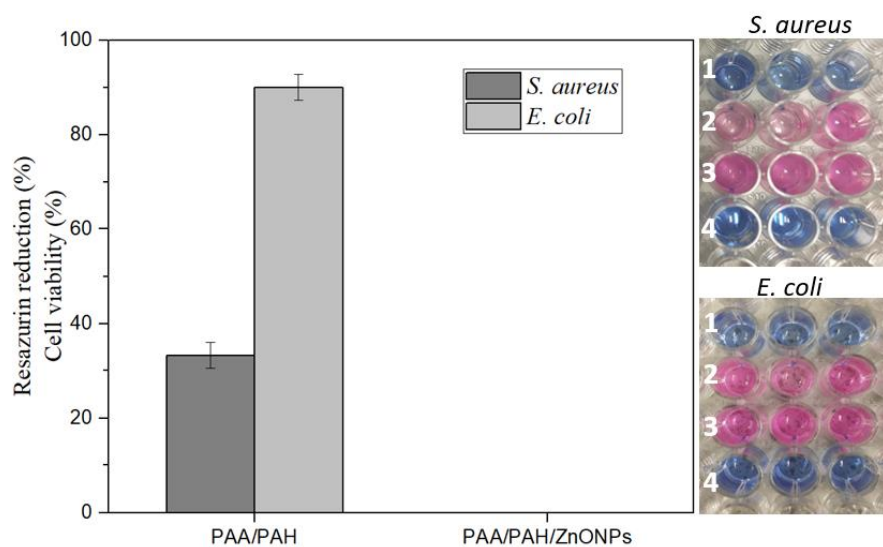
Figure 6.3: Antimicrobial activity of electrospun fibres. 1) PAA/PAH/ZnO, 2) PAA/PAH fibre, 3) positive control and, 4) negative control

The PAA/PAH/ZnONPs fibre composite was efficient to inhibit both bacteria strains as no dye reduction was observed, confirming the role of ZnONPs in the antimicrobial efficacy of the electrospun fibres. This result can also be observed in the

well-plate pictures in Figure 6.3, where the replicates in row 1 did not reduced the resazurin dye, maintaining the blue colour, while the PAA/PAH in row 2 presented some degree of dye reduction in comparison to the row 3, which represents the maximum cell viability. Row 4 showed no dye reduction, as no bacteria was incubated in these wells (negative control).

The final concentration of ZnONPs when testing the PAA/PAH/ZnONPs sample was found to be 900 µg mL^{-1}, once a fibre mat of 0.5 cm^2 (which contains 0.045 mg of ZnONPs) was placed in 0.05 mL of MH broth in each well. Therefore, the antimicrobial activity of the PAA/PAH/ZnONPs was expected as it surpassed the MIC for both bacteria strains. Even though the MIC for *E. coli* was not observed up to a concentration of 100 µg mL^{-1}, total cell growth inhibition indicates that the MIC was achieved when using the 900 µg mL^{-1} concentration.

SEM photomicrographs of the fibre after performing the antimicrobial assay are presented in Figure 6.4. This analysis corroborates with the resazurin assay as no bacteria growth was observed in the PAA/PAH/ZnONPs fibres for both *E. coli* and *S. aureus* strains. In addition, *S. aureus* formed isolated colony clusters in the control sample (PAA/PAH) while the *E. coli* covered nearly the whole surface of the scaffold forming a biofilm, confirming the results observed in the resazurin dye assay.

The SEM photomicrographs also shows that *S. aureus* clusters are formed by spherical cells and are presented only in the surface of the fibres (Figure 6.4B and C). Conversely, *E. coli* cells are rod in shape and are attached to the fibres, using the structure of the material to support their growth, as shown in Figure 6.4E and F. The morphology of the bacteria corroborates with findings in the literature [326–327].

Similar to our findings, Abrigo *et al.* [327] also observed the formation of bacteria colonies of *S. aureus* on the surface a electrospun polystyrene scaffold, while *E. coli* bacteria spread around each fibre, forming a biofilm rather than bacteria clusters.

Bacteria attachment to nanostructures is linked to a range of mechanisms that occurs simultaneously, which poses a challenge in understanding the interaction of bacteria strains with nanomaterials. Some of these mechanisms are dependent on surface chemistry, morphology, and electrostatic and van der Waal forces [328].
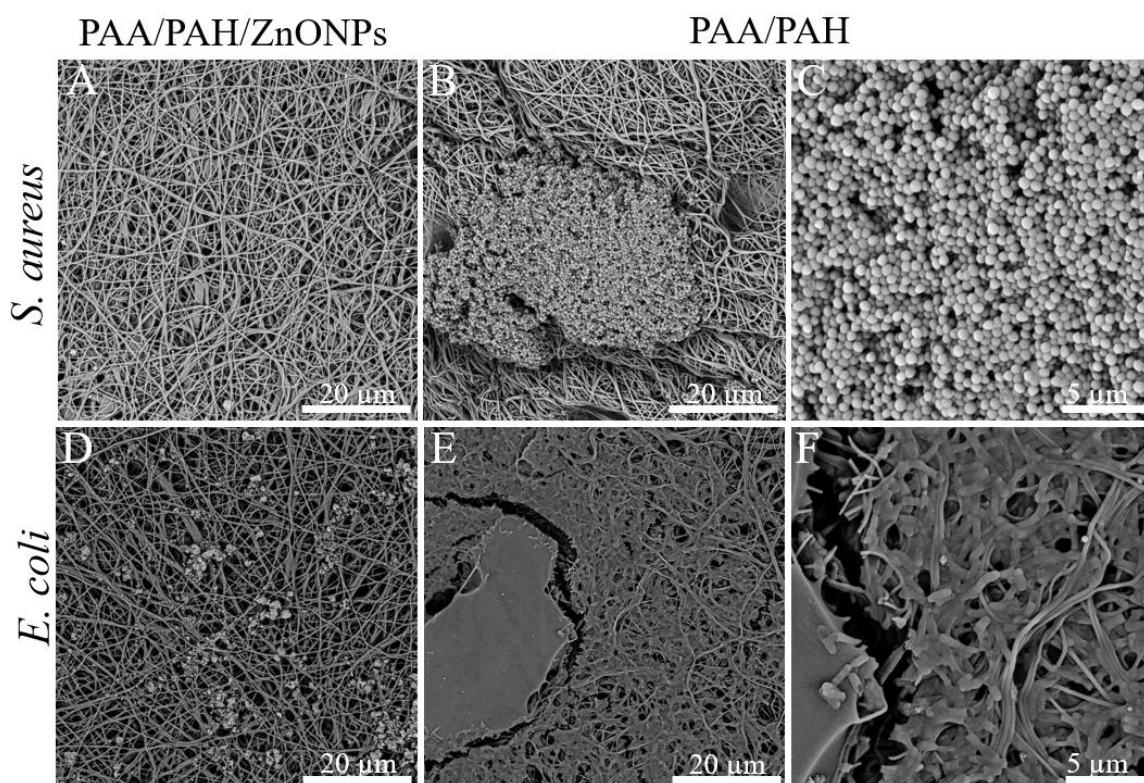
Figure 6.4: SEM photomicrographs of electrospun fibre after incubation with *S. aureus* and *E. coli* A) PAA/PAH/ZnONPs sample after 24 h incubation with *S.aureus,* B) PAA/PAH sample after 24 h incubation with *S.aureus,* C) amplification of image B to highlight the bacteria morphology, D) PAA/PAH/ZnONPs sample after 24 h incubation with *E.coli*, E) PAA/PAH sample after 24 h incubation with *E. coli*, and F) amplification image C to highlight the *E. coli* bacteria morphology and attachment to the fibres

6.5 Summary

Polymer fibres were successfully prepared using the electrospinning technique and posteriorly loaded with green synthesized ZnONPs. The fibre scaffold was formed by uniform PAA/PAH fibres and presented an even distribution of ZnONPs. However, some agglomerates of the nanomaterials were observed.

The electrospun fibres showed a similar morphology to the extracellular matrix of skin tissue and the addition of ZnONPs inhibited both Gram-negative and Gram-positive bacteria strains. These features display the potential of this novel material to be used for wound dressings aiming faster wound healing and infection prevention.

However, in future investigations the particle agglomeration needs to be improved and the cytotoxicity need to be investigated to elucidate the biocompatibility of the material for wound dressing applications. Moreover, the plant extract could be also incorporated to evaluate the effect on the morphological and composition properties of the electrospun fibre, similarly as done for the thin films. In this sense, the plant extract could be added by two methods: in the polymeric solution, or after the crosslinking of the polymers, as the incorporation of ZnONPs.

Conclusions & future perspectives

CHAPTER 7:   General conclusions and future perspectives

7.1   Conclusions and perspectives

This work aimed to develop polymeric antimicrobial biomaterials for biomedical device coatings and wound dressings using PAH and PAA polyelectrolytes. The antimicrobial activity was achieved by adding green synthesized ZnONPs from *Ilex paraguariensis* leaves extract.

The green synthesis of ZnONPs using the plant extract was successfully performed, illustrating a facile and environmentally friendly approach to obtain this nanomaterial. The evaluation of the mechanism route for the green synthesis by cyclic voltammetry and FTIR indicated that the nanoparticles were formed through the complexation of Zn(II) ions with the plant active compounds, which are further thermally degraded to obtain the nanomaterial. The source of zinc ions and plant solvent was found to significantly affect the morphology and particle size of the ZnONPs. Microscopy analysis (FESEM and TEM) has shown that the sample obtained from zinc nitrate and ethanolic solvent (Nit_EtOH) presented a regular spherical shape and size (around 18 nm). These findings were related to the fact that the zinc (II) ions in the synthesis with zinc nitrate were fully complexed by the antioxidants of the plant extract, in comparison to a partial complexation when performing the synthesis with zinc acetate. Regarding the solvent, ethanol increased the extraction of active compounds from the plant leaves, which improved the complexation of Zn(II) ions during the first stage of the synthesis.

The cytotoxicity of the ZnONPs was evaluated using the L929 cell strain of mouse fibroblasts. The results indicated that cell viability was dependent on the ZnONPs

concentration for all samples obtained *via* the green synthesis, and it decreased as the concentration increased. The sample Nit_EtOH conferred the least cytotoxicity among all samples, showing no cytotoxicity up to a concentration of 10 µg mL^{-1} and presenting an LC50 of 18 µg mL^{-1}. When cells were treated with ZnONPs using the LC50 concentration, morphological analysis by SEM and GIEMSA staining showed that all ZnONPs green synthesized induced a degree of the nucleus and cytoplasm condensation. Also, a test performed using protein expression indicated that small and uniform ZnONPs were able to internalize cells and trigger a metabolic process of cell death in high concentrations.

An antimicrobial assay showed that Gram-positive bacteria strains were more susceptible to ZnONPs than Gram-negative ones. While 45 µg mL^{-1} of ZnONPs inhibited *S. aureus* growth, the same concentration reduced only 10% of *E. coli* cell viability. This difference is related to a more complex structure of Gram-negative cells, which are surrounded by lipids and proteins, posing a barrier to nanoparticles and ions internalization. The higher vulnerability of Gram-positive bacteria was also linked to its negatively charged surface, which attracts positive ions, such as Zn(II) ions.

In this sense, the ZnONPs were found to be biocompatible in low concentrations and according to their size and shape, in which more uniform and smaller nanoparticles pose lower cytotoxicity. Thus, the sample Nit_EtOH was further tested in the biomaterials developed in this project and was referred to as solely ZnONPs in the chapters of polymer biomaterials development. Moreover, considering that this sample was able to internalize cells, this study also highlighted the potential application of this nanomaterial to be used in the development of novel therapies within the cell.

The first polymer substrate used in this project was a multilayer thin film using intercalated layers of PAH and PAA, in which ZnONPs and IP extract were added aiming the achievement of antimicrobial properties. The thin films were obtained using a layer-by-layer method by dip-coating, following a full factorial design of experiments. The DOE was performed to evaluate the influence of PAH solution pH, ZnONPs concentration, and the addition of IP extract on the composition of the thin films, which was determined using Zn(II) quantification (ICP-OES).

The statistical analysis of the DOE indicated that the PAH pH and the IP extract significantly affected the adsorption of ZnONPs in the polymer film, considering a 90% confidence interval. Also, the adsorption of nanomaterial follows a linear model, where it increases in more basic PAH pH solution and decreases with the increase of IP extract concentration. These findings were associated with the enhanced stability of ZnONPs in basic conditions, together with a stronger interaction between the nanomaterial and the polyelectrolyte in higher pH solution.

Regarding the IP extract, it is believed that the anions present in the extract are repulsed by the PAA negative charges and attracted by the PAH positively charged groups. These facts can interfere in the deposition of even layers of polyelectrolytes and, therefore, decrease the adsorption of nanoparticles. However, as no study has reported incorporating plant extract in layer-by-layer thin films, this work gives an insight for future investigations, aiming to associate the properties of thin films with the unique characteristic of active compounds naturally present in plants.

The antimicrobial assay performed using *S. aureus* showed no significant antimicrobial activity for the thin films developed in the DOE. Thus, aiming to increase the adsorption of ZnONPs, the number of layers was increased for the sample that

resulted in higher adsorption of nanoparticles according to the DOE. The number of layers was increased from 21 to 81 and 121. While the sample with 81 layers showed no antimicrobial inhibition, the sample with 121 layers presented inconsistent results. The discrepancy was found to be related to a detachment of the thin film from the substrate and to a series of fractures that left the substrate exposed, given space for bacteria growth.

A range of possibilities is seen to improve the thin films.Firstly, the time between coating and testing the samples should be minimized and controlled to avoid possible sample degradation due to aging, especially when working with plant extract, which active compounds are sensitive to oxidation. In addition, the samples must be kept under refrigeration to avoid any degradation before testing. Therefore, the experiment should be repeated taking in consideration this issues. Despite this fact, new approaches regarding the synthesis could be considered. For instance, the plant extract could be incorporated after the deposition of all layers, aiming for high adsorption of nanoparticles. Another approach would be to use a more concentrated solution of ZnONPs to coat the surface of the thin film, which could confer better flexibility and attachment to ZnO coating films.

Thus, the results and conclusions here stated give direction to the development of a promising biomaterial composite that could improve different issues currently seen in the biomedical field. For instance, this material could be used to avoid infections, acting as a flexible and thin coating to implants, catheters, and wound dressings. The main advantage of this material would be the easy production process, which accepts any material shape, and the use of antimicrobial agents to substitute

common antibiotic drugs that are now becoming ineffective due to the development of bacteria resistance.

The second biomaterial developed in this project used the same polyelectrolytes to produce a nanofibre scaffold using the electrospinning technique. This material was chosen not only due to the possibility to incorporate a higher amount of nanoparticles but also because of its unique structure, which resembles the extracellular matrix of skin tissue.

The electrospun fibre scaffold containing the ZnONPs was analysed according to its morphology (FESEM and EDS) and composition (ICP-OES and FTIR). The fibres showed a three-dimensional structure formed by uniform fibres with a diameter of around 230 nm. According to the literature, this morphology favours the wound healing process, mainly due to the high porosity and the facility of cell attachment and proliferation. With the incorporation of ZnONPs, the scaffold became antimicrobial against both *S. aureus* and *E. coli* strains. Moreover, reported studies have shown the ability of ZnO to improve the tissue regeneration process.

These features display that the electrospun fibre scaffold obtained in this work is a promising material to prevent infection and enhance the wound healing process. However, the cytotoxicity of the composite material must be evaluated to confirm that this scaffold meets the requirements for wound dressing biomaterials. Also, future works in this area should include the plant extract, which might improve the properties so far achieved, considering the many benefits that natural antioxidants have for tissue regeneration.

Overall, this work has shown a greener and easy method to obtain ZnONPs, which can be applied not only in the area outlined in this work but also in general

applications that require ZnO. Also, this project has investigated the development of two different polymer biomaterials with antimicrobial characteristics. While the thin films have characteristics to act as an antimicrobial coating, the electrospun scaffold presents a morphological structure required for wound dressings. However, further studies need to be carried out to evaluate the cytotoxicity of the biomaterials and enhance the antimicrobial activity.

Publications and conferences

Publications:

Bandeira, M., Chee, B.S., Frassini, R., Nugent, M., Giovanela, M., Roesch-Ely, Crespo, J.S., Devine, D.M. Antimicrobial electrospun fibrenmat containing green synthesised zinc oxide nanoparticles for wound healing applications, *Materials*, 2021.

Bandeira, M., Possan, A. L., Pavin, S., Raota, C. S., Vebber, M.C. Giovanela, M., Roesch-Ely, M., Devine, D. M., Crespo, J.S. Mechanism of formation, characterization, and cytotoxicity of green synthesised zinc oxide nanoparticles from *Ilex paraguariensis* leaves extract. *Nano-Structure and Nano-objects*, 2020.

Bandeira, M., Giovanela, M., Roesch-Ely, M., Devine, D. M., Crespo, J.S. Green synthesis of zinc oxide nanoparticles: a review of the synthesis methodology and mechanism of formation. *Sustainable Chemistry & Pharmacy*, v. 15, 2020.

Raota, C. S., **Bandeira, M.**, Devine, D. M., Crespo, J.S., Giovanela, M. Section VI: Sustainable Green Nanomaterials for Potential Development in Environmental Industries, *Green Functionalized Nanomaterials for Environmental Applications*. Elsevier,2021.

Venkatesh, C., Laurenti, M., **Bandeira, M.**, Lanzagorta, E. Lucherini L., Cauda, V., Devine, D. Biodegradation and antimicrobial properties of zinc oxide-polymer composite materials for urinary stent applications, Coatings, 2020.

Bavaresco, J. B., **Bandeira, M.**, Raota, C.S., Crespo, J.S., Giovanela, M. Green synthesis of silver nanoparticles from the extract of *yerba mate* leaves (*Ilex paraguariensis*). *Scientia cum Industria*, v.8 (1), 39-45, 2020 (In Portuguese)

Conferences:

Bandeira, M., Pavin, S., Roesch-Ely, M., Crespo, J. S., and Devine, D.M. Green synthesis of zinc oxide nanoparticles from *Ilex paraguariensis* leaves extract for biomedical applications. *Bioengineering in Ireland 2019, Limerick – Ireland, 2019.*

Bandeira, M., Pavin, S., Possan, A. L., Giovanela, M., Roesch-Ely, M., Devine, D.M. Crespo, J. S. Green synthesis of zinc oxide nanoparticles from *Ilex paraguariensis* leaves extract: a study on the synthesis, mechanism of formation and cytotoxicity. *4th Green and Sustainable Chemistry Conference, Dresden – Germany, 2019.*

Bandeira, M., Pavin, S., Roesch-Ely, M., Crespo, J. S., and Devine, D.M. Environmentally friendly synthesis of zinc oxide nanoparticles from *Ilex paraguariensis* leaves extract for biomedical applications. *Athlone Institute of Technology Research Seminar, Athlone – Ireland, 2020.*

References

1. A. P. Reverberi, D. D.M., A. A. G. Bruzzone, R. Teti, & B. Fabiano, Nanotechnology in machining processes : recent advances. *Procedia CIRP*, **79** (2019) 3–8. https://doi.org/10.1016/j.procir.2019.02.002.

2. S. R. D. Mello, C. N. Cruz, M. Chen, M. Kapoor, S. L. Lee, & K. M. Tyner, The evolving landscape of drug products containing nanomaterials in the United States. *Nature Nanotechnology*, **12** (2017) 523–529. https://doi.org/10.1038/nnano.2017.67.

3. F. Ye, Y. Zhao, R. El-sayed, M. Muhammed, & M. Hassan, Advances in nanotechnology for cancer biomarkers. *Nano Today*, **18** (2018) 103–123. https://doi.org/10.1016/j.nantod.2017.12.008.

4. R. Keçili, S. Büyüktiryaki, & C. Hussain, Trends in Analytical Chemistry Advancement in bioanalytical science through nanotechnology : Past , present and future. *Trends in Analytical Chemistry*, **110** (2019) 259–276. https://doi.org/10.1016/j.trac.2018.11.012.

5. M. Anbuvannan, M. Ramesh, G. Viruthagiri, N. Shanmugam, & N. Kannadasan, Synthesis, characterization and photocatalytic activity of ZnO nanoparticles prepared by biological method. *Spectrochimica Acta - Part A: Molecular and Biomolecular Spectroscopy*, **143** (2015) 304–308. https://doi.org/10.1016/j.saa.2015.01.124.

6. A. Singh, N. B. Singh, S. Afzal, T. Singh, & I. Hussain, Zinc oxide nanoparticles: a review of their biological synthesis, antimicrobial activity, uptake, translocation and biotransformation in plants. *Journal of Materials Science*, **53** (2018) 185–201. https://doi.org/10.1007/s10853-017-1544-1.

7. V. G. Bairi, J.-H. Lim, A. Fong, & S. W. Linder, Size characterization of metal oxide nanoparticles in commercial sunscreen products. *Journal of Nanoparticle Research*, **19** (2017) 256. https://doi.org/10.1007/s11051-017-3929-0.

8. S. Bhatia & N. Verma, Photocatalytic activity of ZnO nanoparticles with optimization of defects. *Materials Research Bulletin*, **95** (2017) 468–476. https://doi.org/10.1016/j.materresbull.2017.08.019.

9. S. R. Brintha & M. Ajitha, Synthesis and characterization of ZnO nanoparticles via aqueous solution, sol-gel and hydrothermal methods. *IOSR Journal of Applied Chemistry*, **8** (2015) 66–72. https://doi.org/10.9790/5736-081116672.

10. A. Król, P. Pomastowski, K. Rafińska, V. Railean-Plugaru, & B. Buszewski, Zinc oxide nanoparticles: Synthesis, antiseptic activity and toxicity mechanism. *Advances in Colloid and Interface Science*, **249** (2017) 37–52. https://doi.org/10.1016/j.cis.2017.07.033.

11. P. Anastas & N. Eghbali, Green chemistry: Principles and practice. *Chemical Society Reviews*, **39** (2010) 301–312. https://doi.org/10.1039/b918763b.

12. O. V. Kharissova, H. V. R. Dias, B. I. Kharisov, B. O. Pérez, & V. M. J. Pérez, The greener synthesis of nanoparticles. *Trends in Biotechnology*, **31** (2013) 240–248. https://doi.org/10.1016/j.tibtech.2013.01.003.

13. S. Shamaila, A. K. L. Sajjad, N. ul A. Ryma, S. A. Farooqi, N. Jabeen, S. Majeed, & I. Farooq, Advancements in nanoparticle fabrication by hazard free eco-friendly green routes. *Applied Materials Today*, **5** (2016) 150–199. https://doi.org/10.1016/j.apmt.2016.09.009.

14. S. Iravani, Green synthesis of metal nanoparticles using plants. *Green Chemistry*, **13**

(2011) 2638–2650. https://doi.org/10.1039/c1gc15386b.

15. A. Gour & N. K. Jain, Advances in green synthesis of nanoparticles. *Artificial Cells, Nanomedicine and Biotechnology*, **47** (2019) 844–851. https://doi.org/10.1080/21691401.2019.1577878.

16. M. Bandeira, M. Giovanela, M. Roesch-Ely, D. M. Devine, & J. da Silva Crespo, Green synthesis of zinc oxide nanoparticles: A review of the synthesis methodology and mechanism of formation. *Sustainable Chemistry and Pharmacy*, **15** (2020). https://doi.org/10.1016/j.scp.2020.100223.

17. T. Varadavenkatesan, R. Selvaraj, & R. Vinayagam, Green synthesis of silver nanoparticles using Thunbergia grandiflora flower extract and its catalytic action in reduction of Congo red dye. *Materials Today: Proceedings*, **23** (2019) 39–42. https://doi.org/10.1016/j.matpr.2019.05.441.

18. T. Varadavenkatesan, R. Vinayagam, & R. Selvaraj, Green synthesis and structural characterization of silver nanoparticles synthesized using the pod extract of Clitoria ternatea and its application towards dye degradation. *Materials Today: Proceedings*, **23** (2020) 27–29. https://doi.org/10.1016/j.matpr.2019.04.216.

19. S. Anchan, S. Pai, H. Sridevi, T. Varadavenkatesan, R. Vinayagam, & R. Selvaraj, Biogenic synthesis of ferric oxide nanoparticles using the leaf extract of Peltophorum pterocarpum and their catalytic dye degradation potential. *Biocatalysis and Agricultural Biotechnology*, **20** (2019). https://doi.org/10.1016/j.bcab.2019.101251.

20. A. Dash, M. T. Ahmed, & R. Selvaraj, Mesoporous magnetite nanoparticles synthesis using the Peltophorum pterocarpum pod extract, their antibacterial efficacy against pathogens and ability to remove a pollutant dye. *Journal of Molecular Structure*, **1178** (2019) 268–273. https://doi.org/10.1016/j.molstruc.2018.10.042.

21. O. J. Nava, C. A. Soto-Robles, C. M. Gómez-Gutiérrez, A. R. Vilchis-Nestor, A. Castro-Beltrán, A. Olivas, & P. A. Luque, Fruit peel extract mediated green synthesis of zinc oxide nanoparticles. *Journal of Molecular Structure*, **1147** (2017) 1–6. https://doi.org/10.1016/j.molstruc.2017.06.078.

22. N. Matinise, X. G. Fuku, K. Kaviyarasu, N. Mayedwa, & M. Maaza, ZnO nanoparticles via Moringa oleifera green synthesis: Physical properties & mechanism of formation. *Applied Surface Science*, **406** (2017) 339–347. https://doi.org/10.1016/j.apsusc.2017.01.219.

23. C. S. Raota, A. F. Cerbaro, M. Salvador, A. P. L. Delamare, S. Echeverrigaray, J. Da Silva Crespo, T. B. Da Silva, & M. Giovanela, Green synthesis of silver nanoparticles using an extract of Ives cultivar (Vitis labrusca) pomace: Characterization and application in wastewater disinfection. *Journal of Environmental Chemical Engineering*, **7** (2019) 103383. https://doi.org/10.1016/j.jece.2019.103383.

24. O. J. Nava, P. A. Luque, C. M. Gómez-Gutiérrez, A. R. Vilchis-Nestor, A. Castro-Beltrán, M. L. Mota-González, & A. Olivas, Influence of Camellia sinensis extract on Zinc Oxide nanoparticle green synthesis. *Journal of Molecular Structure*, **1134** (2017) 121–125. https://doi.org/10.1016/j.molstruc.2016.12.069.

25. N. Bala, S. Saha, M. Chakraborty, M. Maiti, S. Das, R. Basu, & P. Nandy, Green synthesis of zinc oxide nanoparticles using Hibiscus subdariffa leaf extract: Effect of temperature on synthesis, anti-bacterial activity and anti-diabetic activity. *RSC Advances*, **5** (2015) 4993–5003. https://doi.org/10.1039/c4ra12784f.

26. M. M. Khan, N. H. Saadah, M. E. Khan, M. H. Harunsani, A. L. Tan, & M. H. Cho, Potentials of Costus woodsonii leaf extract in producing narrow band gap ZnO nanoparticles.

Materials Science in Semiconductor Processing, **91** (2019) 194–200. https://doi.org/10.1016/j.mssp.2018.11.030.

27. K. Singh, J. Singh, & M. Rawat, Green synthesis of zinc oxide nanoparticles using Punica Granatum leaf extract and its application towards photocatalytic degradation of Coomassie brilliant blue R-250 dye. *SN Applied Sciences*, **1** (2019) 1–8. https://doi.org/10.1007/s42452-019-0610-5.

28. G. Sangeetha, S. Rajeshwari, & R. Venckatesh, Green synthesis of zinc oxide nanoparticles by aloe barbadensis miller leaf extract : Structure and optical properties. *Materials Research Bulletin*, **46** (2011) 2560–2566. https://doi.org/10.1016/j.materresbull.2011.07.046.

29. S. Shahriyari Rad, A. M. Sani, & S. Mohseni, Biosynthesis, characterization and antimicrobial activities of zinc oxide nanoparticles from leaf extract of Mentha pulegium (L.). *Microbial Pathogenesis*, **131** (2019) 239–245. https://doi.org/10.1016/j.micpath.2018.01.003.

30. L. G. Riachi & C. A. B. De Maria, Yerba mate: An overview of physiological effects in humans. *Journal of Functional Foods*, **38** (2017) 308–320. https://doi.org/10.1016/j.jff.2017.09.020.

31. E. C. S. Santos, M. A. Bicca, C. H. Blum-Silva, A. P. R. Costa, A. A. dos Santos, E. P. Schenkel, M. Farina, F. H. Reginatto, & T. C. M. de Lima, Anxiolytic-like, stimulant and neuroprotective effects of Ilex paraguariensis extracts in mice. *Neuroscience*, **292** (2015) 13–21. https://doi.org/10.1016/j.neuroscience.2015.02.004.

32. A. B. G. Luz, C. H. B. Da Silva, M. V. P. S. Nascimento, B. M. De Campos Facchin, B. Baratto, T. S. Fröde, F. H. Reginatto, & E. M. Dalmarco, The anti-inflammatory effect of Ilex paraguariensis A. St. Hil (Mate) in a murine model of pleurisy. *International Immunopharmacology*, **36** (2016) 165–172. https://doi.org/10.1016/j.intimp.2016.04.027.

33. D. Hao, X. Gu, P. Xiao, Z. Liang, L. Xu, & Y. Peng, Research progress in the phytochemistry and biology of Ilex pharmaceutical resources. *Acta Pharmaceutica Sinica B*, **3** (2013) 8–19. https://doi.org/10.1016/j.apsb.2012.12.008.

34. B. Felice, M. A. Sánchez, M. C. Socci, L. D. Sappia, M. I. Gómez, M. K. Cruz, C. J. Felice, M. Martí, M. I. Pividori, G. Simonelli, & A. P. Rodríguez, Controlled degradability of PCL-ZnO nanofibrous scaffolds for bone tissue engineering and their antibacterial activity. *Materials Science and Engineering C*, **93** (2018) 724–738. https://doi.org/10.1016/j.msec.2018.08.009.

35. G. Yuvaraja, J. L. Pathak, W. Zhang, Y. Zhang, & X. Jiao, Antibacterial and wound healing properties of chitosan/poly(vinyl alcohol)/zinc oxide beads (CS/PVA/ZnO). *International Journal of Biological Macromolecules*, **103** (2017) 234–241. https://doi.org/10.1016/j.ijbiomac.2017.05.020.

36. D. Banoriya, R. Purohit, & R. K. Dwivedi, Advanced Application of Polymer based Biomaterials. *Materials Today: Proceedings*, **4** (2017) 3534–3541. https://doi.org/10.1016/j.matpr.2017.02.244.

37. F. J. Heiligtag & M. Niederberger, The fascinating world of nanoparticle research. *Materials Today*, **16** (2013) 262–271. https://doi.org/10.1016/j.mattod.2013.07.004.

38. K. N. Thakkar, S. S. Mhatre, & R. Y. Parikh, Biological synthesis of metallic nanoparticles. *Nanomedicine: Nanotechnology, Biology, and Medicine*, **6** (2010) 257–262. https://doi.org/10.1016/j.nano.2009.07.002.

39. D. V. Talapin & E. V. Shevchenko, Introduction: Nanoparticle chemistry. *Chemical*

Reviews, **116** (2016) 10343–10345. https://doi.org/10.1021/acs.chemrev.6b00566.

40. C. J. Murphy, T. K. Sau, A. M. Gole, C. J. Orendorff, J. Gao, L. Gou, S. E. Hunyadi, & T. Li, Anisotropic metal nanoparticles: Synthesis, assembly, and optical applications. *Journal of Physical Chemistry B*, **109** (2005) 13857–13870. https://doi.org/10.1021/jp0516846.

41. M. A. El-Sayed, Small is different: Shape-, size-, and composition-dependent properties of some colloidal semiconductor nanocrystals. *Accounts of Chemical Research*, **37** (2004) 326–333. https://doi.org/10.1021/ar020204f.

42. I. Khan, K. Saeed, & I. Khan, Nanoparticles : Properties , applications and toxicities. *Arabian Journal of Chemistry*, (2017). https://doi.org/10.1016/j.arabjc.2017.05.011.

43. F. Zarpelon, D. Galiotto, C. Aguzolli, L. N. Carli, C. A. Figueroa, I. J. R. Baumvol, G. Machado, J. D. S. Crespo, & M. Giovanela, Removal of coliform bacteria from industrial wastewaters using polyelectrolytes/silver nanoparticles self-assembled thin films. *Journal of Environmental Chemical Engineering*, **4** (2016) 137–146. https://doi.org/10.1016/j.jece.2015.11.013.

44. B. Kumar, K. Jalodia, P. Kumar, & H. K. Gautam, Recent advances in nanoparticle-mediated drug delivery. *Journal of Drug Delivery Science and Technology*, **41** (2017) 260–268. https://doi.org/10.1016/j.jddst.2017.07.019.

45. M. M. Shabat, D. M. El-Amassi, & D. M. Schaadt, Design and analysis of multilayer waveguides containing nanoparticles for solar cells. *Solar Energy*, **137** (2016) 409–412. https://doi.org/10.1016/j.solener.2016.08.041.

46. S. A. Corr, Metal oxide nanoparticles. *Nanoscience*, **1** (2013) 180–207. https://doi.org/10.1039/9781849734844-00180.

47. A. Moezzi, A. M. McDonagh, & M. B. Cortie, Zinc oxide particles: Synthesis, properties and applications. *Chemical Engineering Journal*, **185**–**186** (2012) 1–22. https://doi.org/10.1016/j.cej.2012.01.076.

48. J. L. G. Fierro, *Metal oxides: Chemistry and applications*, 1st ed (Florida: CRC Press, 2005).

49. Z. L. Wang, Nanostructures of zinc oxide. (2004) 26–33.

50. A. Naveed, U. Haq, A. Nadhman, I. Ullah, G. Mustafa, M. Yasinzai, & I. Khan, Synthesis Approaches of Zinc Oxide Nanoparticles: The Dilemma of Ecotoxicity. *Journal of Nanomaterials*, **2017** (2017) 1–14. https://doi.org/10.1155/2017/8510342.

51. L. Spanhel & M. A. Anderson, Semiconductor Clusters in the Sol-Gel Process: Quantized Aggregation, Gelation, and Crystal Growth in Concentrated ZnO Colloids. *Journal of the American Chemical Society*, **113** (1991) 2826–2833. https://doi.org/10.1021/ja00008a004.

52. S. Morandi, A. Fioravanti, G. Cerrato, S. Lettieri, M. Sacerdoti, & M. C. Carotta, Facile synthesis of ZnO nano-structures: Morphology influence on electronic properties. *Sensors and Actuators, B: Chemical*, **249** (2017) 581–589. https://doi.org/10.1016/j.snb.2017.03.114.

53. J. N. Hasnidawani, H. N. Azlina, H. Norita, N. N. Bonnia, S. Ratim, & E. S. Ali, Synthesis of ZnO Nanostructures Using Sol-Gel Method. *Procedia Chemistry*, **19** (2016) 211–216. https://doi.org/http://dx.doi.org/10.1016/j.proche.2016.03.095.

54. R. Bekkari, L. laânab, D. Boyer, R. Mahiou, & B. Jaber, Influence of the sol gel synthesis parameters on the photoluminescence properties of ZnO nanoparticles. *Materials Science in Semiconductor Processing*, **71** (2017) 181–187. https://doi.org/10.1016/j.mssp.2017.07.027.

55. X. Li, G. He, G. Xiao, H. Liu, & M. Wang, Synthesis and morphology control of ZnO

nanostructures in microemulsions. *Journal of Colloid and Interface Science*, **333** (2009) 465–473. https://doi.org/10.1016/j.jcis.2009.02.029.

56. Y. C. Kong, D. P. Yu, B. Zhang, W. Fang, & S. Q. Feng, Ultraviolet-emitting ZnO nanowires synthesized by a physical vapor deposition approach. *Applied Physics Letters*, **78** (2001) 407–409. https://doi.org/10.1063/1.1342050.

57. L. F. Dong, Z. L. Cui, & Z. K. Zhang, Gas sensing properties of nano-ZnO prepared by arc plasma method. *Nanostructured Materials*, **8** (1997) 815–823. https://doi.org/10.1016/S0965-9773(98)00005-1.

58. H. Agarwal, S. Venkat Kumar, & S. Rajeshkumar, A review on green synthesis of zinc oxide nanoparticles – An eco-friendly approach. *Resource-Efficient Technologies*, **3** (2017) 406–413. https://doi.org/10.1016/j.reffit.2017.03.002.

59. R. Wahab, F. Khan, Lutfullah, R. B. Singh, N. K. Kaushik, J. Ahmad, M. A. Siddiqui, Q. Saquib, B. A. Ali, S. T. Khan, J. Musarrat, & A. A. Al-Khedhairy, Utilization of photocatalytic ZnO nanoparticles for deactivation of safranine dye and their applications for statistical analysis. *Physica E: Low-Dimensional Systems and Nanostructures*, **69** (2015) 101–108. https://doi.org/10.1016/j.physe.2015.01.005.

60. M. El-Kemary, H. El-Shamy, & I. El-Mehasseb, Photocatalytic degradation of ciprofloxacin drug in water using ZnO nanoparticles. *Journal of Luminescence*, **130** (2010) 2327–2331. https://doi.org/10.1016/j.jlumin.2010.07.013.

61. M. A. Desai, A. N. Vyas, G. D. Saratale, & S. D. Sartale, Zinc oxide superstructures: Recent synthesis approaches and application for hydrogen production via photoelectrochemical water splitting. *International Journal of Hydrogen Energy*, **44** (2019) 2091–2127. https://doi.org/10.1016/j.ijhydene.2018.08.042.

62. S. Jagtap, S. Rane, S. Arbuj, S. Rane, & S. Gosavi, Optical fiber based humidity sensor using Ag decorated ZnO nanorods. *Microelectronic Engineering*, **187**–**188** (2018) 1–5. https://doi.org/10.1016/j.mee.2017.11.009.

63. G. Bhanjana, N. Dilbaghi, N. K. Singhal, K. H. Kim, & S. Kumar, Zinc oxide nanopillars as an electrocatalyst for direct redox sensing of cadmium. *Journal of Industrial and Engineering Chemistry*, **53** (2017) 192–200. https://doi.org/10.1016/j.jiec.2017.04.025.

64. A. A. Gujel, M. Bandeira, C. Menti, D. Perondi, R. Guégan, M. Roesch-Ely, M. Giovanela, & J. S. Crespo, Evaluation of vulcanization nanoactivators with low zinc content: Characterization of zinc oxides, cure, physico-mechanical properties, Zn2+release in water and cytotoxic effect of EPDM compositions. *Polymer Engineering and Science*, (2017) 1–10. https://doi.org/10.1002/pen.24781.

65. A. Sirelkhatim, S. Mahmud, A. Seeni, N. H. M. Kaus, L. C. Ann, S. K. M. Bakhori, H. Hasan, & D. Mohamad, Review on zinc oxide nanoparticles: Antibacterial activity and toxicity mechanism. *Nano-Micro Letters*, **7** (2015) 219–242. https://doi.org/10.1007/s40820-015-0040-x.

66. E. A. S. Dimapilis, C. S. Hsu, R. M. O. Mendoza, & M. C. Lu, Zinc oxide nanoparticles for water disinfection. *Sustainable Environment Research*, **28** (2018) 47–56. https://doi.org/10.1016/j.serj.2017.10.001.

67. L. E. Shi, Z. H. Li, W. Zheng, Y. F. Zhao, Y. F. Jin, & Z. X. Tang, Synthesis, antibacterial activity, antibacterial mechanism and food applications of ZnO nanoparticles: A review. *Food Additives and Contaminants - Part A Chemistry, Analysis, Control, Exposure and Risk Assessment*, **31** (2014) 173–186. https://doi.org/10.1080/19440049.2013.865147.

68. J. Pulit-Prociak, J. Chwastowski, A. Kucharski, & M. Banach, Functionalization of textiles with silver and zinc oxide nanoparticles. *Applied Surface Science*, **385** (2016) 543–553.

https://doi.org/10.1016/j.apsusc.2016.05.167.

69. H. Mirzaei & M. Darroudi, Zinc oxide nanoparticles: Biological synthesis and biomedical applications. *Ceramics International*, **43** (2016) 907–914. https://doi.org/10.1016/j.ceramint.2016.10.051.

70. P. K. Mishra, H. Mishra, A. Ekielski, S. Talegaonkar, & B. Vaidya, Zinc oxide nanoparticles: a promising nanomaterial for biomedical applications. *Drug Discovery Today*, **22** (2017) 1825–1834. https://doi.org/10.1016/j.drudis.2017.08.006.

71. S. Sruthi, J. Ashtami, & P. V. Mohanan, Biomedical application and hidden toxicity of Zinc oxide nanoparticles. *Materials Today Chemistry*, **10** (2018) 175–186. https://doi.org/10.1016/j.mtchem.2018.09.008.

72. A. Khalid, R. Khan, M. Ul-Islam, T. Khan, & F. Wahid, Bacterial cellulose-zinc oxide nanocomposites as a novel dressing system for burn wounds. *Carbohydrate Polymers*, **164** (2017) 214–221. https://doi.org/10.1016/j.carbpol.2017.01.061.

73. H. R. Bakhsheshi-Rad, E. Hamzah, A. F. Ismail, M. Aziz, M. Kasiri-Asgarani, E. Akbari, S. Jabbarzare, A. Najafinezhad, & Z. Hadisi, Synthesis of a novel nanostructured zinc oxide/baghdadite coating on Mg alloy for biomedical application: In-vitro degradation behavior and antibacterial activities. *Ceramics International*, **43** (2017) 14842–14850. https://doi.org/10.1016/j.ceramint.2017.07.233.

74. M. Laurenti & V. Cauda, ZnO nanostructures for tissue engineering applications. *Nanomaterials*, **7** (2017) 1–34. https://doi.org/10.3390/nano7110374.

75. A. K. Barui, V. Veeriah, S. Mukherjee, J. Manna, K. Patel, S. Patra, K. Pal, S. Murali, R. K. Rana, S. Chatterjee, & C. R. Patra, Zinc oxide nanoflowers make new blood vessels. *Nanoscale*, **24** (2012) 1–12. https://doi.org/10.1039/C2NR32369A.

76. Y. Hanai, H. Tokuda, E. Yasuda, T. Noda, T. Ohta, S. Takai, & O. Kozawa, Up-regulation by zinc of FGF-2-induced VEGF release throughenhancing p44/p42 MAP kinase activation in osteoblasts. *Life Sciences*, **80** (2006) 230–234. https://doi.org/10.1016/j.lfs.2006.09.003.

77. G. Fielding & S. Bose, SiO2 and ZnO dopants in three-dimensionally printed tricalcium phosphate bone tissue engineering scaffolds enhance osteogenesis and angiogenesis in vivo. *Acta Biomaterialia*, **9** (2013) 9137–9148. https://doi.org/10.1016/j.actbio.2013.07.009.

78. M. Javed Akhtar, M. Ahamed, S. Kumar, M. Majeed Khan, J. Ahmad, & S. A. Alrokayan, Zinc oxide nanoparticles selectively induce apoptosis in human cancer cells through reactive oxygen species. *International Journal of Nanomedicine*, **7** (2012) 845–857. https://doi.org/10.2147/IJN.S29129.

79. C. C. Leite, Avaliação da indução de autofagia em linhagem de câncer colorretal tratada com nanopartículas de óxido de zinco, Universidade de Caxias do Sul, 2017.

80. L. Taccola, V. Raffa, C. Riggio, O. Vittorio, M. C. Iorio, R. Vanacore, A. Pietrabissa, & A. Cuschieri, Zinc oxide nanoparticles as selective killers of proliferating cells. *International journal of nanomedicine*, **6** (2011) 1129–1140. https://doi.org/10.2147/IJN.S16581.

81. L. Kou, J. Sun, Y. Zhai, & Z. He, The endocytosis and intracellular fate of nanomedicines: Implication for rational design. *Asian Journal of Pharmaceutical Sciences*, **8** (2013) 1–8. https://doi.org/10.1016/j.ajps.2013.07.001.

82. S. Salatin & A. Yari Khosroushahi, Overviews on the cellular uptake mechanism of polysaccharide colloidal nanoparticles. *Journal of Cellular and Molecular Medicine*, **21** (2017) 1668–1686. https://doi.org/10.1111/jcmm.13110.

83. N. Oh & J. H. Park, Endocytosis and exocytosis of nanoparticles in mammalian cells.

International Journal of Nanomedicine, **9** (2014) 51–63. https://doi.org/10.2147/IJN.S26592.

84. S. Polo & P. P. Di Fiore, Endocytosis conducts the cell signaling orchestra. *Cell*, **124** (2006) 897–900. https://doi.org/10.1016/j.cell.2006.02.025.

85. W. S. Garrett & I. Mellman, Studies of endocytosis. *Dendritic Cells*, Second Edi, (Academic Press, 2001), pp. 213–230. https://doi.org/10.1016/B978-012455851-9/50055-9.

86. N. Mizushima, Autophagy : process and function. *Genes & Development*, **21** (2007) 2861–2873. https://doi.org/10.1101/gad.1599207.

87. S. Shimizu, T. Yoshida, M. Tsujioka, & S. Arakawa, Autophagic cell death and cancer. *International Journal of Molecular Sciences*, **15** (2014) 3145–3153. https://doi.org/10.3390/ijms15023145.

88. K. N. Yu, T. J. Yoon, A. Minai-Tehrani, J. E. Kim, S. J. Park, M. S. Jeong, S. W. Ha, J. K. Lee, J. S. Kim, & M. H. Cho, Zinc oxide nanoparticle induced autophagic cell death and mitochondrial damage via reactive oxygen species generation. *Toxicology in Vitro*, **27** (2013) 1187–1195. https://doi.org/10.1016/j.tiv.2013.02.010.

89. S. T. Stern, P. P. Adiseshaiah, & R. M. Crist, Autophagy and lysosomal dysfunction as emerging mechanisms of nanomaterial toxicity. *Particle and Fibre Toxicology*, **9** (2012) 1. https://doi.org/10.1186/1743-8977-9-20.

90. Y. Y. Kao, Y. M. Chiung, Y. C. Chen, T. J. Cheng, & P. S. Liu, Zinc oxide nanoparticles interfere with zinc ion homeostasis to cause cytotoxicity. *Toxicological Sciences*, **125** (2012) 462–472. https://doi.org/10.1093/toxsci/kfr319.

91. V. V. Makarov, A. J. Love, O. V. Sinitsyna, S. S. Makarova, I. V. Yaminsky, M. E. Taliansky, & N. O. Kalinina, "Green" nanotechnologies: Synthesis of metal nanoparticles using plants. *Acta Naturae*, **6** (2014) 35–44. https://doi.org/10.1039/c1gc15386b.

92. P. Singh, Y.-J. Kim, D. Zhang, & D.-C. Yang, Biological synthesis of nanoparticles from plants and microorganisms. *Trends in Biotechnology*, **34** (2016) 588–599. https://doi.org/.1037//0033-2909.I26.1.78.

93. M. R. Parra & F. Z. Haque, Aqueous chemical route synthesis and the effect of calcination temperature on the structural and optical properties of ZnO nanoparticles. *Journal of Materials Research and Technology*, **3** (2014) 363–369. https://doi.org/10.1016/j.jmrt.2014.07.001.

94. P. Dhadapani, A. S. Siddarth, S. Kamalasekaran, S. Maruthamuthu, & G. Rajagopal, Bio-approach: Ureolytic bacteria mediated synthesis of ZnO nanocrystals on cotton fabric and evaluation of their antibacterial properties. *Carbohydrate Polymers*, **103** (2014) 448–455. https://doi.org/.1037//0033-2909.I26.1.78.

95. U. Manzoor, F. T. Zahra, S. Rafique, M. T. Moin, & M. Mujahid, Effect of the synthesis temperature, nucleation time and postsynthesis heat treatment of ZnO nanoparticles and its sensing properties. *Journal of Nanomaterials*, **2015** (2015) 1–6.

96. S. Shaziman, A. S. Ismailrosdi, M. H. Mamat, & A. S. Zoolfakar, Influence of Growth Time and Temperature on the Morphology of ZnO Nanorods via Hydrothermal. *IOP Conference Series: Materials Science and Engineering*, **99** (2015) 1–8. https://doi.org/10.1088/1757-899X/99/1/012016.

97. S. Azizi, M. B. Ahmad, F. Namvar, & R. Mohamad, Green biosynthesis and characterization of zinc oxide nanoparticles using brown marine macroalga Sargassum muticum aqueous extract. *Materials Letters*, **116** (2014) 275–277. https://doi.org/10.1016/j.matlet.2013.11.038.

98. S. Nagarajan & K. A. Kuppusamy, Extracellular synthesis of zinc oxide nanoparticle using seaweeds o f gulf of Mannar , India. *Journal of Nanobiotechnology*, **11** (2013) 1–11.

99. S. Busi, J. Rajkumari, S. Pattnaik, P. Parasuraman, & S. Hnamte, Extracellular synthesis of zinc oxide nanoparticles using Acinetobacter schindleri SIZ7 and its antimicrobial property against foodborne pathogens. *Journal of Microbiology, Biotechnology and Food Sciences*, **05** (2016) 407–411. https://doi.org/10.15414/jmbfs.2016.5.5.407-411.

100. R. M. Tripathi, A. S. Bhadwal, R. K. Gupta, P. Singh, A. Shrivastav, & B. R. Shrivastav, ZnO nanoflowers: Novel biogenic synthesis and enhanced photocatalytic activity. *Journal of Photochemistry and Photobiology B: Biology*, **141** (2014) 288–295. https://doi.org/10.1016/j.jphotobiol.2014.10.001.

101. E. Selvarajan & V. Mohanasrinivasan, Biosynthesis and characterization of ZnO nanoparticles using Lactobacillus plantarum VITES07. *Materials Letters*, **112** (2013) 180–182. https://doi.org/10.1016/j.matlet.2013.09.020.

102. B. N. Singh, A. K. S. Rawat, W. Khan, A. H. Naqvi, & B. R. Singh, Biosynthesis of stable antioxidant ZnO nanoparticles by Pseudomonas aeruginosa Rhamnolipids. *PLoS ONE*, **9** (2014) 1–12. https://doi.org/10.1371/journal.pone.0106937.

103. M. A. Rauf, M. Owais, R. Rajpoot, F. Ahmad, N. Khan, & S. Zubair, Biomimetically synthesized ZnO nanoparticles attain potent antibacterial activity against less susceptible: S. aureus skin infection in experimental animals. *RSC Advances*, **7** (2017) 36361–36373. https://doi.org/10.1039/c7ra05040b.

104. R. Raliya & J. C. Tarafdar, ZnO Nanoparticle Biosynthesis and Its Effect on Phosphorous-Mobilizing Enzyme Secretion and Gum Contents in Clusterbean (Cyamopsis tetragonoloba L.). *Agricultural Research*, **2** (2013) 48–57. https://doi.org/10.1007/s40003-012-0049-z.

105. V. N. Kalpana, B. A. S. Kataru, N. Sravani, T. Vigneshwari, A. Panneerselvam, & V. Devi Rajeswari, Biosynthesis of zinc oxide nanoparticles using culture filtrates of Aspergillus niger: Antimicrobial textiles and dye degradation studies. *OpenNano*, **3** (2018) 48–55. https://doi.org/10.1016/j.onano.2018.06.001.

106. S. Gunalan, R. Sivaraj, & V. Rajendran, Green synthesized ZnO nanoparticles against bacterial and fungal pathogens. *Progress in Natural Science: Materials International*, **22** (2012) 693–700. https://doi.org/10.1016/j.pnsc.2012.11.015.

107. G. Sathishkumar, C. Rajkuberan, K. Manikandan, S. Prabukumar, J. DanielJohn, & S. Sivaramakrishnan, Facile biosynthesis of antimicrobial zinc oxide (ZnO) nanoflakes using leaf extract of Couroupita guianensis Aubl. *Materials Letters*, **222** (2018) 200. https://doi.org/10.1016/j.matlet.2018.03.170.

108. A. K. Singh, P. Pal, V. Gupta, T. P. Yadav, V. Gupta, & S. P. Singh, Green synthesis, characterization and antimicrobial activity of zinc oxide quantum dots using Eclipta alba. *Materials Chemistry and Physics*, **203** (2018) 40–48. https://doi.org/10.1016/j.matchemphys.2017.09.049.

109. P. Sutradhar & M. Saha, Green synthesis of zinc oxide nanoparticles using tomato (Lycopersicon esculentum) extract and its photovoltaic application. *Journal of Experimental Nanoscience*, **11** (2017) 314–327. https://doi.org/10.1080/17458080.2015.1059504.

110. M. Sorbiun, E. Shayegan Mehr, A. Ramazani, & S. Taghavi Fardood, Green Synthesis of Zinc Oxide and Copper Oxide Nanoparticles Using Aqueous Extract of Oak Fruit Hull (Jaft) and Comparing Their Photocatalytic Degradation of Basic Violet 3. *International Journal of Environmental Research*, **12** (2018) 29–37. https://doi.org/10.1007/s41742-

018-0064-4.

111. M. Khatami, H. Q. Alijani, H. Heli, & I. Sharifi, Rectangular shaped zinc oxide nanoparticles: Green synthesis by Stevia and its biomedical efficiency. *Ceramics International*, **44** (2018) 15596–15602. https://doi.org/10.1016/j.ceramint.2018.05.224.

112. M. Fazlzadeh, R. Khosravi, & A. Zarei, Green synthesis of zinc oxide nanoparticles using Peganum harmala seed extract, and loaded on Peganum harmala seed powdered activated carbon as new adsorbent for removal of Cr(VI) from aqueous solution. *Ecological Engineering*, **103** (2017) 180–190. https://doi.org/10.1016/j.ecoleng.2017.02.052.

113. A. Das, R. Chadha, N. Maiti, & S. Kapoor, Synthesis of pH sensitive gold nanoparticles for potential application in radiosensitization. *Materials Science & Engineering C*, **55** (2015) 34–41. https://doi.org/10.1016/j.msec.2015.05.048.

114. O. Velgosová, A. Mraziková, & R. Marcincaková, Influence of pH on green synthesis of Ag nanoparticles. *Materials Letters*, **180** (2016) 336–339. https://doi.org/10.1016/j.matlet.2016.04.045.

115. K. Chitra & G. Annadurai, Antibacterial Activity of pH-Dependent Biosynthesized Silver Nanoparticles against Clinical Pathogen. *BioMed Research International*, **2014** (2014) 1–6. https://doi.org/10.1155/2014/725165.

116. N. R. N. Roselina, A. Azizan, K. Mei, A. Jumahat, & M. A. A. Bakar, Effect of pH on formation of Nickel Nanostructures through Chemical Reduction Method. *Procedia Engineering*, **68** (2013) 43–48. https://doi.org/10.1016/j.proeng.2013.12.145.

117. S. S. Alias, A. B. Ismail, & A. A. Mohamad, Effect of pH on ZnO nanoparticle properties synthesized by sol-gel centrifugation. *Journal of Alloys and Compounds*, **499** (2010) 231–237. https://doi.org/10.1016/j.jallcom.2010.03.174.

118. C. Chinnasamy, P. Tamilselvam, B. Karthick, B. Sidharth, & M. Senthilnathan, Green Synthesis , Characterization and Optimization Studies of Zinc Oxide Nano Particles Using Costusigneus Leaf Extract. *Materials Today: Proceedings*, **5** (2018) 6728–6735. https://doi.org/10.1016/j.matpr.2017.11.331.

119. N. Ain Samat & R. Md Nor, Sol-gel synthesis of zinc oxide nanoparticles using Citrus aurantifolia extracts. *Ceramics International*, **39** (2013) S545–S548. https://doi.org/10.1016/j.ceramint.2012.10.132.

120. M. Shah, D. Fawcett, S. Sharma, S. K. Tripathy, & G. E. J. Poinern, *Green synthesis of metallic nanoparticles via biological entities* (2015). https://doi.org/10.3390/ma8115377.

121. C. M. Pelicano, E. Magdaluyo, & A. Ishizumi, Temperature Dependence of Structural and Optical Properties of ZnO Nanoparticles Formed by Simple Precipitation Method. *MATEC Web of Conferences*, **43** (2016) 02001. https://doi.org/10.1051/matecconf/20164302001.

122. M. Ovais, A. T. Khalil, M. Ayaz, I. Ahmad, S. K. Nethi, & S. Mukherjee, Biosynthesis of metal nanoparticles via microbial enzymes: A mechanistic approach. *International Journal of Molecular Sciences*, **19** (2018) 1–20. https://doi.org/10.3390/ijms19124100.

123. S. A. Kumar, M. K. Abyaneh, S. W. Gosavi, S. K. Kulkarni, R. Pasricha, A. Ahmad, & M. I. Khan, Nitrate reductase-mediated synthesis of silver nanoparticles from AgNO 3. *Biotechnology Letters*, **29** (2007) 439–445. https://doi.org/10.1007/s10529-006-9256-7.

124. N. Pantidos & L. Horsfall, Biological Synthesis of Metallic Nanoparticles by Bacteria,

Fungi and Plants. *Journal of Nanomedicine & Nanotechnology*, **05** (2014) 1–10. https://doi.org/10.4172/2157-7439.1000233.

125. N. I. Hulkoti & T. C. Taranath, Biosynthesis of nanoparticles using microbes-A review. *Colloids and Surfaces B: Biointerfaces*, **121** (2014) 474–483. https://doi.org/10.1016/j.colsurfb.2014.05.027.

126. X. Li, H. Xu, Z.-S. Chen, & G. Chen, Biosynthesis of Nanoparticles by Microorganisms and Their Applications. *Journal of Nanomaterials*, **2011** (2011) 1–16. https://doi.org/10.1155/2011/270974.

127. T. Klaus, R. Joerger, & C.-G. Granqvist, Silver-based crystalline nanoparticles, microbially fabricated. *Proceedings of the National Academy of Sciences of the United States of America*, **96** (1999) 13611–4.

128. J. Markus, R. Mathiyalagan, Y. Kim, R. Abbai, S. Singh, S. Ahn, Z. E. J. Perez, J. Hurh, & D. C. Yang, Intracellular synthesis of gold nanoparticles with antioxidant activity by probiotic Lactobacillus kimchicus DCY51 isolated from Korean kimchi. *Enzyme and microbial Technology*, **95** (2016) 85–93. https://doi.org/.1037//0033-2909.I26.1.78.

129. H. Argawal, S. Menon, S. V. Kumar, & S. Rajeshkumar, Mechanistic study on antibacterial action of zinc oxide nanoparticles synthesized using green route. *Chemico-Biological Interactions*, **286** (2018) 60–70. https://doi.org/.1037//0033-2909.I26.1.78.

130. C. A. McDevitt, A. D. Ogunniyi, E. Valkov, M. C. Lawrence, B. Kobe, A. G. McEwan, & J. C. Paton, A molecular mechanism for bacterial susceptibility to Zinc. *PLoS Pathogens*, **7** (2011) 1–9. https://doi.org/10.1371/journal.ppat.1002357.

131. G. Grass, M. D. Wong, B. P. Rosen, R. L. Smith, & C. Rensing, ZupT Is a Zn(II) Uptake System in Escherichia coli. *Journal of Bacteriology*, **184** (2002) 864–866. https://doi.org/10.1128/JB.184.3.864.

132. Z. Molnár, V. Bódai, G. Szakacs, B. Erdélyi, Z. Fogarassy, G. Sáfrán, T. Varga, Z. Kónya, E. Tóth-Szeles, R. Szucs, & I. Lagzi, Green synthesis of gold nanoparticles by thermophilic filamentous fungi. *Scientific Reports*, **8** (2018) 1–12. https://doi.org/10.1038/s41598-018-22112-3.

133. A. Zielonka & M. Klimek-ochab, Fungal synthesis of size-defined nanoparticles Related content. *Advances in natural Sciences: nanoscience and nanotechnology*, **8** (2017) 1–9. https://doi.org/10.1088/2043-6254/aa84d4.

134. K. B. Narayanan & N. Sakthivel, Biological syntheiss of metal nanoparticles by microbes. *Advances in Colloid and Interface Science*, **156** (2010) 1–13. https://doi.org/10.1016/j.cis.2010.02.001.

135. G. Li, D. He, Y. Qian, B. Guan, S. Gao, Y. Cui, K. Yokoyama, & L. Wang, Fungus-mediated green synthesis of silver nanoparticles using aspergillus terreus. *International Journal of Molecular Sciences*, **13** (2012) 466–476. https://doi.org/10.3390/ijms13010466.

136. S. Ahmed, M. Ahmad, B. L. Swami, & S. Ikram, A review on plants extract mediated synthesis of silver nanoparticles for antimicrobial applications : A green expertise. *Journal of Advanced Research*, **7** (2016) 17–28. https://doi.org/10.1016/j.jare.2015.02.007.

137. D. P. Xu, Y. Li, X. Meng, T. Zhou, Y. Zhou, J. Zheng, J. J. Zhang, & H. Bin Li, Natural antioxidants in foods and medicinal plants: Extraction, assessment and resources. *International Journal of Molecular Sciences*, **18** (2017) 20–31. https://doi.org/10.3390/ijms18010096.

138. A. Altemimi, N. Lakhssassi, A. Baharlouei, D. Watson, & D. Lightfoot, Phytochemicals: Extraction, Isolation, and Identification of Bioactive Compounds from Plant Extracts.

Plants, **6** (2017) 1–23. https://doi.org/10.3390/plants6040042.

139. P. Maisuthisakul, S. Pasuk, & P. Ritthiruangdej, Relationship between antioxidant properties and chemical composition of some Thai plants. *Journal of Food Composition and Analysis*, **21** (2008) 229–240. https://doi.org/10.1016/j.jfca.2007.11.005.

140. B. Guldiken, G. Ozkan, G. Catalkaya, F. D. Ceylan, I. E. Yalcinkaya, & E. Capanoglu, Phytochemicals of herbs and spices: health versus toxicological effects. *Food and Chemical Toxicology*, **119** (2018) 37–49. https://doi.org/.1037//0033-2909.I26.1.78.

141. S. J. S. Flora, Structural, chemical and biological aspects of antioxidants for strategies against metal and metalloid exposure. *Oxidative Medicine and Cellular Longevity*, **2** (2009) 191–206. https://doi.org/10.4161/oxim.2.4.9112.

142. S. Ahmed, S. Ali, & S. Ikram, A review on biogenic synthesis of ZnO nanoparticles using plant extracts and microbes : A prospect towards green chemistry. *Journal of Photochemistry and Photobiology B: Biology*, **166** (2017) 272–284. https://doi.org/10.1016/j.jphotobiol.2016.12.011.

143. N. A. Anjum, M. Hasanuzzaman, M. A. Hossain, P. Thangavel, A. Roychoudhury, S. S. Gill, M. A. M. Rodrigo, V. Adam, M. Fujita, R. Kizek, A. C. Duarte, E. Pereira, & I. Ahmad, Jacks of metal/metalloid chelation trade in plantsâ€"an overview. *Frontiers in Plant Science*, **6** (2015) 1–17. https://doi.org/10.3389/fpls.2015.00192.

144. M. Saxena, J. Saxena, R. Nema, D. Singh, & A. Gupta, Pytochemistry of Medicinal Plants. *Journal of Pharmacognosy and Phytochemistry*, **1** (2013) 168–182.

145. G. Sharma, A. K. Gupta, D. Ganjewala, C. Gupta, D. Prakash, & others, Phytochemical composition, antioxidant and antibacterial potential of underutilized parts of some fruits. *International Food Research Journal*, **24** (2017) 1167–1173.

146. A. T. Oz & E. Kafkas, Phytochemicals in Fruits and Vegetables. *Superfood Funct. Food - An Overv. Their Process. Util.* (2017), pp. 175–184. https://doi.org/10.5772/66987.

147. M. Gupta, R. S. Tomar, S. Kaushik, R. K. Mishra, & D. Sharma, Effective antimicrobial activity of green ZnO nano particles of Catharanthus roseus. *Frontiers in Microbiology*, **9** (2018) 1–13. https://doi.org/10.3389/fmicb.2018.02030.

148. D. Kelman, E. K. Posner, K. J. McDermid, N. K. Tabandera, P. R. Wright, & A. D. Wright, Antioxidant activity of Hawaiian marine algae. *Marine Drugs*, **10** (2012) 403–416. https://doi.org/10.3390/md10020403.

149. Z. Zhang, F. Wang, X. Wang, X. Liu, Y. Hou, & Q. Zhang, Extraction of the polysaccharides from five algae and their potential antioxidant activity in vitro. *Carbohydrate Polymers*, **82** (2010) 118–121. https://doi.org/10.1016/j.carbpol.2010.04.031.

150. M. Plaza, S. Santoyo, L. Jaime, G. García-Blairsy Reina, M. Herrero, F. J. Señoráns, & E. Ibáñez, Screening for bioactive compounds from algae. *Journal of Pharmaceutical and Biomedical Analysis*, **51** (2010) 450–455. https://doi.org/10.1016/j.jpba.2009.03.016.

151. R. Ishwarya, B. Vaseeharan, S. Kalyani, B. Banumathi, M. Govindarajan, N. S. Alharbi, S. Kadaikunnan, M. N. Al-anbr, J. M. Khaled, & G. Benelli, Facile green synthesis of zinc oxide nanoparticles using Ulva lactuca seaweed extract and evaluation of their photocatalytic, antibiofilm and insecticidal activity. *Journal of Photochemistry and Photobiology B: Biology*, **178** (2018) 249–258. https://doi.org/10.1016/j.jphotobiol.2017.11.006.

152. M. Khatami, R. S. Varma, N. Zafarnia, H. Yaghoobi, M. Sarani, & V. G. Kumar, Applications of green synthesized Ag, ZnO and Ag/ZnO nanoparticles for making clinical antimicrobial wound-healing bandages. *Sustainable Chemistry and Pharmacy*, **10** (2018) 9–15. https://doi.org/10.1016/J.SCP.2018.08.001.

153. A. Raja, S. Ashokkumar, R. Pavithra Marthandam, J. Jayachandiran, C. P. Khatiwada, K. Kaviyarasu, R. Ganapathi Raman, & M. Swaminathan, Eco-friendly preparation of zinc oxide nanoparticles using Tabernaemontana divaricata and its photocatalytic and antimicrobial activity. *Journal of Photochemistry and Photobiology B: Biology*, **181** (2018) 53–58. https://doi.org/10.1016/j.jphotobiol.2018.02.011.

154. S. S. Roshitha, V. Mithra, V. Saravanan, S. K. Sadasivam, & M. Gnanadesigan, Photocatalytic degradation of methylene blue and safranin dyes using chitosan zinc oxide nano-beads with Musa × paradisiaca L. pseudo stem. *Bioresource Technology Reports*, **5** (2019) 339–342. https://doi.org/10.1016/j.biteb.2018.08.004.

155. F. Namvar, S. Azizi, H. S. Rahman, R. Mohamad, A. Rasedee, M. Soltani, & R. A. Rahim, Green synthesis, characterization, and anticancer activity of hyaluronan/zinc oxide nanocomposite. *OncoTargets and Therapy*, **9** (2016) 4549–4559. https://doi.org/10.2147/OTT.S95962.

156. R. Dobrucka, J. Dlugaszewska, & M. Kaczmarek, Cytotoxic and antimicrobial effect of biosynthesized SnO2 nanoparticles using Pruni spinosae flos extract. *Inorganic and Nano-Metal Chemistry*, **48** (2018) 367–376. https://doi.org/10.1080/24701556.2019.1569054.

157. N. Thovhogi, E. Park, E. Manikandan, M. Maaza, & A. Gurib-Fakim, Physical properties of CdO nanoparticles synthesized by green chemistry via Hibiscus Sabdariffa flower extract. *Journal of Alloys and Compounds*, **655** (2016) 314–320. https://doi.org/10.1016/j.jallcom.2015.09.063.

158. Rahmayeni, A. Alfina, Y. Stiadi, H. J. Lee, & Zulhadjri, Green synthesis and Characterization of ZnO-CoFe2O4 Semiconductor Photocatalysts Prepared Using Rambutan (Nephelium lappaceum L.) Peel Extract. *Materials Research*, **22** (2019) 1–11. https://doi.org/10.1590/1980-5373-MR-2019-0228.

159. K. R. Basavalingiah, S. Harishkumar, Udayabhanu, G. Nagaraju, D. Rangappa, & Chikkahanumantharayappa, Highly porous, honeycomb like Ag–ZnO nanomaterials for enhanced photocatalytic and photoluminescence studies: green synthesis using Azadirachta indica gum. *SN Applied Sciences*, **1** (2019). https://doi.org/10.1007/s42452-019-0863-z.

160. X. Fuku, K. Kaviyarasu, N. Matinise, & M. Maaza, Punicalagin Green Functionalized Cu/Cu2O/ZnO/CuO Nanocomposite for Potential Electrochemical Transducer and Catalyst. *Nanoscale Research Letters*, **11** (2016) 1–12. https://doi.org/10.1186/s11671-016-1581-8.

161. J. J. Marques, *Erva-mate: guia para aplicação das boas práticas agrícolas* (Lajeado: Emater/RS, 2013).

162. L. C. Barbosa Lessa, *História do chimarrão* (Porto Alegre: Sulina, 1986).

163. Embrapa, Sistema de Produção da Erva-mate. (n.d.).

164. IBGE, Produção da Extração Vegetal e da Silvicultura. (2016). https://www.ibge.gov.br/estatisticas-novoportal/economicas/agricultura-e-pecuaria/9105-producao-da-extracao-vegetal-e-da-silvicultura.html?=&t=destaques (accessed July 26, 2018).

165. G. B. Freitas, A. Andriola, A. G. Gauer, & L. S. Silveira Ienk, ERVA-MATE, MUITO MAIS QUE UMA TRADIÇÃO, UM VERDADEIRO POTENCIAL TERAPÊUTICO. *Revista Eletrônica de Farmácia*, **VIII** (2011) 101–113.

166. N. D. S. Lima, E. De Oliveira, A. P. S. Da Silva, L. D. A. Maia, E. G. De Moura, & P. C. Lisboa, Effects of Ilex paraguariensis (yerba mate) treatment on leptin resistance and

inflammatory parameters in obese rats primed by early weaning. *Life Sciences*, **115** (2014) 29–35. https://doi.org/10.1016/j.lfs.2014.09.003.

167. R. Filip, Antifungal Activity of the aqueous Extract of Ilex Paraguariensis against Malassezia furfur. *Phitotherapy Research*, **24** (2010) 715–719. https://doi.org/10.1002/ptr.

168. R. A. Jacques, Caracterização química da erva-mate (Ilex paraguariensis): Aplicação de diferentes processos de extração e influência das condições de plantios sobre a composição química, Universidade Federal do Rio Grande do Sul, 2005.

169. C. H. Blum-Silva, A. B. G. Luz, M. V. P. S. Nascimento, B. M. de Campos Facchin, B. Baratto, T. S. Fröde, L. P. Sandjo, E. M. Dalmarco, & F. H. Reginatto, Qualitative and quantitative analysis data of the major constituents of Ilex paraguariensis leaves by UPLC-PDA and QTOF-MS. *Data in Brief*, **8** (2016) 295–299. https://doi.org/10.1016/j.dib.2016.05.022.

170. F. L. G. Dutra, R. Hoffmann-Ribani, & M. Ribani, Determinação de compostos fenólicos por cromatografia líquida de alta eficiência isocrática durante estacionamento da erva-mate. *Quimica Nova*, **33** (2010) 119–123. https://doi.org/10.1590/S0100-40422010000100022.

171. K. A. S. Berté, M. R. Beux, P. K. W. D. S. Spada, M. Salvador, R. Ho, & R. F. H. Santos, Chemical Composition and Antioxidant Activity of Yerba-Mate (Ilex paraguariensis A . St . -Hil ., Aquifoliaceae) Extract as Obtained by Spray Drying. *Journal of Agricultural and Food Chemistry*, **59** (2011) 5523–5527. https://doi.org/10.1021/jf2008343.

172. C. Anesini, S. Turner, L. Cogoi, & R. Filip, Study of the participation of caffeine and polyphenols on the overall antioxidant activity of mate (Ilex paraguariensis). *LWT - Food Science and Technology*, **45** (2012) 299–304. https://doi.org/10.1016/j.lwt.2011.06.015.

173. R. G. Peres, F. G. Tonin, M. F. M. Tavares, & D. B. Rodriguez-Amaya, HPLC-DAD-ESI/MS identification and quantification of phenolic compounds in ilex paraguariensis beverages and on-line evaluation of individual antioxidant activity. *Molecules*, **18** (2013) 3859–3871. https://doi.org/10.3390/molecules18043859.

174. M. E. G. Lacerda, C. A. Filho, & M. A. Kaplan, Comparative Evaluation of Methyl Xanthine Percentages in Commercial Samples of Black Tea and Mate Tea Avaliação Comparativa dos Teores de Metilxantinas em Amostras de Chá Preto e Chá Mate. *Brazilian Journal of Food Technology*, **3** (2000) 17–21.

175. S. C. B. Gnoatto, S. E. P., & V. L. Bassani, HPLC Method to Assay Total Saponins in Ilex paraguariensis Aqueous Extract Simone. *Journal of Brazilian Chemical Society*, **16** (2005) 723–26. https://doi.org/10.1590/S0103-50532005000500007.

176. L. Mertz, What is biocompatibility? A new definition based on the latest technology. *IEEE Pulse*, **4** (2013) 14–15.

177. D. Williams, Concepts in biocompatibility: new biomaterials, new paradigms and new testing regimes. *Biocompat. Perform. Med. devices* (Cambridge: Woodhead Publishing, 2012), pp. 3–17.

178. Q. Chen & G. A. Thouas, Metallic implant biomaterials. *Materials Science and Engineering R: Reports*, **87** (2015) 1–57. https://doi.org/10.1016/j.mser.2014.10.001.

179. J. Jacob, Biomaterials: Contact lenses. *An Introd. to Mater. Med.*, 3rd ed, (Oxford: Academic Press, 2013), pp. 909–916.

180. R. A. Bapat, T. V. Chaubal, C. P. Joshi, P. R. Bapat, H. Choudhury, M. Pandey, B. Gorain, & P. Kesharwani, An overview of application of silver nanoparticles for biomaterials in

dentistry. *Materials Science and Engineering C*, **91** (2018) 881–898. https://doi.org/10.1016/j.msec.2018.05.069.

181. L. F. Santos, I. J. Correia, A. S. Silva, & J. F. Mano, Biomaterials for drug delivery patches. *European Journal of Pharmaceutical Sciences*, **118** (2018) 49–66. https://doi.org/10.1016/j.ejps.2018.03.020.

182. P. Zarrintaj, B. Bakhshandeh, M. R. Saeb, F. Sefat, I. Rezaeian, M. R. Ganjali, S. Ramakrishna, & M. Mozafari, Oligoaniline-based conductive biomaterials for tissue engineering. *Acta Biomaterialia*, **72** (2018) 16–34. https://doi.org/10.1016/j.actbio.2018.03.042.

183. B. D. Ratner, The biocompatibility manifesto: Biocompatibility for the twenty-first century. *Journal of Cardiovascular Translational Research*, **4** (2011) 523–527. https://doi.org/10.1007/s12265-011-9287-x.

184. S. Bhat & A. Kumar, Biomaterials and bioengineering tomorrow's healthcare. *Biomatter*, **3** (2013). https://doi.org/10.4161/biom.24717.

185. W. He & R. Benson, Polymeric Biomaterials. *Appl. Plast. Handb.*, 2nd ed, (Oxford: William Andrew, 2017), pp. 145–164.

186. P. Grossen, D. Witzigmann, S. Sieber, & J. Huwyler, PEG-PCL-based nanomedicines: A biodegradable drug delivery system and its application. *Journal of Controlled Release*, **260** (2017) 46–60. https://doi.org/10.1016/j.jconrel.2017.05.028.

187. M. Arora, Polymethylmethacrylate bone cements and additives: A review of the literature. *World Journal of Orthopedics*, **4** (2013) 67. https://doi.org/10.5312/wjo.v4.i2.67.

188. E. Caló & V. V. Khutoryanskiy, Biomedical applications of hydrogels: A review of patents and commercial products. *European Polymer Journal*, **65** (2015) 252–267. https://doi.org/10.1016/j.eurpolymj.2014.11.024.

189. V. K. Vendra, L. Wu, & S. Krishnan, Polymer Thin Films for Biomedical Applications. *Nanomater. Life Sci.* (Weinheim: Wiley-VCH, 2010), pp. 1–53.

190. S. Parham, A. Z. Kharazi, H. R. Bakhsheshi-Rad, H. Ghayour, A. F. Ismail, H. Nur, & F. Berto, Electrospun Nano-fibers for biomedical and tissue engineering applications: A comprehensive review. *Materials*, **13** (2020) 1–25. https://doi.org/10.3390/ma13092153.

191. B. Azimi, H. Maleki, L. Zavagna, J. Gustavo, D. Ossa, S. Linari, A. Lazzeri, & S. Danti, Bio-Based Electrospun Fibers for Wound Healing. *Journal of Functional Bomaterials*, **11** (2020). https://doi.org/10.3390/jbf11030067.

192. M. Hess, R. G. Jones, J. Kahovec, T. Kitayama, P. Kratochvíl, P. Kubisa, W. Mormann, R. F. T. Stepto, D. Tabak, J. Vohlídal, & E. S. Wilks, Terminology of polymers containing ionizable or ionic groups and of polymers containing ions (IUPAC Recommendations 2006). *Pure and Applied Chemistry*, **78** (2006) 2067–2074. https://doi.org/10.1351/pac200678112067.

193. V. S. Meka, M. K. G. Sing, M. R. Pichika, S. R. Nali, V. R. M. Kolapalli, & P. Kesharwani, A comprehensive review on polyelectrolyte complexes. *Drug Discovery Today*, **22** (2017) 1697–1706. https://doi.org/10.1016/j.drudis.2017.06.008.

194. J. Choi & M. F. Rubner, Influence of the degree of ionization on weak polyelectrolyte multilayer assembly. *Macromolecules*, **38** (2005) 116–124. https://doi.org/10.1021/ma048596o.

195. P. Atkins & L. Jones, *Princípios da química: questionando a vida moderna e o meio ambiente* (Porto Alegre: Bookman, 2006).

196. S. E. Burke & C. J. Barrett, Acid-base equilibria of weak polyelectrolytes in multilayer thin films. *Langmuir*, **19** (2003) 3297–3303. https://doi.org/10.1021/la026500i.

197. H. Frey, Applications and Developments of Thin Film Technology. In H. Frey, & H.R. Khan,eds., *Handb. Thin-Film Technol.* (Berlin, Heidelberg: Springer Berlin Heidelberg, 2015), pp. 1–3. https://doi.org/10.1007/978-3-642-05430-3_1.

198. S. M. Skovdal, N. P. Jørgensen, E. Petersen, S. Jensen-Fangel, R. Ogaki, G. Zeng, M. I. Johansen, M. Wang, H. Rohde, & R. L. Meyer, Ultra-dense polymer brush coating reduces Staphylococcus epidermidis biofilms on medical implants and improves antibiotic treatment outcome. *Acta Biomaterialia*, **76** (2018) 46–55. https://doi.org/10.1016/j.actbio.2018.07.002.

199. L. Séon, P. Lavalle, P. Schaaf, & F. Boulmedais, Polyelectrolyte Multilayers: A Versatile Tool for Preparing Antimicrobial Coatings. *Langmuir*, **31** (2015) 12856–12872. https://doi.org/10.1021/acs.langmuir.5b02768.

200. S. Karki, H. Kim, S. J. Na, D. Shin, K. Jo, & J. Lee, Thin films as an emerging platform for drug delivery. *Asian Journal of Pharmaceutical Sciences*, **11** (2016) 559–574. https://doi.org/10.1016/j.ajps.2016.05.004.

201. M. Mozafari, A. Ramedani, Y. N. Zhang, & D. K. Mills, Thin films for tissue engineering applications. *Thin Film Coatings Biomater. Biomed. Appl.* (Cambridge: Woodhead Publishing, 2016), pp. 167–195.

202. P. H. Li & P. K. Chu, Thin film depositions technologies and processing of biomaterials. *Thin Film Coatings Biomater. Biomed. Appl.* (Cambridge: Woodhead Publishing, 2016), pp. 3–28.

203. S. Pahal, R. Gakhar, A. M. Raichur, & M. M. Varma, Polyelectrolyte multilayers for bio-applications: recent advancements. *IET Nanobiotechnology*, **11** (2017) 903–908. https://doi.org/10.1049/iet-nbt.2017.0007.

204. A. R. M. Oliveira & A. J. G. Zarbin, Um procedimento simples e barato para a construção de um equipamento "dip-coating" para deposição de filmes em laboratório. *Quimica Nova*, **28** (2005) 141–144. https://doi.org/10.1590/S0100-40422005000100024.

205. A. Pallotta, M. Parent, I. Clarot, M. Luo, V. Borr, P. Dan, V. Decot, P. Menu, R. Safar, O. Joubert, P. Leroy, & A. Boudier, Blood Compatibility of Multilayered Polyelectrolyte Films Containing Immobilized Gold Nanoparticles. *Particle and Particle Systems Characterization*, **34** (2017) 1–8. https://doi.org/10.1002/ppsc.201600184.

206. S. R. Pattabhi, A. M. Lehaf, J. B. Schlenoff, & T. C. S. Keller, Human mesenchymal stem cell osteoblast differentiation, ECM deposition, and biomineralization on PAH/PAA polyelectrolyte multilayers. *Journal of Biomedical Materials Research - Part A*, **103** (2015) 1818–1827. https://doi.org/10.1002/jbm.a.35322.

207. M. Sailer, K. Lai Wing Sun, O. Mermut, T. E. Kennedy, & C. J. Barrett, High-throughput cellular screening of engineered ECM based on combinatorial polyelectrolyte multilayer films. *Biomaterials*, **33** (2012) 5841–5847. https://doi.org/10.1016/j.biomaterials.2012.05.001.

208. H. W. Chien, S. F. Tan, K. L. Wei, & W. B. Tsai, Modulation of the functions of osteoblast-like cells on poly(allylamine hydrochloride) and poly(acrylic acid) multilayer films. *Colloids and Surfaces B: Biointerfaces*, **88** (2011) 297–303. https://doi.org/10.1016/j.colsurfb.2011.07.005.

209. A. Jaklenec, A. C. Anselmo, J. Hong, A. J. Vegas, M. Kozminsky, R. Langer, P. T. Hammond, & D. G. Anderson, High Throughput Layer-by-Layer Films for Extracting Film Forming Parameters and Modulating Film Interactions with Cells. *ACS Applied Materials*

and Interfaces, **8** (2016) 2255–2261. https://doi.org/10.1021/acsami.5b11081.

210. F. Trista, G. Palestino, J. Menchaca, E. Pérez, H. Atmani, F. Cuisinier, & G. Ladam, Tunable Protein-Resistance of Polycation-Terminated Polyelectrolyte Multilayers. *Biomacromolecules*, **10** (2009) 2275–2283. https://doi.org/10.1021/bm900453s.

211. S. Anandhakumar & A. M. Raichur, Polyelectrolyte/silver nanocomposite multilayer films as multifunctional thin film platforms for remote activated protein and drug delivery. *Acta Biomaterialia*, **9** (2013) 8864–8874. https://doi.org/10.1016/j.actbio.2013.06.012.

212. F. Tian, J. Kaňka, F. Yang, J. Min, & P. T. Hammond, Role of silica nanoparticles in monitoring and prolonging release of drug-eluting polyelectrolyte coatings using long-period fiber grating platform. *Sensors and Actuators, B: Chemical*, **252** (2017) 831–839. https://doi.org/10.1016/j.snb.2017.06.048.

213. N. Dal'Acqua, A. C. R. Faria, M. C. Vebber, H. da Silva Barud, M. Giovanela, G. Machado, & J. da Silva Crespo, Hydrogen photocatalytic production from the self-assembled films of PAH/PAA/TiO2 supported on bacterial cellulose membranes. *International Journal of Hydrogen Energy*, **43** (2018) 15794–15806. https://doi.org/10.1016/j.ijhydene.2018.06.176.

214. M. C. Vebber, J. da Silva Crespo, & M. Giovanela, Self-assembled thin films of PAA/PAH/TiO 2 for the photooxidation of ibuprofen. Part I: Optimization of photoactivity using design of experiments and surface response methodology. *Chemical Engineering Journal*, **360** (2019) 1447–1458. https://doi.org/10.1016/j.cej.2018.10.189.

215. J. Xue, T. Wu, Y. Dai, & Y. Xia, Electrospinning and electrospun nanofibers: Methods, materials, and applications. *Chemical Reviews*, **119** (2019) 5298–5415. https://doi.org/10.1021/acs.chemrev.8b00593.

216. C. J. Luo, S. D. Stoyanov, E. Stride, E. Pelan, & M. Edirisinghe, Electrospinning versus fibre production methods: From specifics to technological convergence. *Chemical Society Reviews*, **41** (2012) 4708–4735. https://doi.org/10.1039/c2cs35083a.

217. P. J. Rivero, D. M. Redin, & R. J. Rodríguez, Electrospinning: A powerful tool to improve the corrosion resistance of metallic surfaces using nanofibrous coatings. *Metals*, **10** (2020). https://doi.org/10.3390/met10030350.

218. S. Maeda, T. Kato, H. Kogure, & N. Hosoya, Rapid response of thermo-sensitive hydrogels with porous structures. *Applied Physics Letters*, **106** (2015). https://doi.org/10.1063/1.4919585.

219. S. Sukigara, M. Gandhi, J. Ayutsede, M. Micklus, & F. Ko, Regeneration of Bombyx mori silk by electrospinning - Part 1: Processing parameters and geometric properties. *Polymer*, **44** (2003) 5721–5727. https://doi.org/10.1016/S0032-3861(03)00532-9.

220. N. Bhardwaj & S. C. Kundu, Electrospinning: A fascinating fiber fabrication technique. *Biotechnology Advances*, **28** (2010) 325–347. https://doi.org/10.1016/j.biotechadv.2010.01.004.

221. F. Topuz, M. A. Abdulhamid, T. Holtzl, & G. Szekely, Nanofiber engineering of microporous polyimides through electrospinning: Influence of electrospinning parameters and salt addition. *Materials and Design*, **198** (2021) 109280. https://doi.org/10.1016/j.matdes.2020.109280.

222. H. Shao, J. Fang, H. Wang, & T. Lin, Effect of electrospinning parameters and polymer concentrations on mechanical-to-electrical energy conversion of randomly-oriented electrospun poly(vinylidene fluoride) nanofiber mats. *RSC Advances*, **5** (2015) 14345–

14350. https://doi.org/10.1039/c4ra16360e.

223. M. Boas, A. Gradys, G. Vasilyev, M. Burman, & E. Zussman, Electrospinning polyelectrolyte complexes: PH-responsive fibers. *Soft Matter*, **11** (2015) 1739–1747. https://doi.org/10.1039/c4sm02618g.

224. M. Mahmud, A. Perveen, A. Matin, & T. Arafat, Effects of binary solvent mixtures on the electrospinning behavior of poly (vinyl alcohol). *Materials Research Express*, **5** (2018). https://doi.org/10.1088/2053-1591/aadf1f.

225. W. K. Son, J. H. Youk, T. S. Lee, & W. H. Park, The effects of solution properties and polyelectrolyte on electrospinning of ultrafine poly(ethylene oxide) fibers. *Polymer*, **45** (2004) 2959–2966. https://doi.org/10.1016/j.polymer.2004.03.006.

226. A. Chunder, S. Sarkar, Y. Yu, & L. Zhai, Fabrication of ultrathin polyelectrolyte fibers and their controlled release properties. *Colloids and Surfaces B: Biointerfaces*, **58** (2007) 172–179. https://doi.org/10.1016/j.colsurfb.2007.03.004.

227. C. Huang & N. L. Thomas, Fabrication of porous fibers via electrospinning: strategies and applications. *Polymer Reviews*, **60** (2020) 595–647. https://doi.org/10.1080/15583724.2019.1688830.

228. J. Cui, F. Li, Y. Wang, Q. Zhang, W. Ma, & C. Huang, Electrospun nanofiber membranes for wastewater treatment applications. *Separation and Purification Technology*, **250** (2020) 117116. https://doi.org/10.1016/j.seppur.2020.117116.

229. S. Agarwal, J. H. Wendorff, & A. Greiner, Use of electrospinning technique for biomedical applications. *Polymer*, **49** (2008) 5603–5621. https://doi.org/10.1016/j.polymer.2008.09.014.

230. S. Nemati, S. jeong Kim, Y. M. Shin, & H. Shin, Current progress in application of polymeric nanofibers to tissue engineering. *Nano Convergence*, **6** (2019) 1–16. https://doi.org/10.1186/s40580-019-0209-y.

231. M. Cavo, F. Serio, N. R. Kale, E. D'Amone, G. Gigli, & L. L. Del Mercato, Electrospun nanofibers in cancer research: From engineering of: From vitro 3D cancer models to therapy. *Biomaterials Science*, **8** (2020) 4887–4905. https://doi.org/10.1039/d0bm00390e.

232. S. P. Miguel, D. R. Figueira, D. Simões, M. P. Ribeiro, P. Coutinho, P. Ferreira, & I. J. Correia, Electrospun polymeric nanofibres as wound dressings: A review. *Colloids and Surfaces B: Biointerfaces*, **169** (2018) 60–71. https://doi.org/10.1016/j.colsurfb.2018.05.011.

233. M. Rychter, A. Baranowska-Korczyc, & J. Lulek, Progress and perspectives in bioactive agent delivery via electrospun vascular grafts. *RSC Advances*, **7** (2017) 32164–32184. https://doi.org/10.1039/c7ra04735e.

234. F. Zheng, S. Wang, S. Wen, M. Shen, M. Zhu, & X. Shi, Characterization and antibacterial activity of amoxicillin-loaded electrospun nano-hydroxyapatite/poly(lactic-co-glycolic acid) composite nanofibers. *Biomaterials*, **34** (2013) 1402–1412. https://doi.org/10.1016/j.biomaterials.2012.10.071.

235. G. Jin, M. P. Prabhakaran, D. Kai, S. K. Annamalai, K. D. Arunachalam, & S. Ramakrishna, Tissue engineered plant extracts as nanofibrous wound dressing. *Biomaterials*, **34** (2013) 724–734. https://doi.org/10.1016/j.biomaterials.2012.10.026.

236. A. M. Abdelgawad, S. M. Hudson, & O. J. Rojas, Antimicrobial wound dressing nanofiber mats from multicomponent (chitosan/silver-NPs/polyvinyl alcohol) systems. *Carbohydrate Polymers*, **100** (2014) 166–178. https://doi.org/10.1016/j.carbpol.2012.12.043.

237. T. Maver, M. Kurečič, T. Pivec, U. Maver, L. Gradišnik, P. Gašparič, B. Kaker, A. Bratuša, S. Hribernik, & K. Stana Kleinschek, Needleless electrospun carboxymethyl cellulose/polyethylene oxide mats with medicinal plant extracts for advanced wound care applications. *Cellulose*, **27** (2020) 4487–4508. https://doi.org/10.1007/s10570-020-03079-9.

238. W. Zhang, S. Ronca, & E. Mele, Electrospun nanofibres containing antimicrobial plant extracts. *Nanomaterials*, **7** (2017) 1–17. https://doi.org/10.3390/nano7020042.

239. Z. Hadisi, M. Farokhi, H. R. Bakhsheshi-Rad, M. Jahanshahi, S. Hasanpour, E. Pagan, A. Dolatshahi-Pirouz, Y. S. Zhang, S. C. Kundu, & M. Akbari, Hyaluronic Acid (HA)-Based Silk Fibroin/Zinc Oxide Core–Shell Electrospun Dressing for Burn Wound Management. *Macromolecular Bioscience*, **20** (2020) 1–17. https://doi.org/10.1002/mabi.201900328.

240. T. Yamaguchi, H. Takamura, T. Matoba, & J. Terao, HPLC method for evaluation of the free radical-scavenging activity of foods by using 1,1-diphenyl-2-picrylhydrazyl. *Bioscience, Biotechnology and Biochemistry*, **62** (1998) 1201–1204. https://doi.org/10.1271/bbb.62.1201.

241. V. L. Singleton, J. A. Rossi Jr., & Rossi J A Jr., Colorimetry of Total Phenolics with Phosphomolybdic-Phosphotungstic Acid Reagents. *American Journal of Enology and Viticulture*, **16** (1965) 144–158. https://doi.org/10.12691/ijebb-2-1-5.

242. A. J. Bard & L. R. Faulkner, *Electrochemical methods: fundamentals and applications* (New York: John Wiley & Sons, 1994).

243. N. Elgrishi, K. J. Rountree, B. D. McCarthy, E. S. Rountree, T. T. Eisenhart, & J. L. Dempsey, A Practical Beginner's Guide to Cyclic Voltammetry. *Journal of Chemical Education*, **95** (2018) 197–206. https://doi.org/10.1021/acs.jchemed.7b00361.

244. V. Uvarov & I. Popov, Metrological characterization of X-ray diffraction methods at different acquisition geometries for determination of crystallite size in nano-scale materials. *Materials Characterization*, **85** (2013) 111–123. https://doi.org/10.1016/j.matchar.2013.09.002.

245. C. T. Rueden, J. Schindelin, M. C. Hiner, B. E. DeZonia, A. E. Walter, E. T. Arena, & K. W. Eliceiri, ImageJ2: ImageJ for the next generation of scientific image data. *BMC Bioinformatics*, **18** (2017) 1–26. https://doi.org/10.1186/s12859-017-1934-z.

246. Biological evaluation of medical devices (ISO 10993-5). *International Organization for Standardization*, (2009).

247. D. C. Montgomery, *Design and Analysis of experiments* (New York: John Wiley & Sons, 1996).

248. *Method 3050B: Acid Digestion of Sediments, Sludges, and Soils,* (Washington, DC, 1996).

249. G. Yuvaraja, J. L. Pathak, W. Zhang, Y. Zhang, & X. Jiao, Antibacterial and wound healing properties of chitosan/poly(vinyl alcohol)/zinc oxide beads (CS/PVA/ZnO). *International Journal of Biological Macromolecules*, **103** (2017) 234–241. https://doi.org/10.1016/j.ijbiomac.2017.05.020.

250. P. V. Gnaneshwar, S. V. Sudakaran, S. Abisegapriyan, J. Sherine, S. Ramakrishna, M. H. A. Rahim, M. M. Yusoff, R. Jose, & J. R. Venugopal, Ramification of zinc oxide doped hydroxyapatite biocomposites for the mineralization of osteoblasts. *Materials Science and Engineering C*, **96** (2019) 337–346. https://doi.org/10.1016/j.msec.2018.11.033.

251. M. Zhai, Y. Xu, B. Zhou, & W. Jing, Keratin-chitosan/n-ZnO nanocomposite hydrogel for antimicrobial treatment of burn wound healing: Characterization and biomedical application. *Journal of Photochemistry and Photobiology B: Biology*, **180** (2018) 253–258. https://doi.org/10.1016/j.jphotobiol.2018.02.018.

252. P. P. Fu, Q. Xia, H. M. Hwang, P. C. Ray, & H. Yu, Mechanisms of nanotoxicity: Generation of reactive oxygen species. *Journal of Food and Drug Analysis*, **22** (2014) 64–75. https://doi.org/10.1016/j.jfda.2014.01.005.

253. C. B. Anders, J. E. Eixenberger, N. A. Franco, R. J. Hermann, K. D. Rainey, J. J. Chess, A. Punnoose, & D. G. Wingett, ZnO nanoparticle preparation route influences surface reactivity, dissolution and cytotoxicity. *Environmental Science: Nano*, **5** (2018) 572–588. https://doi.org/10.1039/c7en00888k.

254. P. Chen, H. Wang, M. He, B. Chen, B. Yang, & B. Hu, Size-dependent cytotoxicity study of ZnO nanoparticles in HepG2 cells. *Ecotoxicology and Environmental Safety*, **171** (2019) 337–346.

255. A. Punnoose, K. Dodge, J. W. Rasmussen, J. Chess, D. Wingett, & C. Anders, Cytotoxicity of ZnO nanoparticles can be tailored by modifying their surface structure: A green chemistry approach for safer nanomaterials. *ACS Sustainable Chemistry and Engineering*, **2** (2014) 1666–1673. https://doi.org/10.1021/sc500140x.

256. F. T. Thema, E. Manikandan, M. S. Dhlamini, & M. Maaza, Green synthesis of ZnO nanoparticles via Agathosma betulina natural extract. *Materials Letters*, **161** (2015) 124–127. https://doi.org/10.1016/j.matlet.2015.08.052.

257. A. Diallo, B. D. Ngom, E. Park, & M. Maaza, Green synthesis of ZnO nanoparticles by Aspalathus linearis: Structural & optical properties. *Journal of Alloys and Compounds*, **646** (2015) 425–430. https://doi.org/10.1016/j.jallcom.2015.05.242.

258. A. Talha Khalil, S. Hameed, S. Afridi, H. E. A. Mohamed, & Z. K. Shinwari, Sageretia thea mediated biosynthesis of metal oxide nanoparticles for catalytic degradation of crystal violet dye. *Materials Today: Proceedings*, (2020). https://doi.org/10.1016/j.matpr.2020.04.687.

259. M. A. Vieira, M. Maraschin, C. M. Pagliosa, R. Podestá, K. N. de Simas, I. I. Rockenbach, R. D. de M. C. Amboni, & E. R. Amante, Phenolic acids and methylxanthines composition and antioxidant properties of mate (ilex paraguariensis) residue. *Journal of Food Science*, **75** (2010) 280–285. https://doi.org/10.1111/j.1750-3841.2010.01548.x.

260. A. C. Colpo, H. Rosa, M. E. Lima, C. E. F. Pazzini, V. B. De Camargo, F. E. M. Bassante, R. Puntel, D. Ávila Silva, A. Mendez, & V. Folmer, Yerba mate (Ilex paraguariensis St . Hill .) -based beverages : How successive extraction influences the extract composition and its capacity to chelate iron and scavenge free radicals q. *Food Chemistry*, **209** (2016) 185–195. https://doi.org/10.1016/j.foodchem.2016.04.059.

261. A. A. Esmelindro, J. dos S. Girardi, A. Mossi, J. A., & C. Dariva, Influence of Agronomic Variables on the Composition of Mate Tea Leaves (Ilex paraguariensis) Extracts Obtained from CO 2 Extraction at 30 ° C and 175 bar. *Journal of Agricultural and Food Chemistry*, **52** (2004) 1990–1995.

262. M. R. Khelladi, L. Mentar, A. Beniaiche, L. Makhloufi, & A. Azizi, A study on electrodeposited zinc oxide nanostructures. *Journal of Materials Science: Materials in Electronics*, **24** (2013) 153–159. https://doi.org/10.1007/s10854-012-0973-5.

263. N. Ait Ahmed, M. Eyraud, H. Hammache, F. Vacandio, S. Sam, N. Gabouze, P. Knauth, K. Pelzer, & T. Djenizian, New insight into the mechanism of cathodic electrodeposition of zinc oxide thin films onto vitreous carbon. *Electrochimica Acta*, **94** (2013) 238–244. https://doi.org/10.1016/j.electacta.2013.01.103.

264. J. D. Lee, *Concise inorganic chemistry*, 5th ed (Oxford: Blackwell Science Ltd, 1996).

265. E. L. Cardozo, O. Ferrarese-Filho, L. C. Filho, M. de L. L. Ferrarese, C. M. Donaduzzi, & J. A. Sturion, Methylxanthines and phenolic compounds in mate (Ilex paraguariensis St.

Hil.) progenies grown in Brazil. *Journal of Food Composition and Analysis*, **20** (2007) 553–558. https://doi.org/10.1016/j.jfca.2007.04.007.

266. N. Rukk, R. S. Kusmina, Lyudmila G. Shamshiev, G. A. Davydova, E. A. Mironova, A. M. Ermakov, G. A. Buzanov, A. Y. Skeyabina, A. N. Streletski, G. A. Vorobeva, V. M. Retivov, P. A. Volkov, S. Belus, E. Kozhukova, & V. Krasnoperova, Zinc(II) and cadmium(II) halide complexes with caffeine: Synthesis, X-ray crystal structure, cytotoxicity and genotoxicity studies. *Inorganica Chimica Acta*, **487** (2019) 184–200. https://doi.org/.1037//0033-2909.I26.1.78.

267. E. L. A. Mohamed & E. L. H. Hicham, Synthesis and Characterization of caffeine Complexes [M (caf) 4X2] M = Ni (II), Cu (II), Zn (II), Cd (II) X = SCN - , CN - ; caf : caffeine. *Research Journal of Chemical Sciences*, **4** (2014) 42–48.

268. K. Rajam, S. Rajendran, & N. N. Banu, Effect of Caffeine-Zn2+ System in Preventing Corrosion of Carbon Steel in Well Water. *Journal of Chemistry*, **2013** (2013) 1–11. https://doi.org/10.1155/2013/521951.

269. H. Wang, T. L. Hu, R. M. Wen, Q. Wang, & X. H. Bu, In vitro controlled release of theophylline from metal-drug complexes. *Journal of Materials Chemistry B*, **1** (2013) 3879–3882. https://doi.org/10.1039/c3tb20633e.

270. H. EL Hamdani & M. EL Amane, Preparation, spectral, antimicrobial properties and anticancer molecular docking studies of new metal complexes [M(caffeine) 4] (PF 6) 2; M = Fe(II), Co(II), Mn(II), Cd(II), Zn(II), Cu(II), Ni(II). *Journal of Molecular Structure*, **1184** (2019) 262–270. https://doi.org/10.1016/j.molstruc.2019.02.049.

271. L. Findoráková, K. Győryová, J. Kovářová, V. Balek, F. A. Nour El-Dien, & L. Halás, Novel zinc(II) benzoate complex compounds with caffeine and urea synthesis and characterization. *Journal of Thermal Analysis and Calorimetry*, **95** (2009) 923–928. https://doi.org/10.1007/s10973-008-8581-6.

272. S. K. Srivastava & V. B. Singh, Ab initio and DFT studies of the structure and vibrational spectra of anhydrous caffeine. *Spectrochimica Acta - Part A: Molecular and Biomolecular Spectroscopy*, **115** (2013) 45–50. https://doi.org/10.1016/j.saa.2013.06.005.

273. A. T. Khalil, M. Ovais, I. Ullah, M. Ali, Z. K. Shinwari, & M. Maaza, Physical properties, biological applications and biocompatibility studies on biosynthesized single phase cobalt oxide (Co3O4) nanoparticles via Sageretia thea (Osbeck.). *Arabian Journal of Chemistry*, **13** (2020) 606–619. https://doi.org/10.1016/j.arabjc.2017.07.004.

274. N. Mayedwa, N. Mongwaketsi, S. Khamlich, K. Kaviyarasu, N. Matinise, & M. Maaza, Green synthesis of nickel oxide, palladium and palladium oxide synthesized via Aspalathus linearis natural extracts: physical properties & mechanism of formation. *Applied Surface Science*, **446** (2018) 266–272. https://doi.org/10.1016/j.apsusc.2017.12.116.

275. G. Sharmila, C. Muthukumaran, & E. Sangeetha, Green fabrication , characterization of Pisonia alba leaf extract derived MgO nanoparticles and its biological applications. *Nano-Structures & Nano-Objects*, **20** (2019) 100380. https://doi.org/10.1016/j.nanoso.2019.100380.

276. K. Rekha, M. Nirmala, M. G. Nair, & A. Anukaliani, Structural , optical , photocatalytic and antibacterial activity of zinc oxide and manganese doped zinc oxide nanoparticles. *Physica B: Physics of Condensed Matter*, **405** (2010) 3180–3185. https://doi.org/10.1016/j.physb.2010.04.042.

277. S. K. K. Shaat, H. Musleh, H. Zayed, J. Asad, & N. Aldahoudi, Nano-Structures & Nano-

Objects Structural parameters of hydrothermally synthesized ZnO nanostructure and their based solar cells. *Nano-Structures & Nano-Objects*, **23** (2020) 100515. https://doi.org/10.1016/j.nanoso.2020.100515.

278. J. Meseguer, I. Pérez-Grande, & A. Sanz-Andrés, Phase Change capacitors. *Spacecr. Therm. Control*, 1st ed, (Cambridge: Woodhead Publishing, 2012), pp. 209–224.

279. A. Krężel & W. Maret, The biological inorganic chemistry of zinc ions. *Archives of Biochemistry and Biophysics*, **611** (2016) 3–19. https://doi.org/10.1016/j.abb.2016.04.010.

280. S. Pai, H. Sridevi, T. Varadavenkatesan, & R. Vinayagam, Photocatalytic zinc oxide nanoparticles synthesis using Peltophorum pterocarpum leaf extract and their characterization. *Optik - International Journal for Light and Electron Optics*, **185** (2019) 248–255. https://doi.org/10.1016/j.ijleo.2019.03.101.

281. R. Vinayagam, R. Selvaraj, P. Arivalagan, & T. Varadavenkatesan, Synthesis, characterization and photocatalytic dye degradation capability of Calliandra haematocephala -mediated zinc oxide nanoflowers. *Journal of Photochemistry & Photobiology, B: Biology*, **203** (2020) 111760. https://doi.org/10.1016/j.jphotobiol.2019.111760.

282. S. Singh, M. Joshi, P. Panthari, B. Malhotra, A. C. Kharkwal, & H. Kharkwal, Citrulline rich structurally stable zinc oxide nanostructures for superior photo catalytic and optoelectronic applications : A green synthesis approach. *Nano-Structures & Nano-Objects*, **11** (2017) 1–6. https://doi.org/10.1016/j.nanoso.2017.05.006.

283. E. G. Goh, X. Xu, & P. G. McCormick, Effect of particle size on the UV absorbance of zinc oxide nanoparticles. *Scripta Materialia*, **78**–**79** (2014) 49–52. https://doi.org/10.1016/j.scriptamat.2014.01.033.

284. S. Syama, S. C. Reshma, P. J. Sreekanth, H. K. Varma, & P. V. Mohanan, Effect of Zinc Oxide nanoparticles on cellular oxidative stress and antioxidant defense mechanisms in mouse liver. *Toxicological and Environmental Chemistry*, **95** (2013) 495–503. https://doi.org/10.1080/02772248.2013.789606.

285. I. M. M. Paino, F. J. Gonçalves, F. L. Souza, & V. Zucolotto, Zinc Oxide Flower-Like Nanostructures That Exhibit Enhanced Toxicology Effects in Cancer Cells. *ACS Applied Materials and Interfaces*, **8** (2016) 32699–32705. https://doi.org/10.1021/acsami.6b11950.

286. K. M. Kim, M. K. Kim, H. J. Paek, S. J. Choi, & J. M. Oh, Stable fluorescence conjugation of ZnO nanoparticles and their size dependent cellular uptake. *Colloids and Surfaces B: Biointerfaces*, **145** (2016) 870–877. https://doi.org/10.1016/j.colsurfb.2016.06.006.

287. M. C. Santimano, A. Martin, M. Kowshik, & A. Sarkar, Zinc oxide nanoparticles cause morphological changes in human A549 cell line through alteration in the expression pattern of small GTPases at mRNA Level. *Journal of Bionanoscience*, **7** (2013) 300–306. https://doi.org/10.1166/jbns.2013.1134.

288. Z. Emami-Karvani & P. Chehrazi, Antibacterial activity of ZnO nanoparticle on Gram-positive and Gram-negative bacteria. *African Journal of Microbiology Research*, **5** (2011) 1368–1373. https://doi.org/10.5897/AJMR10.159.

289. M. Premanathan, K. Karthikeyan, K. Jeyasubramanian, & G. Manivannan, Selective toxicity of ZnO nanoparticles toward Gram-positive bacteria and cancer cells by apoptosis through lipid peroxidation. *Nanomedicine: Nanotechnology, Biology, and Medicine*, **7** (2011) 184–192. https://doi.org/10.1016/j.nano.2010.10.001.

290. B. Lallo da Silva, B. L. Caetano, B. G. Chiari-Andréo, R. C. L. R. Pietro, & L. A. Chiavacci,

Increased antibacterial activity of ZnO nanoparticles: Influence of size and surface modification. *Colloids and Surfaces B: Biointerfaces*, **177** (2019) 440–447. https://doi.org/10.1016/j.colsurfb.2019.02.013.

291. H. Esmailzadeh, P. Sangpour, F. Shahraz, J. Hejazi, & R. Khaksar, Effect of nanocomposite packaging containing ZnO on growth of Bacillus subtilis and Enterobacter aerogenes. *Materials Science and Engineering C*, **58** (2016) 1058–1063. https://doi.org/10.1016/j.msec.2015.09.078.

292. S. S. Bari & S. Mishra, Recent Advances in Nanostructured Polymer Composites for Biomedical Applications. *Nanostructured Polym. Compos. Biomed. Appl.* (Elsevier Inc., 2019), pp. 489–506. https://doi.org/10.1016/b978-0-12-816771-7.00024-7.

293. C. Venkatesh, M. Laurenti, M. Bandeira, E. Lanzagorta, L. Lucherini, V. Cauda, & D. M. Devine, Biodegradation and antimicrobial properties of zinc oxide–polymer composite materials for urinary stent applications. *Coatings*, **10** (2020). https://doi.org/10.3390/coatings10101002.

294. D. Campoccia, L. Montanaro, & C. R. Arciola, A review of the biomaterials technologies for infection-resistant surfaces. *Biomaterials*, **34** (2013) 8533–8554. https://doi.org/10.1016/j.biomaterials.2013.07.089.

295. X. Zhang, C. Gong, O. U. Akakuru, Z. Su, A. Wu, & G. Wei, The design and biomedical applications of self-assembled two-dimensional organic biomaterials. *Chemical Society Reviews*, **48** (2019) 5564–5595. https://doi.org/10.1039/c8cs01003j.

296. X. Ding, C. Yang, T. P. Lim, L. Y. Hsu, A. C. Engler, J. L. Hedrick, & Y. Y. Yang, Antibacterial and antifouling catheter coatings using surface grafted PEG-b-cationic polycarbonate diblock copolymers. *Biomaterials*, **33** (2012) 6593–6603. https://doi.org/10.1016/j.biomaterials.2012.06.001.

297. S. Park, U. Han, D. Choi, & J. Hong, Layer-by-layer assembled polymeric thin films as prospective drug delivery carriers: Design and applications. *Biomaterials Research*, **22** (2018) 1–13. https://doi.org/10.1186/s40824-018-0139-5.

298. M. Kaushik, R. Niranjan, R. Thangam, B. Madhan, V. Pandiyarasan, C. Ramachandran, D. H. Oh, & G. D. Venkatasubbu, Investigations on the antimicrobial activity and wound healing potential of ZnO nanoparticles. *Applied Surface Science*, **479** (2019) 1169–1177. https://doi.org/10.1016/j.apsusc.2019.02.189.

299. V. Tiwari, N. Mishra, K. Gadani, P. S. Solanki, N. A. Shah, & M. Tiwari, Mechanism of anti-bacterial activity of zinc oxide nanoparticle against Carbapenem-Resistant Acinetobacter baumannii. *Frontiers in Microbiology*, **9** (2018) 1–10. https://doi.org/10.3389/fmicb.2018.01218.

300. H. Duan, D. Wang, & Y. Li, Green chemistry for nanoparticle synthesis. *Chemical Society Reviews*, **44** (2015) 5778–5792. https://doi.org/10.1039/c4cs00363b.

301. A. Mocanu, G. Isopencu, C. Busuioc, O. M. Popa, P. Dietrich, & L. Socaciu-Siebert, Bacterial cellulose films with ZnO nanoparticles and propolis extracts: Synergistic antimicrobial effect. *Scientific Reports*, **9** (2019) 1–10. https://doi.org/10.1038/s41598-019-54118-w.

302. D. Kwon, J. Park, J. Park, S. Y. Choi, & T. H. Yoon, Effects of surface-modifying ligands on the colloidal stability of ZnO nanoparticle dispersions in in vitro cytotoxicity test media. *International Journal of Nanomedicine*, **9** (2014) 57–65. https://doi.org/10.2147/IJN.S57924.

303. S. Liufu, H. Xiao, & Y. Li, Adsorption of polyelectrolyte on the surface of ZnO nanoparticles and the stability of colloidal dispersions. *Chinese Science Bulletin*, **50**

(2005) 1570–1575. https://doi.org/10.1360/982004-575.

304. R. Marsalek, Particle Size and Zeta Potential of ZnO. *APCBEE Procedia*, **9** (2014) 13–17. https://doi.org/10.1016/j.apcbee.2014.01.003.

305. S. S. Shiratori & M. F. Rubner, pH-dependent thickness behavior of sequentially adsorbed layers of weak polyelectrolytes. *Macromolecules*, **33** (2000) 4213–4219. https://doi.org/10.1021/ma991645q.

306. Z. Tang, Y. Wang, & N. A. Kotov, Semiconductor Nanoparticles on Solid Substrates : Film Structure , Intermolecular Interactions , and Polyelectrolyte Effects. *Langmuir*, **18** (2002) 7035–7040. https://doi.org/10.1021/la025601d.

307. X. Wu, C. Liu, H. Chen, Y. Zhang, L. Li, & N. Tang, Layer-by-Layer Deposition of Hyaluronan and Quercetin-Loaded Chitosan Nanoparticles onto Titanium for Improving Blood Compatibility. *Coatings*, **10** (2020). https://doi.org/10.3390/coatings10030256.

308. Z. Diaconeasa, Time-dependent degradation of polyphenols from thermally-processed berries and their in vitro antiproliferative effects against melanoma. *Molecules*, **23** (2018). https://doi.org/10.3390/molecules23102534.

309. A. Shpichka, D. Butnaru, E. A. Bezrukov, R. B. Sukhanov, A. Atala, V. Burdukovskii, Y. Zhang, & P. Timashev, Skin tissue regeneration for burn injury. *Stem Cell Research and Therapy*, **10** (2019) 1–16. https://doi.org/10.1186/s13287-019-1203-3.

310. S. Wang, Y. Xiong, J. Chen, A. Ghanem, Y. Wang, J. Yang, & B. Sun, Three Dimensional Printing Bilayer Membrane Scaffold Promotes Wound Healing. *Frontiers in Bioengineering and Biotechnology*, **7** (2019) 1–11. https://doi.org/10.3389/fbioe.2019.00348.

311. E. M. Tottoli, R. Dorati, I. Genta, E. Chiesa, S. Pisani, & B. Conti, Skin wound healing process and new emerging technologies for skin wound care and regeneration. *Pharmaceutics*, **12** (2020) 1–30. https://doi.org/10.3390/pharmaceutics12080735.

312. J. Qu, X. Zhao, Y. Liang, T. Zhang, P. X. Ma, & B. Guo, Antibacterial adhesive injectable hydrogels with rapid self-healing, extensibility and compressibility as wound dressing for joints skin wound healing. *Biomaterials*, **183** (2018) 185–199. https://doi.org/10.1016/j.biomaterials.2018.08.044.

313. J. Jiang, J. Pi, & J. Cai, The Advancing of Zinc Oxide Nanoparticles for Biomedical Applications. *Bioinorganic Chemistry and Applications*, **2018** (2018) 18. https://doi.org/10,1155/2018/1062562.

314. M. Batool, S. Khurshid, Z. Qureshi, & W. M. Daoush, Adsorption, antimicrobial and wound healing activities of biosynthesised zinc oxide nanoparticles. *Chemical Papers*, **75** (2021) 893–907. https://doi.org/10.1007/s11696-020-01343-7.

315. C. P. Gong, Y. Luo, & Y. Y. Pan, Novel synthesized zinc oxide nanoparticles loaded alginate-chitosan biofilm to enhanced wound site activity and anti-septic abilities for the management of complicated abdominal wound dehiscence. *Journal of Photochemistry and Photobiology B: Biology*, **192** (2019) 124–130. https://doi.org/10.1016/j.jphotobiol.2019.01.019.

316. A. Keirouz, M. Zakharova, J. Kwon, C. Robert, V. Koutsos, A. Callanan, X. Chen, G. Fortunato, & N. Radacsi, High-throughput production of silk fibroin-based electrospun fibers as biomaterial for skin tissue engineering applications. *Materials Science and Engineering C*, **112** (2020). https://doi.org/10.1016/j.msec.2020.110939.

317. T. Blachowicz & A. Ehrmann, Recent developments in electrospun ZnO nanofibers: A short review. *Journal of Engineered Fibers and Fabrics*, **15** (2020) 1–6. https://doi.org/10.1177/1558925019899682.

318. E. Ferrone, R. Araneo, A. Notargiacomo, M. Pea, & A. Rinaldi, ZnO nanostructures and electrospun ZnO–polymeric hybrid nanomaterials in biomedical, health, and sustainability applications. *Nanomaterials*, **9** (2019) 1–33. https://doi.org/10.3390/nano9101449.

319. H. Chhabra, R. Deshpande, M. Kanitkar, A. Jaiswal, V. P. Kale, & J. R. Bellare, A nano zinc oxide doped electrospun scaffold improves wound healing in a rodent model. *RSC Advances*, **6** (2016) 1428–1439. https://doi.org/10.1039/c5ra21821g.

320. Y. Chen, W. Lu, Y. Guo, Y. Zhu, & Y. Song, Electrospun gelatin fibers surface loaded ZnO particles as a potential biodegradable antibacterial wound dressing. *Nanomaterials*, **9** (2019) 1–13. https://doi.org/10.3390/nano9040525.

321. R. Ahmed, M. Tariq, I. Ali, R. Asghar, P. Noorunnisa Khanam, R. Augustine, & A. Hasan, Novel electrospun chitosan/polyvinyl alcohol/zinc oxide nanofibrous mats with antibacterial and antioxidant properties for diabetic wound healing. *International Journal of Biological Macromolecules*, **120** (2018) 385–393. https://doi.org/10.1016/j.ijbiomac.2018.08.057.

322. K. T. Shalumon, K. H. Anulekha, S. V. Nair, S. V. Nair, K. P. Chennazhi, & R. Jayakumar, Sodium alginate/poly(vinyl alcohol)/nano ZnO composite nanofibers for antibacterial wound dressings. *International Journal of Biological Macromolecules*, **49** (2011) 247–254. https://doi.org/10.1016/j.ijbiomac.2011.04.005.

323. M. Bandeira, A. L. Possan, S. S. Pavin, C. S. Raota, M. C. Vebber, M. Giovanela, M. Roesch-Ely, D. M. Devine, & J. S. Crespo, Mechanism of formation, characterization and cytotoxicity of green synthesized zinc oxide nanoparticles obtained from Ilex paraguariensis leaves extract. *Nano-Structures and Nano-Objects*, **24** (2020) 100532. https://doi.org/10.1016/j.nanoso.2020.100532.

324. I. Jun, H. S. Han, J. R. Edwards, & H. Jeon, Electrospun fibrous scaffolds for tissue engineering: Viewpoints on architecture and fabrication. *International Journal of Molecular Sciences*, **19** (2018) 745. https://doi.org/10.3390/ijms19030745.

325. A. R. Esfahani, Z. Zhang, Y. Y. L. Sip, L. Zhai, & A. H. M. A. Sadamani, Removal of heavy metals from water using electrospun polyelectrolyte complex fiber mats. *Journal of Water Process Engineering*, **37** (2020). https://doi.org/10.1016/j.jwpe.2020.101438.

326. C. E. Peña-González, E. Pedziwiatr-Werbicka, T. Martín-Pérez, E. M. Szewczyk, J. L. Copa-Patiño, J. Soliveri, J. Pérez-Serrano, R. Gómez, M. Bryszewska, J. Sánchez-Nieves, & F. J. de la Mata, Antibacterial and antifungal properties of dendronized silver and gold nanoparticles with cationic carbosilane dendrons. *International Journal of Pharmaceutics*, **528** (2017) 55–61. https://doi.org/10.1016/j.ijpharm.2017.05.067.

327. M. Abrigo, P. Kingshott, & S. L. McArthur, Electrospun polystyrene fiber diameter influencing bacterial attachment, proliferation, and growth. *ACS Applied Materials and Interfaces*, **7** (2015) 7644–7652. https://doi.org/10.1021/acsami.5b00453.

328. C. J. Mortimer & L. Burke, Microbial Interactions with Nanostructures and their Importance for the Development of Electrospun Nanofibrous Materials used in Regenerative Medicine and Filtration. *Journal of Microbial & Biochemical Technology*, **8** (2016) 195–201. https://doi.org/10.4172/1948-5948.1000285.